



Thermal Performance of Nanoparticle Reinforced Enzymatic Construction Materials: Photothermal Heating System Proposal

A Major Qualifying Project
submitted to the Faculty of
WORCESTER POLYTECHNIC INSTITUTE
in partial fulfillment of the requirements for the
degree of Bachelor of Science

Authors

Anne McNamara, Worcester Polytechnic Institute
Georgy Zhukov, Worcester Polytechnic Institute

Date

April 3rd, 2023

Advisors

Prof. Dr. Nima Rahbar, Worcester Polytechnic Institute
Prof. Dr. Steven Van Dessel, Worcester Polytechnic Institute

This report represents work of WPI undergraduate students submitted to the faculty as evidence of a degree requirement. WPI routinely publishes these reports on its website without editorial or peer review. For more information about the project's program at WPI, see <http://www.wpi.edu/Academics/Projects>

TABLE OF CONTENTS

Table of Figures	5
Table of Tables	7
Authorship	8
MQP Design Statement	10
Professional Licensure Statement	12
Abstract	1
Keywords	1
1.0 Introduction	2
2.0 Background	3
2.1 History of Heating	3
2.1.1 Systems Through Time	3
2.1.1.1 Beginnings of Heating Systems in Dwellings	3
2.1.1.2 Prominent Heating Systems of Today	6
2.1.1.3 Emerging Heating Systems	11
2.1.2 Comparison Between Systems	12
2.1.2.1 Energy Efficiency of Systems	13
2.1.2.2 System Costs and Expected Lifetime	14
2.1.2.3 Associated Emissions	15
2.2 Greenhouse Gas Emissions and Buildings	15
2.2.1 Addressing the Issue: Executive Order 14057	16
2.2.2 Building Operation: Heating	18
2.2.3 Green Strategies	19
2.3 ECM-n Summary	21
2.3.1 Introduction of New Building Material	21
2.3.1.1 Existing Zero-Carbon Construction Materials	21
2.3.2 Material Properties	23
2.3.2.1 Structural Strength and Self-healing	23
2.3.2.2 Photothermal Capabilities	24
2.3.3 ECM-n as a Heating Element	25
2.4 Data Retrieval	26
2.4.1 Quantification of ECM-n Properties	26
2.4.1.1 Thermal Properties - Instruments & Processes	26
2.4.1.2 Optical Absorbance - Instruments & Processes	28
2.4.2 Software	29
2.4.2.1 COMSOL	30
3.0 METHODOLOGY	31
3.1 Photothermal Heating System Design	31

3.1.1	System Context	31
3.1.2	System Composition	32
3.1.3	System Overview	33
3.2	Creation of ECM-n Sample	34
3.2.1	Mold Making	35
3.2.2	ECM-n Mixing Procedure	35
3.2.3	Procedure Modifications	36
3.2.3.1	Alternative to Laser Curing	36
3.2.3.2	Slurry Modification	37
3.2.3.3	Slurry with Surfactant Modification	37
3.3	ECM-n Properties - Tests and Experiments	38
3.3.1	Thermogravimetric Analyzer (TGA)	38
3.3.2	Differential Scanning Calorimeter (DSC)	39
3.3.3	Guarded Longitudinal Comparative Calorimetry (GLCC)	39
3.3.4	Spectrometry Tests	41
3.3.3.1	UV-VIS Range	42
3.3.3.2	IR Range	43
3.4	Energy Simulation	44
3.4.1	Hand Calculations	44
3.4.2	COMSOL	45
3.4.2.1	General	46
3.4.2.2	Inputs and Outputs	47
4.0	RESULTS AND ANALYSIS	48
4.1	ECM-n Properties	48
4.1.1	Thermal Properties	49
4.1.2	Optical Properties	52
4.2	Energy Simulation	55
4.2.1	Hand Calculations	55
4.2.2	Model Reaches Steady-State Conditions	56
4.3	Passive Photothermal Heating System Design	58
4.3.1	Proposed Design	58
4.3.1.1	Comprehensive Figure of System Overview	59
4.3.1.2	Building Envelope	59
4.3.1.3	Efficiencies	61
5.0	DISCUSSION & CONCLUSION	62
5.1	Heating System Considerations	62
5.1.1	Laser Heating	62
5.1.2	Building envelope	63

5.2 ECM-n Properties	63
5.2.1 Thermal Properties	63
5.2.2 VIS Range Spectrophotometer	64
5.2.3 Comprehensive Analysis of Absorbance Data	64
5.3 Takeaways	65
6.0 ACKNOWLEDGEMENTS	67
BIBLIOGRAPHY	68
APPENDIX	2
Appendix A – Visual Summary of Heat Pumps	2
Appendix B - ECM-N Sample Creation Procedures	3
Appendix C – NETZSCH-PROTEUS-70 Software Settings for TGA Procedure	6
Appendix D – Software Settings for DSC Procedure	8
Appendix E – Methods Summary for Guarded Longitudinal Comparative Calorimetry	11
Appendix F – XPS Insulation Product Specification Sheet	13
Appendix G – Supplemental DSC Results	15
Appendix H – Spectrometry Results Data of ECM-n Specimen, Absorbance Peaks	16
Appendix I – Hand Calculations	17
Appendix J – Model Heating Visualization - Isothermal Lines	18

Table of Figures

Figure 1. Early Age Roman Hypocaust Section.	5
Figure 2. Natural Gas Furnace.	7
Figure 3. Oil Furnace.	8
Figure 4. Electric Furnace.	9
Figure 5. Annual Global CO2 Emissions by Sector.	17
Figure 6. Building Materials' Contribution to Annual Global CO2 Emissions.	17
Figure 7. Annual Buildings' Energy Consumption by Type.	18
Figure 8. Energy Infrastructure Breakdown by Source.	19
Figure 9. Geographic map of Natural Ventilation hours in 1854 locations.	20
Figure 10. Laser-Induced Curing of ECM-n.	24
Figure 11. Comparison of Multiscale Microstructure and Mineralization.	25
Figure 12. Temperature Gradient.	27
Figure 13. Experimental Setups to Measure Reflected and Transmitted Light.	29
Figure 14. Passive Photothermal Heating System Design.	31
Figure 15. System Energy Flow Chart.	32
Figure 16. System Section with Solar Collectors.	33
Figure 17. COMSOL Section Cut of ECM-n Wall Depicting Point Heat Source Distribution.	34
Figure 18. Partially Cured 2" Cube ECM-n Sample Flipped Upside Down.	37
Figure 19. Guarded Longitudinal Comparative Calorimeter Experimental Assembly Section.	40
Figure 20. Guarded Longitudinal Comparative Calorimeter Laboratory Setup.	40
Figure 21. Zoomed Experimental Setup for Measuring Reflectivity of the ECM-n Sample.	43
Figure 22. Full Scope Experimental Setup for Measuring Reflectivity of the ECM-n Sample.	43
Figure 23. Section Cut View of the COMSOL Model.	47
Figure 24. Isometric View of the COMSOL Model.	47
Figure 25. Isometric Wireframe View.	48
Figure 26. Cross Section of Building Envelope Composition.	48
Figure 27. TGA Data for ECM-n Sample.	49
Figure 28. Annotated DSC Data Showing Crystallization.	50
Figure 29. GLCC Temperature Program Graph.	51
Figure 30. Recorded Temperatures During the Thermal Conductivity Experiment.	51
Figure 31. Guarded Longitudinal Comparative Calorimeter Laboratory Setup.	51
Figure 32. Temperature Measurements at Different Points of the Experimental Setup.	52
Figure 33. Calculated Values of Heat Flux and Heat Flow.	52
Figure 34. Geometry Settings and Calculated.	52
Figure 35. Results of Thermal Conductivity of ECM-n Based on Excel Calculations.	52
Figure 36. Spectrometry Results Data of ECM-n Specimen.	53
Figure 37. Reflectance Percentage over the IR Range.	54

Figure 38. Absorbance of ECM-n Sample at NIR and IR Ranges.	55
Figure 39. Temperature Integration Results of Interior Walls.	57
Figure 40. Normal Energy Flux for Interior Surface of Walls.	57
Figure 41. Temperature vs. Time Graph Depicting the Interior and Outer Side of ECM-n Wall.	57
Figure 42. Colored Thermal Gradient for Single Wall.	58
Figure 43. Passive Photothermal Heating System Design.	59
Figure 44. Altered Imbedded Fiber Cable in ECM-n Wall.	60
Figure 45. Seasonal Solar Power Intensity in Boston, Massachusetts.	61
Figure 46. Transverse Intensity Profile of a Gaussian Beam.	62
Figure 47. Solar Spectra & Proportional Energy Content of Solar Power.	64
Figure 48. Heat Pump Visual Summary.	2
Figure 49. Example Data Given by TecaLog Software Manual.	12
Figure 50. XPS R-Values from Dupont.	13
Figure 51. Physical Properties of XPS from Dupont.	14
Figure 52. DSC Data for ECM-n Sample.	15
Figure 53. Appendix H, 1 of 4.	16
Figure 54. Appendix H, 2 of 4.	16
Figure 55. Appendix H, 3 of 4.	16
Figure 56. Appendix H, 4 of 4.	16
Figure 57. Variables and Equations Legend.	17
Figure 58. Model Component Material Properties.	17
Figure 59. Wall Model in Excel.	17
Figure 60. Results from Hand Calculations in Excel.	17
Figure 61. Heat Gradient of Point Heat Source Distributions.	18

Table of Tables

Table 1: System Efficiency Comparison Table	14
Table 2: Fuel to Electricity Comparison	14
Table 3: Hand Calculation Known Property Summary Table	44
Table 4: Hand Calculation Results Summary Table	56

Authorship

Section	Primary Author(s)	Editor(s)
Table of Contents	McNamara	McNamara
Table of Figures	McNamara	McNamara
Table of Tables	McNamara	McNamara
MQP Design Statement	McNamara	Zhukov
Professional License Statement	McNamara	Zhukov
Abstract	Zhukov, McNamara	McNamara, Zhukov
1.0 Introduction	McNamara	Zhukov
2.0 Background		
2.1 History of Heating	McNamara	Zhukov
2.2 Greenhouse Gas Emissions and Buildings	Zhukov	McNamara, Zhukov
2.3 ECM-n Summary	McNamara	Zhukov
2.4 Data Retrieval	McNamara	Zhukov
3.0 Methodology		
3.1 Passive Photothermal Heating System Design	McNamara	McNamara, Zhukov
3.2 Creation of ECM-n Sample	McNamara	Zhukov, McNamara
3.3 ECM-n Properties - Tests and Experiments	McNamara	Zhukov, McNamara
3.4 Energy Simulation	Zhukov, McNamara	McNamara, Zhukov
4.0 Results and Analysis		
4.1 ECM-n Properties	McNamara	McNamara
4.2 Energy Simulation	Zhukov, McNamara	McNamara, Zhukov
4.3 Passive Photothermal Heating System Design	McNamara	McNamara, Zhukov

5.0 Discussions		
5.1 Heating System Considerations	Zhukov	McNamara, Zhukov
5.2 ECM-n Properties	Zhukov	McNamara, Zhukov
5.3 Takeaways	McNamara	McNamara, Zhukov
6.0 Acknowledgments	McNamara	McNamara, Zhukov
7.0 Bibliography	McNamara, Zhukov	McNamara
Appendix		
A	McNamara	McNamara, Zhukov
B	Zhukov	McNamara
C	McNamara	McNamara, Zhukov
D	McNamara	McNamara, Zhukov
E	McNamara, Zhukov	McNamara
F	Zhukov, McNamara	McNamara
G	Zhukov	McNamara, Zhukov
H	McNamara	McNamara, Zhukov
I	Zhukov	McNamara, Zhukov

MQP Design Statement

The Major Qualifying Project (MQP) at Worcester Polytechnic Institute is a requirement for all undergraduate students of all departments. The project is designed as a culminating project to bring together knowledge learned from courses throughout our time at the college. The Architectural Engineering department requires that all students participate in the MQP. To meet this requirement, a building envelope design proposal and engineering recommendations were studied around the application of a new construction material as a heating system. The integration of multiple engineering and science disciplines, including architectural, mechanical, chemical, and material science, were required to develop a strategic experiential procedure and initial design phases of the project that incorporates the sustainability and energy efficiency innovation desired by stakeholders. All measurements and calculations were completed using SI units.

This MQP, specific to the Architectural Engineering major, also satisfies the Capstone Project requirement set by the Accreditation Board for Engineering and Technology (ABET). The team consisted of two architectural engineering students. Both student contributors utilized a variety of coursework to show design competence in their curriculum areas. The team also communicated and collaborated with faculty advisors, graduate students, and entrepreneurial advisors throughout the design process. This was accomplished through weekly advisory meetings, a semester-long value-creation class, and guidance from graduate students.

To meet the ABET requirements for a Capstone Project it is required that the four architectural engineering curriculum areas are demonstrated within the project's scope. The four curriculum areas are building structures, building mechanical systems, building electrical systems, and construction/construction management. For the MQP, students are expected to reach the synthesis level in one of these areas, the application level in a second area, and the comprehension level in the remaining two areas. Building mechanical systems is a prioritized area in this MQP, as the project's main focus was to design a new photothermal heating system. The comprehension level of construction/ construction management was met. The design development kept the feasibility and potential for large-scale manufacturing in the construction industry at the forefront of the design process.

Building Physics, Principles Of HVAC Design For Buildings, and Advanced HVAC System Design courses provided us with theory and background knowledge of how mechanical

systems in buildings operate. This technical knowledge helped develop the problem statement for this project, as well as perform heat loss calculations. The latter was necessary to determine the thermal performance of the system “at a glance” prior to computational thermal modeling in software. Architectural Design Studio Class V- Building Envelope Design class provided very detailed technical specifications of the building envelope compositions which meet the IECC code for the specified designed climate zones.

Courses such as Construction Project Management and Legal Aspects of Professional Practice assisted in understanding the timeline of projects and the order of contractor work and the construction projects. For mechanical system design, this information brings more feasibility by breaking the system down into components for more detailed analysis. It helped to know how ultimately the system would need to be implemented in real-world applications. Furthermore, familiarity developed using various software programs learned in Architectural Design Studio courses, allowed the team to quickly learn COMSOL software.

Professional Licensure Statement

Across the world, professional licensure is a challenging, long-term commitment for engineers. However, the rigor and duration are worthwhile investments in a young engineer's career development. The professional licensure program was developed to ensure that designs are subject to examination and verification from certified Professional Engineers. With processes such as this in place, engineers are able to minimize risks to the public.

The professional licensure program varies across the globe but relevant to the work done in this project, this report will focus on the process in the United States. Within the United States, the professional licensure process again varies by state but the general process is outlined by the National Council of Examiners for Engineering and Surveying (NCEES). The process has four primary steps, the first being the successful completion of a Bachelor of Science degree in engineering from an Accreditation Board for Engineers and Technology (ABET) accredited program. Upon the receipt of the Bachelor of Science degree, aspiring Professional Engineers must register for and pass the Fundamentals of Engineering (FE) Exam which is conducted by the NCEES. After passing the FE, one becomes an Engineer in Training (E.I.T). Once an Engineer is in Training, three to five years of work experience must be completed under the supervision of a Professional Engineer. The length of the work experience varies on a state level and may be shortened based on different factors, including the completion of a Master's Degree. After completing the specified amount of work experience, the E.I.T. is eligible to sit for the discipline-specific Professional Engineering (PE) exam. The disciplines architectural engineer graduates may take the PE exam vary, but are typically one of the following: Civil Engineering, Architectural Engineering, or Fire Protection Engineering. After passing the PE exam, the aspiring Professional Engineer can apply for a license in their desired state of practice.

The benefits of becoming an accredited Professional Engineer are numerous. Having the PE license can prove beneficial in terms of titles in the workplace; there are opportunities for career growth, and it shows a higher level of commitment to the engineering profession. These benefits have the potential to launch candidates who have earned a PE into positions with higher salaries and more authority in the workplace, in terms of projects and responsibility. Once the FE and PE exams have been passed in one state, registering as a PE in any state in the United States is fairly straightforward. This flexibility and security in the job are afforded by completing this professional licensure process (Fong, 2019).

Abstract

Building operations and the construction sectors are both responsible for 38% of the total CO₂ emissions worldwide (Architecture 2030, 2022). Energy consumption and associated CO₂ emissions must be diminished to put the United States on track for the Federal Sustainability Plan (Executive Order 14057). The Enzymatic Construction Material with nanoparticles (ECM-n) is a new carbon-negative alternative to concrete that offers promise to reduce carbon dioxide emissions. In addition to the material's self-healing features, structural ECM-n is also effective in converting electromagnetic radiation into heat. Focusing on the heating capabilities, this project investigates the photothermal heating performance of a wall assembly with the ECM-n. The proposed heating system design capitalizes on ECM-n's photothermal properties. It as well reduces the system's negative environmental impact by harnessing solar energy to heat the building. Experiments were conducted to determine ECM-n's thermal and optical properties. Based on the found data, a model was developed using COMSOL software to optimize the heating performance of a typical building enclosure using the ECM-n. The "Thermal Performance of Nanoparticle Reinforced Enzymatic Construction Materials" project has the potential to contribute to the reduction of carbon emissions and provide a means to meet global environmental goals and legislation.

Keywords

- Enzymatic Construction Material
- Nanoparticles
- Photothermal Heating
- Carbon-negative
- Sustainable Building Construction
- Carbon Emission Reduction

1.0 Introduction

Building operations make up 27% of annual global CO₂ emissions, the highest contributing building operation, to this statistic, is heating systems (IEA, n. d.). The high contribution of building heating is due to the prominence of natural gas and oils being used in outdated systems with poor energy efficiency. Another significant contributor to annual global CO₂ emissions is the production of construction materials. Concrete is the world's leading construction material resulting in 4.1 billion tons being produced annually (Watts, 2019).

Emerging technologies and research usher in a wave of new construction materials with a smaller carbon footprint. The Enzymatic Construction Material (ECM), is a self-healing carbon-negative material with strong structural properties (Wang et al., 2022). ECM was modified to include nanoparticles for its curing process, the newly modified material is an Enzymatic Construction Material with nano-particles (ECM-n) (Wang et al., 2022). The addition of the nanoparticles improved the material's strength and thermal properties. These bolstered properties can be capitalized on to potentially develop a heating system that would mitigate the current demand for concrete and fossil fuel-based heating systems. Creating an alternative to address these issues could lead to the reduction of global carbon emissions, which is a critical component of environmental goals and legislation being enforced globally.

The goal of this project was to study a new heating system that takes advantage of the ECM-n's thermal properties. To approach this problem it was necessary to first develop a comprehensive understanding of other heating systems currently used. From there, another goal was to consider the environmental impact heating systems have and design a passive photothermal heating system to reduce the negative environmental impacts these systems typically have. To successfully design a system, a complete knowledge of ECM-n and its properties was needed. Given that the thermal properties of the material were initially unknown, it was essential to run testing with the material and determine the associated thermal properties. Once the thermal properties were determined, they were used in modeling software to optimize and design a hybrid heating system and building enclosure using the ECM-n. These goals were accomplished through the data extraction processes and by iterative design in the modeling software.

2.0 Background

This chapter provides the background information necessary to understand the approach taken in the project's design process. The historical development and importance of heating systems are first outlined, opening up the discussion about the associative carbon emissions and how they may be diminished with legislation. Then a summary of the project's primary material focus and experimental backgrounds are given. Finally, the inspiration and background for this project are explained.

2.1 History of Heating

As the project goals were to investigate and design a new heating system using a new construction material, it was beneficial to initially have a comprehensive understanding of heating systems. Heating systems have progressed significantly since the days of open fires in caves, and as humanity progressed in both technological development and record-keeping. From such, it is possible to follow the advancement of these systems.

2.1.1 Systems Through Time

There are 3 main mediums that deliver heat energy from heat sources to zones: air, water, and electrical resistance. The latter was not available in homes until the late 1900s (Vogele, 2018). In the sections below, the chapter covers the beginnings of heating systems in homes, the most commonly used systems today: fossil-fuel-powered systems, and the modern systems that are being developed and advanced.

2.1.1.1 Beginnings of Heating Systems in Dwellings

Hearths and Fireplaces

The earliest records of residential heating include hearths and fireplaces, stoves, and underfloor systems. The records include an excavated central hearth from Greece, dated 2500 B.C., as well as crude fireplace heating found in Europe as early as 800s A.D (Karakanas, 2004). There are records of castles in the same European area and date using an early version of a chimney.

The earliest fireplaces were made of simple stones (Karakanas, 2004). With advancements in the casting of metal, these new improvements conceived the early fireplace. Cast iron firebacks, and raised grates, and specialized cast hearths could all be implemented (Hodgkinson, 2012). The cast iron firebacks protected stones in the fireplace. Fire grates, invented by Louis Savot in France during the early 1600s, led to the development of the circulating fireplace (Garrison, 1927). These specialized hearths were designed to have a narrower width, a streamlined flue for a stronger draft, and ducts under, behind, and above the hearth. Having a large hearth was extremely beneficial because, in addition to being a heat source itself, it was frequently used for cooking.

The first comprehensive manual on fireplace design was written in 1713 France (Jandot, 2020). Following this publication, fireplace construction reached a high point with the work by

Benjamin Thompson – later known as Count Rumford – publishing, *Chimney Fireplaces* in 1796 (Maurig, 1999). The outlined design later led to what is now known as the Rumford fireplace. The improved design was smaller and shallower with widely angled covings so they would radiate better.

Stoves

Similarly to the rise of fireplace heating in the 800s A.D., stoves made of clay bricks also became prominent at this time (Solov'ev, 1999). Metal stoves first appeared in the 1500s in Europe. They were primarily made of cast iron hearth firebacks that were welded together (Hodgkinson, 2012). Following this, cast iron sections were produced specifically for this purpose and Holland and Germany became leading centers for iron stove manufacturing (Edgerton, 1961). By the late 1500s in Europe, masonry stoves became commonplace (Goldstone, 2009). These stoves became known as Russian or Swedish stoves and were very large. They later became more ornate in appearance and commonly had tile coverings (Stuart, 1845).

In the 1600s, the *Furnus Acapnos* or “*smokeless stove*” was invented in France by Dalesme (Garrison, 1927). This was one of the first advanced designs for a stove. Dalesme’s design allowed for the introduction of fresh fuel in the same compartment as the combustion air. This new strategy allowed for all the combustion products to be directed over the already-burning fuel which resulted in complete combustion. This smokeless stove was an innovative technological advance but it did not catch on. The advantages were not directly visible so very few housekeepers at the time were willing to take on the management of the complex system of which they did not understand the benefits.

Chimneys

The origin of chimneys is unclear but it is thought that the first use of a chimney in Europe was in the 12th century. During an earthquake in Venice in 1347, many chimneys were destroyed, however, it is known that there were chimneys present in Padua, Italy by 1368 (Hammerl, 1994). Although present in Europe, the chimney as it is known today was not commonly found in homes in Europe until the 16th and 17th centuries (Cullingford, 2001). This is due in large part to the chimney’s original design. The fireplaces found in homes were very large as they were used for cooking, however, a brick chimney was unable to eliminate the smoke from the home efficiently for a fireplace so it was not until the 18th century that central chimneys were considered to be effective at removing smoke from the homes.

Early chimneys were built larger than modern chimneys so that a chimney sweep would be able to climb into them. Having such a large chimney resulted in harsh drafts which then led to the added feature of a divider screen. The divider screen was used to shield the occupants of the home from the drafts (Crowley, 2003).

Radiant Heating Systems

Radiant heating is the process of electromagnetic waves being intercepted and absorbed and then converted into heat. Radiant energy is absorbed by objects and our bodies and warms space or people. It is a similar process to sunlight being absorbed by your clothes and making a person warm (Kubba, 2012). Radiant heating, specifically radiant heating systems are known to be used as early as 1300 B.C. These original radiant panel systems were underfloor heating systems. They were used in the Middle East at this time, notably in mosques in Turkey where they had underfloor heating system installed (Bean, 2010).

In 80 B.C., the Romans began to use radiant heating. The first implementation of this technology came from designs by Sergius Orata. At the beginning of their use of these systems, they heated only the floors but later expanded their designs to include walls and they eventually designed early warm-air heating systems, introducing heated air through floor openings. Prominently, from 10 B.C. through 324 A.D., the Romans used the Roman hypocaust heating system to heat upper-class Roman houses as well as at least 17 major public baths (Fagan, 2001).

The Roman hypocaust heating system had several iterations. The early design consisted of a chamber that had pillars that held up the stone floors. The chambers had a fire at one end and combustion gasses passed through the chamber, under the floor, to the opposite side. The chamber through which these gasses moved through was the hypocaust (Figure 1). Later iterations of heating systems that used the hypocaust, used either tile flues or hollow tile walls to conduct the heated combustion products to eave vents. Creating the early warm-air heating systems. For these later, advanced designs, the fire which was formerly in the hypocaust was moved to a separate furnace chamber. Eventually, the Romans' famed hypocaust chamber was eliminated and floor ducts connected the furnace to the wall flues (Basaran, 2007).

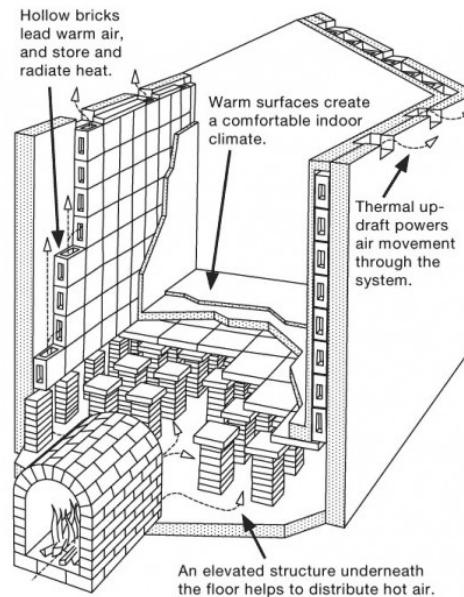


Figure 1. Early Age Roman Hypocaust Section.
Citation (Romans in Britain, n. d.).

The system was proven to be very efficient by modern tests at the Constantinian Baths. Modern testing found that the hypocaust heated the floor up to 95°F. The walls were heated to the temperature range of 66°F to 90°F. The system had an efficiency rating of about 90%. However, these systems were difficult to control compared to modern systems and took approximately two days to pre-heat (DeLaine, 1988).

2.1.1.2 Prominent Heating Systems of Today

The central air heating system first originated in the 13th century with the radiant heating systems of Ancient Rome. After the collapse of the Roman Empire, the central air heating systems of hot air, steam, or hot water did not come to fruition until the late 18th century. In 1793, William Strutt designed a furnace (Egerton, 1968). Strutt's design heated outside air in an underground passage before it conditioned a room. James Watt from Scotland created the first functional central boiler system in his home. This invention involved high-pressure steam distribution through pipes (Fleming, 1952). Early hot water-based heating systems were used in Russia in the early 1700s to heat Peter the Great's palace (Stuart, 1845). The system was not widely used, outside of conditioning greenhouses, until later on. Last, in the 1830s, hot water heating systems developed rapidly and were implemented in churches and factories all over England. The final element of the central air system, the radiator, was not invented until the late 1850s by a Russian inventor, Franz San Galli (Patil, 2018). The radiator was adopted widely across Europe and the United States.

Central air systems work by converting electricity to heat or by burning propane or natural gas to generate heat. In a furnace, an integral part of the central air system, the heat produced moves through a heat exchanger, increasing the air temperature to make hot air. To make the air hot, air from the building's ductwork is blown over the heat exchanger. Finally, the furnace's blower forces the heated air into the supply ductwork, which then distributes the warmed air throughout the building. (Goodman, n. d.) These central air systems include forced-air systems, which include furnaces, ductwork, and blowers.

Gas Furnaces

The two most common types of gas furnaces are the natural gas furnace and the oil furnace. In a natural gas furnace, gas is mixed with air inside a burner and ignited in the combustion chamber. From there, a blower pulls cool air from rooms throughout the building, into the furnace through the air ducts. That cool air is then heated over the heat exchanger which is connected to the combustion chamber. The warm air can then flow through the ductwork and heat the room. The exhaust gasses created by the burning in the combustion chamber are vented to the exterior through a flue in the roof or by a side wall vent ("Furnaces: How They Work | AHRI" n.d.). A diagram, Figure 2, is shown below of the various components of the system.

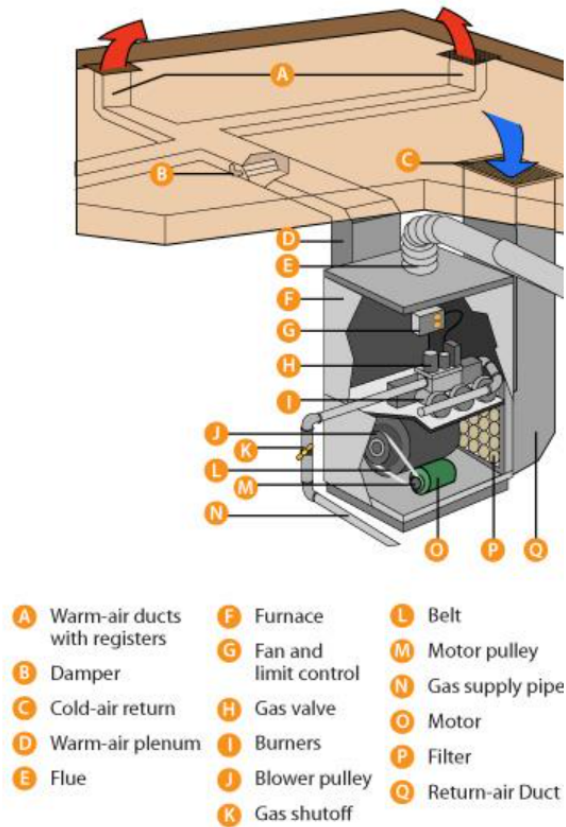


Figure 2. Natural Gas Furnace.
 (“Furnaces: How They Work | AHRI” n.d.)

An oil furnace is another popular furnace in a central air/ forced-air heating system. An oil furnace works similarly to a natural gas furnace. Their main difference is the fuel source and the combustion. The oil is turned into small particles or atomized, and the small particles are burned. The air absorbs the heat produced by the combustion as it crosses the heat exchanger. The blower then moves the warmed air into the ductwork, consequently, throughout the building. The fumes and exhaust gasses are vented to the building’s exterior (“Furnaces: How They Work | AHRI”, n. d.). Figure 3 is shown below of the various components of the system.

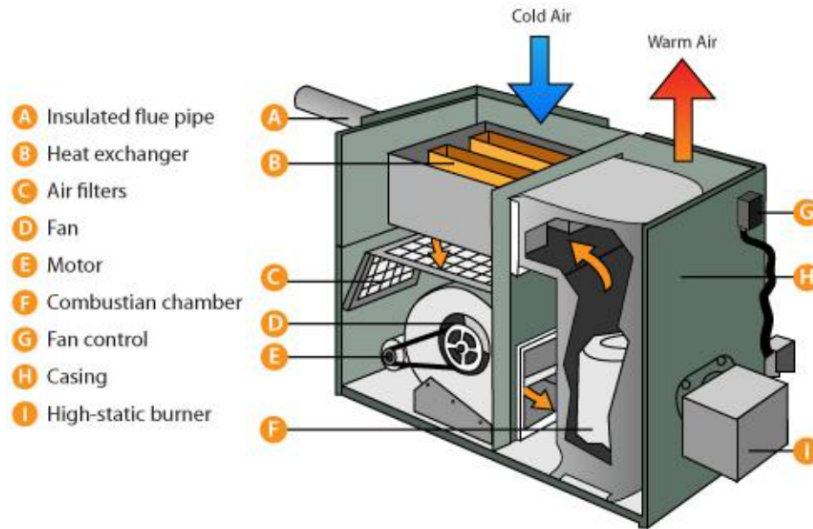


Figure 3. Oil Furnace.
 (“Furnaces: How They Work | AHRI” n.d.)

Electric Heating

The general concept of electric heating can be reduced to electrical energy being converted into heat through, commonly, the use of an electric resistor. Electric heating is frequently used in space heating, water heating, and other industrial processes. Using electricity for heat has risen in popularity due to its convenience and cleanliness—compared to combustible fuels. Electric heating also requires less auxiliary equipment, opening up more building areas for occupant use. Although it is more costly than other combustible fuel-powered heating systems, electric heating’s benefits are worth the investment. This electric heat comes in the forms of electric coils, strips, and convectors in walls and under windows, or as baseboard radiation. Electric heating also allows for unconventional applications. Electric heat can be moved through wires in the ceiling or floor of a building to be radiant heating (Kubba, 2017).

Another common application of electric heating is an electric furnace, as mentioned earlier. An electric furnace works similarly to a gas furnace but rather draws from electric currents. The electric furnaces pull air into the system through a heat exchanger. In the heat exchanger, electric heating elements, electrically-heated coils, warm the air, and the warm air is then pushed by a blower into the ductwork through a building or home. A diagram, Figure 4, is shown below of the various components of the system.

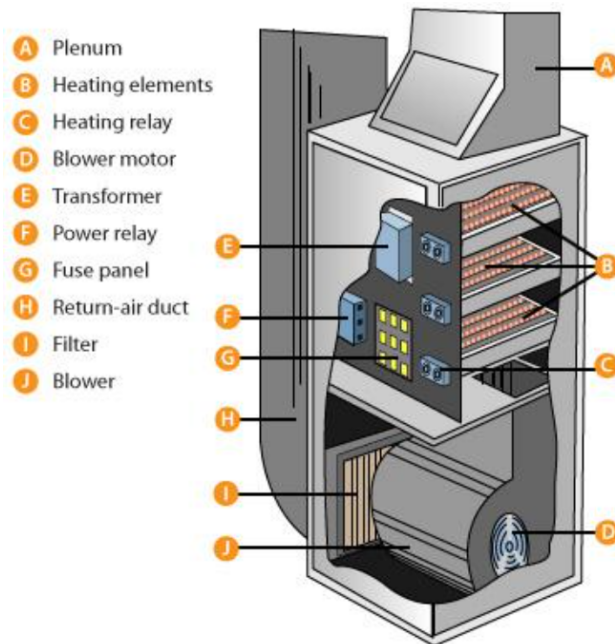


Figure 4. Electric Furnace.
 (“Furnaces: How They Work | AHRI” n.d.).

Electric furnaces have three to six electric-resistance heating elements that are 3.5 to 7kW which move electrically charged particles through metal wires producing heat. Also found in an electric furnace are the contactor, sequencer, and transformer. A contractor controls the voltage going into the system and works with the thermostat to prompt the furnace to produce heat. A sequencer turns the heating elements on and off. By doing this the current through the system is minimized. Using an appropriate sequencer is important because if the heating elements in a furnace all energize at once, a breaker could blow. A transformer is essential as it serves the electric furnace by providing power to the control circuits for the thermostat, contractors, and sequencers. It transfers electrical energy between circuits. Given that there can be multiple currents flowing through a furnace, a transformer contributes significantly to ensuring that power can flow smoothly through the furnace system (Vogele, 2017).

Radiant Systems

Radiant systems use radiation heat transfer and convection to warm the air in a space. This radiant heat transfer begins with the delivery of heat through; floors, ceiling panels, radiators, or walls to warm the space with infrared radiation. Radiant heat systems are most typically applied in flooring, to promote natural air convection (Kosonen, 2017). There are a variety of radiant heat systems: radiant air floors, electric radiant floors, and hot water (hydronic) radiant floors. Air-heated radiant floor systems are rarely used because they are not cost-effective for residential uses. Air’s heat capacity is significantly lower than that of water and therefore requires a large amount of energy to pump air through the slab to make the system effective in heating. Alternatives to radiant heat systems include baseboard heating and forced-air systems. If

compared, radiant heating is more efficient as there are no losses in ductwork in this system (DOE, n. d.). Radiant heat systems rely significantly on the convection of warm to cold air. As the air around the flooring heats up, lighter warm air then rises through convection, pushing heavier cool air down to the heated floors. This natural circulation is what makes this particular system the most comfortable for occupants.

Electric-radiant floor systems use electric resistance heaters on the floor to deliver the heat. Due to the costs associated with electricity, the electric-radiant floor systems work most efficiently in a cost-effective manner when used in tandem with a significant thermal mass. An affordable and practical thermal mass may be a thick concrete floor. The electric cables can ‘charge’ the thermal mass with heat during evenings when energy costs are lower and last 8-10 hours. Electric-radiant floors are also practical to use in smaller additions where it is not possible or efficient to extend a forced-air system (Ihm et al., 2005).

Hydronic-radiant floors are the most popular and cost-effective radiant heating systems. The heat is delivered by pumping heated water from a boiler through tubing under the flooring. Hydronic-radiant floors can be controlled by using zoning valves or pumps to control the hot water flow to the system which is then tied to the thermostats which regulate room temperatures. Ultimately, the installation of hydronic-radiant systems is more costly than electric-radiant systems. However, with the long-term costs of running water through the system compared to the cost of electricity continuously over time, the hydronic system is the better investment (Warmup, 2022). As is true for all radiant-heating systems, the costs of installation for the system depend on location, the size of the home, the type of installation (wet or dry), the floor covering, remoteness of the site, and the cost of labor (DOE, n. d.).

Heating, Ventilation, and Air Conditioning (HVAC) Overview

The heating, ventilation, and air conditioning (HVAC) system functions to condition a space as needed by, warming air when it's cool outside and cooling air when it's warm outside. The term HVAC is all-encompassing. It includes the air conditioner, furnace, heat pumps, indoor air quality equipment, thermostats, and similar control systems. HVAC units can be adapted to control humidity levels and improve the air quality of conditioned a space. At the most basic level, the HVAC system is designed to move air, to heat or cool. To do this a heating unit, a cooling unit, and ductwork are the three essential components of the system (ASHRAE, 2020).

There are various types of HVAC systems: Split Systems, Hybrid Heat Pump, Ductless Mini-Split, Ducted Mini-Split, or Packaged Systems. Split system may be made up of a furnace and air conditioner, an air handler unit (AHU) and heat pump, or a furnace and heat pump. A hybrid heat pump system is a central heating system with an electric heat pump that works in tandem with a furnace. The heat pump exchanges heat between colder outside and warmed inside, which makes it more efficient than conventional systems when outside temperatures are above 0 degrees Celsius (Linton, 1990). In harsher temperatures, the furnace is usually used to heat the home. The heat exchange system brings more savings within mild temperatures, however the efficiency drop makes it unreliable for colder climates. A ductless mini-split system has a

compressor and condenser, and an indoor air handler that blows cool air into the space. A ducted mini-split uses tubes rather than larger ducts. The tubes move air into a room from an outdoor compressor and condenser. These systems have better air circulation than the ductless mini-split. Finally, a packaged system houses all the components of a split system outside. These systems are quieter than a split system, take up less space in the house, and have lower installation costs (ASHRAE, 2020).

2.1.1.3 Emerging Heating Systems

As technology advances, the newer systems emerging in prominence are taking an innovative approach to building enclosure conditioning. These systems, specifically focusing on the heating systems utilize clean energy sources and can be more efficient than older approaches. Moving away from oil and natural gasses, most emerging energy systems use electricity which can be generated by renewables such as solar, wind, hydro, or geothermal energy. Some systems are passive or partially passive for parts of the day. This means that no combustion or electricity is required to harness the energy of the source to create heat in the system. The efficiencies of the systems are discussed in Section 2.1.2.1.

Heat Pumps

Heat pumps transfer heat between the building interior and the outside air using electricity. The heat pump works similarly to a central air conditioner whose design is based on the principle of heat being attracted to cooler temperatures. The most typical heat pump has three main units that make up the system. There is an air handling unit on the interior of the building, the exterior has the heat pump itself and the third component is the compressor which controls the refrigerant. The refrigerant circulates between the other two units absorbing and releasing heat as needed until the interior space reaches the specified temperature on the thermostat. There are various kinds of heat pumps, described above is the split system air source heat pump. There can also be geothermal-based heat pumps that pull heat from the ground. Other variations of the heat pumps can include ground source heat pumps, mini-split air source heat pumps, air-to-water heat pumps, and packaged unit air source heat pumps (DOE, n. d.).

The condenser unit of the system is the most complex as it involves an expansion valve, evaporator, compressor, condenser, and reversing valve. The condenser and evaporator act as heat exchangers. The evaporator is the exterior heat exchanger, which warms cold refrigerant with outside air and evaporates as its temperature increases. The cold air then is expelled to the outside. The refrigerant then moves to the compressor. The compressor increases the pressure of the gasified refrigerant. As the pressure increases, so does the temperature of the refrigerant. The refrigerant then moves into the interior heat exchanger, the condenser. The condenser takes hot gasified refrigerant and releases the heat to the inside air and condenses the refrigerant to a liquid as it cools after letting the hot air move to the interior. The refrigerant moves to the expansion valve last and again, as the pressure of the liquid refrigerant drops, the temperature also drops allowing the refrigerant to be cool as it moves to the exterior to attract warm air. The reversing

valve would force the refrigerant to flow in the opposite direction and a cooling process would be the result. Some fans draw outside/ inside air through the respective heat exchangers. The temperature of the air changes from cool to warm and vice versa depending on the heating/cooling mode and which exchanger/ direction the air moves across the system (Sun-Aire, 2017). A visual summary can be found in Appendix A.

Heat pumps work best in milder climates and require electricity to power the compressor, fans, pumps, and controls. Overall, these systems are fairly clean as they only require electricity and are the most energy-efficient system widely available.

Solar Heating

Moving into solar heating systems, there are solar collecting devices that convert light into heat which can be used for other building applications. This emerging technology utilizes renewable solar energy to heat water, air, or other fluids for use in residential, commercial, or industrial applications. The process uses solar collectors which absorb sunlight and convert it into heat that is transferred to a fluid. This heated fluid or material is then circulated through a building's heating system to provide warmth and comfort to the occupants. There are three different types of active solar heating systems, including 1) Liquid-based systems, 2) Air-based systems, and 3) Hybrid systems. Liquid-based systems use a fluid such as water or antifreeze, to transfer heat from the solar collector to a storage tank or directly to a building's heating system. An air-based system uses air as the transfer medium to distribute the heat to the building's heating system. A hybrid system combines both liquid-based and air-based systems to provide optimal heating performance (DOE, n. d.).

One main benefit of the system is its low environmental impact. The system uses renewable energy from the sun and as a result, reduces reliance on non-renewable energy sources. This not only helps to reduce greenhouse gas emissions and air pollution, but it also reduces the overall carbon footprint of a building or facility. If the overall output of the active solar system is too low to sustain the building's loads, it can be integrated with the building's existing heating systems to decrease energy demand from the grid. The initial cost of installing the system is higher than that of traditional systems, however, the variety of applications and long-term energy savings offset the initial investment (Manfred Starlinger, n. d.).

2.1.2 Comparison Between Systems

As concerns about climate change and energy efficiency become more prevalent in society, the heating systems used in buildings have come under increasing scrutiny. In this section, the energy efficiencies of various heating systems, as well as the costs, lifetime, and emissions associated with the systems, are examined. Throughout history, humans have been advancing our heating practices, increasing the efficiency of systems. Looking back at history broadly; society has managed to develop from wide, drafty chimneys and hearths to the most efficient system, the heat pump which relies on renewable energy sources. When comparing heating systems, the provided background information focuses on systems widely used and

installed today, in 2023. It is important to note that heating systems that use fossil fuels are difficult to compare to renewable or passive energy sources when looking at the energy efficiency criteria.

2.1.2.1 Energy Efficiency of Systems

The energy efficiency of heating systems is typically measured based on what kind of system it is. This makes it difficult to compare them as each system is rated in its energy efficiency metric. Boilers and furnaces use an annual fuel utilization efficiency (AFUE) rating, which is a measure of how much heat the system produces relative to the amount of fuel it consumes. AFUE ratings are expressed as percentages, where the higher percentages indicate greater efficiency (Central-Air-Conditioner-and-Refrigeration, n. d.). Boilers and furnaces are required to have a minimum AFUE rating of 80%, however, older systems may have a 56-70% AFUE and newer systems can have AFUE ratings from 90% to 98.5%, (DOE, n. d.).

A heat pump is used for both heating and cooling and each has its metric for energy efficiency. The cooling aspect uses the seasonal energy efficiency ratio (SEER) for energy efficiency. SEER is a measure of the efficiency of central air systems and is calculated as the ratio of the cooling output to the electrical energy input over an entire cooling season. A heat pump's heating energy efficiency is measured by the heating seasonal performance factor (HSPF) or the coefficient of performance (COP), depending on the type of heat pump. Average HSPF ratings for heat pumps are between 6.8-10 and COP ranges are from 2-4 (DOE, n. d.). Radiant floor heating is one of the most energy-efficient ways to heat your home. They are considered at least 20 to 25% more energy-efficient than forced-air heating systems (DOE, n. d.).

Table 1: System Efficiency Comparison Table

Type of System	Energy Efficiency Rating Ranges	Expected Lifetime of System	Fuel Source
Furnaces	59-98.5%	15-30 years	Natural gas, propane, heating oil, biodiesel blends, electricity
Boilers	50-90%	15-30 years	Natural gas, propane, heating oil, biodiesel blends, electricity
Heat Pumps	6.8-10 HSPF	15 years	Electricity, geothermal energy
Active Solar Heating	19%	20+ years	Solar energy
Electric Heating	95-100%	20+ years	Electricity

Table 2: Fuel to Electricity Comparison

Fuel Source	Amount Required to Generate 1 kWh of Electricity	Cost
Coal	1.12 pounds/kWh	\$0.02/ kWh
Natural Gas	7.36 cubic feet/kWh	\$0.05/ kWh
Petroleum Liquids	0.08 gallons/kWh	\$0.28/ kWh
Solar Power for a Single PV Panel (1.7 m ²)	4.5 hours/kWh	-

Sources: ("Frequently Asked Questions (FAQs) - U.S. Energy Information Administration (EIA)," n.d.)

("Solar Panel Calculator | How Many Solar Panels Do I Need?," n.d.)

(U.S. Energy Information Administration 2016)

("United States Natural Gas Industrial Price (Dollars per Thousand Cubic Feet)" 2009)

("Today in Energy - Daily Prices - Prices - U.S. Energy Information Administration (EIA)" 2016)

2.1.2.2 System Costs and Expected Lifetime

The systems with the most expensive upfront costs associated with them are the systems less widely adopted, such as the active solar heating and radiant heat flooring. However, with a

larger upfront cost, the long-term savings are worth the extra costs. These systems tend to use clean energy sources, are more energy efficient, and have long life expectancies.

One of the most common and least costly heating systems is a forced-air system, which uses a furnace to heat air that is then circulated throughout the building via air ducts. The average cost of installing a residential forced-air system is estimated to be between \$5,000 to \$10,000. The long-term savings associated with this system depend upon the energy efficiency rating of the system. A forced-air system typically lasts about 15-20 years (HomeAdvisor, n. d.).

Contrarily, radiant heat flooring is one of the most expensive heating systems. Hydronic radiant floor heating systems use a system of pipes beneath the flooring to circulate hot water providing consistent even heating throughout the building. The average cost of installing this system in a residential application is approximately \$14,000 to \$48,000 (HomeAdvisor, n. d.). The long-term savings this system comes with are significant. Compared to forced-air systems, hydronic radiant floor heating systems can reduce a homeowner's heating bills by up to 30%, and for a system that can last up to 35 years with appropriate maintenance, this is a beneficial investment.

The presented costs and lifetimes are the extreme ends of the spectrum. Regardless of the system, proper care and maintenance, effective insulation, and climate conditions should also be factored into the decision of implementing a heating system. An important consideration should also be that the higher sticker-price systems, later result in savings on an energy bill and utilize renewable energy sources which are important environmentally.

2.1.2.3 Associated Emissions

Fossil fuel-powered heating systems can have a significant impact on the environment through the emissions they produce. The most common types of associated emissions include carbon dioxide, nitrogen oxides, and sulfur dioxide (DOE, n. d.). Carbon dioxide is a greenhouse gas that contributes to climate change, while nitrogen oxides and sulfur dioxide can cause respiratory problems and contribute to air pollution.

Forced-air systems, which use fossil-powered furnaces to heat air, are less efficient and produce higher levels of emissions than other heating systems. The Department of Energy reports that “upgrading your furnace or boiler from 56% to 90% efficiency in an average cold-climate house will save 1.5 tons of carbon dioxide emissions each year if you heat with natural gas” (Weinberger, 2022). According to the U.S. Energy Information Administration, residential and commercial buildings accounted for 12% of carbon dioxide emissions in the United States alone in 2021 (IEA, 2022). It is important to consider not only the cost of heating but also its environmental impact when choosing a heating system.

2.2 Greenhouse Gas Emissions and Buildings

Greenhouse gases (GHGs) are the main cause of global warming. They accumulate in the upper layers of the Earth's atmosphere and trap incoming solar heat. GHGs keep temperatures at the surface of the Earth 33 degrees warmer than they otherwise could be, making the planet

habitable (Purkey et al., n. d.). However, the abundance of GHGs only accelerates climate change, causing global warming.

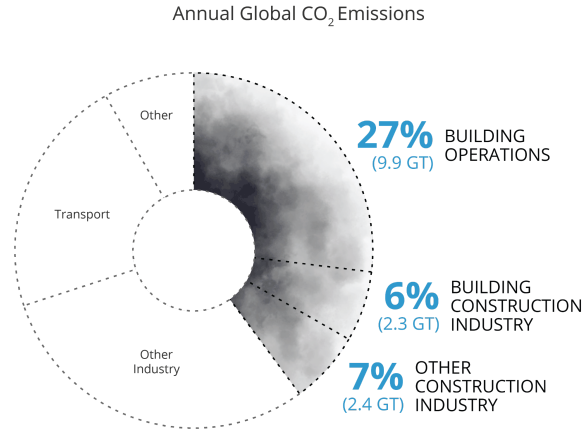
This overheating effect is called the enhanced greenhouse effect, and it is spurred by the release of unwanted amounts of greenhouse gasses into the atmosphere. In the atmosphere, 80.9% of the emissions are carbon dioxide (CO₂), which is a product of burning fossil fuels, and cement manufacturing (EPA, 2017). During the combustion of fossil fuels, the chemical reaction takes the form of the organic compound and oxygen under high temperatures. One of the resulting products is carbon dioxide. A similar process happens in the making of cement. Raw limestone is burned in a furnace to produce pure lime. The reaction is accompanied by the release of CO₂ until all limestone has reacted (Screed, n. d.).

2.2.1 Addressing the Issue: Executive Order 14057

The impacts of climate change affect every facet of modern living. Starting approximately 30 years ago, federal and private organizations around the world have worked to diminish the emissions of CO₂ in the atmosphere by proposing new policies on sustainability and resiliency (EPA, n. d.). An example of the first global take on the issue of global warming was presented by the Paris Agreement. This document was released by the United Nations and tasked involved countries to “limit global warming to 1.5°C by the end of this century” (UNFCCC, n. d.). The United States re-entered this agreement in 2020, setting the ground for a greener future.

In 2020, following the adoption of The Paris Agreement, President Biden signed Executive Order 14057, or Federal Sustainability Plan which aims to combat CO₂ emissions and have a net-zero emission infrastructure prevail by 2050 (Federal Chief Sustainability Officer, n. d.). The plan also sets intermediate goals between now and 2050, such as decreasing energy consumption by 50% by 2030 and fostering more dynamic implementation (The White House, 2021). It aims to impose zero-emission policies in transportation, energy, and building operation sectors as the main emitters of CO₂.

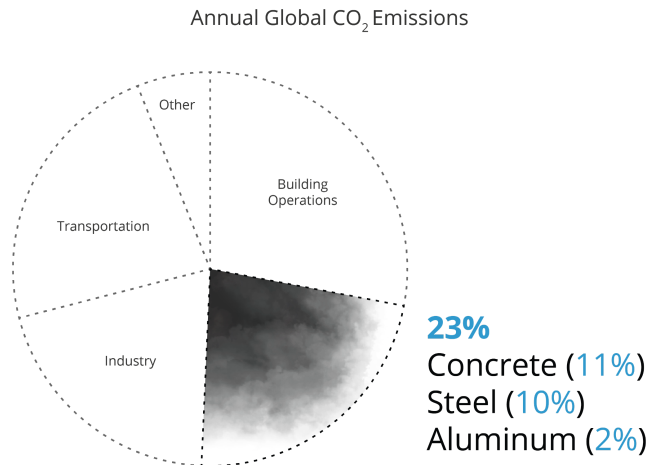
Many argue that the biggest contributor to climate change is transportation. However, the emissions caused by Internal Combustion Engines (ICEs) are only 11.9% of the total CO₂ emissions (Ritchie, 2020) whereas construction and building operation sectors combined produce 30% of that total. Now, the car industry is well-equipped for green conversion, even though transportation yields two-thirds less carbon dioxide than the energy economy of buildings does. Global building operation consumption increases exponentially, adding up to the amount produced the year before. Data showed a five percent increase in 2021 from 2020 consumption. Expanding economies and increasing demand for natural gas in some countries spurred the escalation in GHG emissions (IEA, 2022). The other reason is that high-efficiency strategies in buildings and low-emissions structural material production are not dominating the market, just yet.



© Architecture 2030. All Rights Reserved. Data Source: IEA (2022), Buildings, IEA, Paris
Building Construction Industry and Other Construction Industry represent emissions from concrete, steel, and aluminum for buildings and infrastructure respectively.

*Figure 5. Annual Global CO₂ Emissions by Sector.
 Citation, (Architecture 2030, 2022).*

Production of any construction material is accompanied by the generation of CO₂, but the leaders in associated emissions are steel, aluminum, and concrete (Fig. 6). Concrete alone stands for 11% of the total carbon content (Fig. 6), and it is the second most used material in the world, giving away the first place to water (Gagg, 2014). Per every pound of cement created 0.9 pounds of carbon dioxide is released. Other common structural materials like steel and aluminum yield more carbon emissions per cubic meter but are less used by the volume of produced material. Even though concrete, aluminum, and steel are cheap and reliable, due to their high carbon footprint, they will be substituted by greener alternatives very soon.



© Architecture 2030. All Rights Reserved.
 Data Sources: Global ABC Global Status Report 2018, EIA

*Figure 6. Building Materials' Contribution to Annual Global CO₂ Emissions.
 Citation, (Architecture 2030, 2022).*

Executive Order 14057 claims: “All new construction and major modernization projects larger than 25,000 GSF entering the planning stage will be designed, constructed, and operated to be net-zero emissions by 2030” (Federal Chief Sustainability Officer, n. d.). This means that any middle-sized residential complex, to the large-scale commercial projects, will be required to have all consumed energy be sustainable. Although it does not mean that the electrical grid will be eliminated, just that buildings will use it differently. For example, if some building uses an electrical grid to balance the loads, all of that energy has to be compensated with clean, renewable alternatives. This type of building operation is called net-zero emission. It is calculated based on the annual energy consumption of the building (Project Drawdown, n. d.).

2.2.2 Building Operation: Heating

To achieve net zero in new buildings, the standardized design approach for buildings has to be modified in various directions. With advancing technology in engineering, new high-efficient systems are introduced merely every year, opening the floodgates for new sustainable architecture. Water heating, lighting, and cooking have a significant contribution to the energy consumption of the building, but all of it is overshadowed by the energy directed to the conditioning of air, especially in northern regions (Fig. 7). Temperature differences in colder climates exterior conditions and comfortable 26°C interior conditions, results in higher energy consumption and lesser energy-saving strategies, being available for buildings in the north.

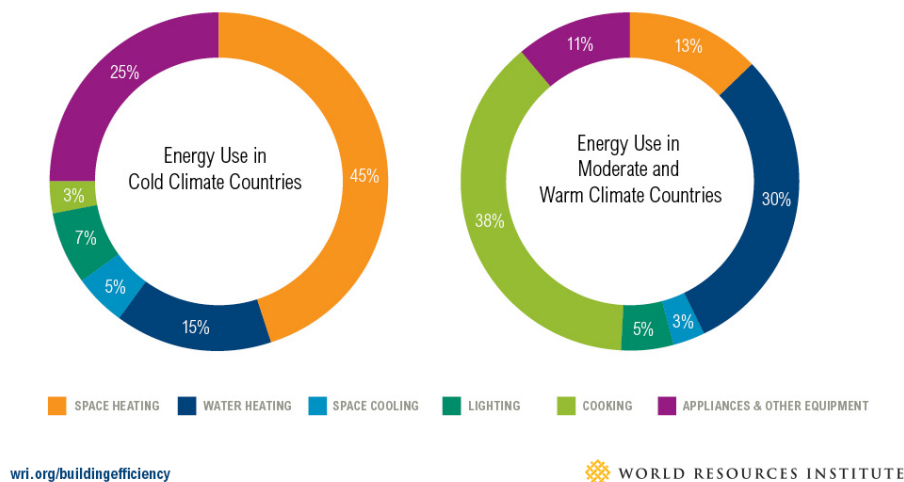


Figure 7. Annual Buildings' Energy Consumption by Type. Consumption in Cold (left) vs. Warm (right) Climates. (Accelerating Building Efficiency, 2021).

The recent popularization of ground heat pumps pushed the industry to the next level (see Section 2.1.1.3), bringing efficient heating to extreme climates. However, this is only one side of a coin. Buildings' energy performance, as well, depends on the rate of heat loss throughout the year. Factors like thermal bridging and air leakage are the main contributors to that. Modern

building envelope systems are designed to diminish the effect of thermal bridges by providing sufficient thermal and moisture insulation. With access to high-performance enclosures, architects now have more freedom of expression in buildings, maintaining the standard of occupational comfort inside.

So, the problem is not exclusively about how much energy buildings consume, but more importantly how much useful energy is delivered. Tesla, in its annual investor presentation on March 1st, 2023 (Fig. 8), claimed that only $\frac{1}{3}$ of global energy is delivered as intended, and the rest of the produced energy is lost (2023 Investor Day, 2023). Buildings need to incorporate more strategies that can maximize their efficiency based on free sources. Natural ventilation and geothermal heating are examples of such strategies with zero operational costs. The aim is to design net-zero buildings that consume 2-3 times less energy than their rivals, converting up to 90% of the total energy to useful energy.



*Figure 8. Energy Infrastructure Breakdown by Source.
(2023 Investor Day, 2023).*

2.2.3 Green Strategies

In North America, the pioneering non-profit organization that popularized sustainable architecture for building owners is U.S. Green Building Council (USGBC). It introduced a special rating system called Leadership in Energy and Environmental Design (LEED) that determined how sustainable and energy efficient the architecture of a building/campus is. The evaluation is based on LEED-established criteria that track the building's energy consumption, amount of CO₂ released during operation, sustainability of construction, and more (USGBC, n.d.).

LEED in cooperation with federal and local governments has incentivized building owners to take the first steps towards highly efficient building design. Since greener buildings incorporate newer technologies, more upscale materials, and higher soft costs, ultimately, reduced operational costs offer a 2-3 year return on the investment. This estimation includes benefits such as tax-credit equity and better terms for project financing (EPA, 2016). Various

non-profit organizations across the United States have grant programs open to provide financial assistance for LEED-certified buildings. On the local level, certain state governments have issued a set of incentives to help LEED become more accessible to building owners. They provide financial help and sometimes priority building permit acquisition (“LEED Certification Incentives in Other States” 2019).

Aside from LEED certification federal and local administrations attempt to speed up the adoption of green strategies by focusing on end-users’ needs. The climate change urge offered utility companies in the United States generous money rebates for on-site renewable energy generation, with the main focus on solar panels. In particular, Massachusetts alone has introduced numerous money rebates for active strategies that make homes and businesses more energy and carbon-efficient (Massachusetts Department of Energy Resources, n. d.). The database containing all the benefits can be found in a single software called Commonwealth Energy Tool for Savings (energyCENT) (Massachusetts Department of Energy Resources, n. d.).

This explanatory approach benefits the Federal Sustainability Plan immensely since northern regions need to adapt faster than, for example, California. In mild climates, passive strategies in buildings are more feasible and less costly to achieve, since the high solar gain and moderate winds can supply buildings with heat and natural ventilation throughout the year. In places like Boston, Massachusetts, natural ventilation strategies are limited, whereas, in Sacramento, California, natural ventilation can be used all year round (Fig. 9).

Another example of uprising energy saving strategies is harvesting solar to save on lighting loads. Solar light collectors are an effective way to reduce energy consumption in buildings by providing natural lighting and reducing the need for artificial lighting during daylight hours (Solar Impulse, n. d.). In terms of integration with building mechanical systems, solar light collectors can be easily integrated into a building's lighting system by connecting them to light fixtures or a centralized lighting control system.

Therefore, there is a need for new passive energy strategies and carbon-neutral construction materials. This paper proposes an innovative heating approach, using solar power in tandem with the new sustainable construction material with photothermal potential.

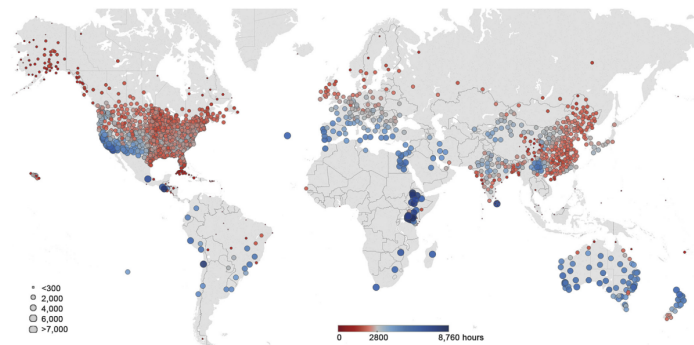


Figure 9. Geographic map of Natural Ventilation hours in 1854 locations.
Citation, (Chen et al., 2017).

2.3 ECM-n Summary

2.3.1 Introduction of New Building Material

The foundation of this project comes from the March 2022 scientific publication, “*A Self-Healing Enzymatic Construction Material*,” by authors Shuai Wang, Suzanne F. Scarlata, and Nima Rahbar. The publication presents a ground-breaking approach to creating self-healing carbon-negative construction material called Enzymatic Construction Material (ECM). This self-healing material is capable of repairing itself in response to damage by the absorption of carbon dioxide. The publication describes a material made of a polymeric network and an enzyme-based healing system, which when combined can regenerate the material. The structural integrity of the material is bolstered by the polymeric network. Meanwhile, the enzyme-based system works to catalyze and create a chemical reaction to bind any broken parts of the material back together (Wang et al., 2022). From this research, it was proven that the material can heal itself multiple times and can retain its mechanical properties even after repeated damage and repair cycles.

The research is significant given it presents a new solution to the problem of material degradation and damage in construction applications. Utilizing ECM could reduce the need for costly repairs and maintenance leading to significant economic and environmental benefits. Furthermore, the use of enzymes in the healing system is a promising environmentally-friendly alternative to traditional repair methods, which have previously relied upon toxic chemicals. This material, unlike its main competitor, self-healing concrete, has zero-carbon dioxide content and overall is a negative-emission construction material (Wang et al., 2022).

In September 2022, authors Shuai Wang, Suzanne F. Scarlata, and Nima Rahbar published a second paper, “*Curing and Self-Healing of Enzymatic Construction Materials Using Nanoparticles*,” which presents a modified approach to the creation of the self-healing enzymatic construction material. In this iteration, the addition of nanoparticles was implemented to the material making it an enzymatic construction material with nanoparticles (ECM-n). The nanoparticles, which are made of calcium carbonate, act as a curing agent by reacting with the polymeric network to increase its strength and stability. With the addition of nanoparticles, the material improved its strength and stability after curing with the nanoparticles, making it more resistant to damage. The components of the material are sand, gelatin, calcium carbonate, carbon dioxide, enzyme, and nanoparticles. The enzymes and carbon dioxide are used to drive the crystallization process which absorbs the carbon dioxide. The calcium crystal structures work with the nanoparticles and gelatin to give the sand the structure to combine to make a sufficient construction material (Wang et al., 2022).

2.3.1.1 Existing Zero-Carbon Construction Materials

Fungal-Based Construction Materials

One existing zero-carbon construction material is a fungal-based construction material that uses mycelium. Mycelium is the vegetative part of the fungus, consisting of a mass of

thread-like structures known as hyphae. This material has shown potential as a sustainable alternative to traditional construction materials due to its low environmental impact and ability to be grown quickly and efficiently (Saxton, 2020).

Mycelium can be grown in various shapes and forms. Mycelium-based materials are typically created by growing the mycelium on a substrate, which the mycelium consumes and the result is a strong, durable material that can be modeled into different shapes and sizes. Mycelium, like the ECM-n, has a low environmental impact. However, mycelium-based materials are biodegradable and even have a low carbon footprint, as they consume carbon dioxide during the growth process.

The mycelium-based material is still being developed so there are characteristics of the material that could be stronger to make this material a more desirable alternative to existing construction materials. The load-bearing capacity of the material is minimal (Jones et al., 2020). There are no self-healing capabilities of the material whereas other zero-carbon construction materials are capable of such. Furthermore, the long-term health effects of the material are unknown which is a concern for the longevity and safety of buildings constructed with the material (Bonnefin, n. d.).

Bacterial-Based Construction Materials

Another alternative construction material emerging is Living Building materials. Bacteria have long been used in construction, particularly in the production of concrete, since 2006 (Amran et al., 2022). However, the emerging building material out of the biotechnology realm is the creation of living building materials. These materials are created by genetically engineering bacteria to produce a variety of different substances, including cellulose and calcium carbonate (“Living Materials Laboratory / Wil v. Srubar III” n.d.).

Living building materials are created by growing bacteria in a controlled environment. The bacteria are genetically modified to produce different substances, including cellulose, which can be used to create a wide range of different building materials. The most significant advantage of living building materials is their adaptability. The bacteria can be programmed to respond to different environmental conditions. This allows the material to change and adapt to its surroundings making the material particularly well-suited to construction applications in extreme environments, such as deep sea or space.

The Living Building material is still being developed and the material is not yet entirely optimized for application in construction. The material has a mediocre compressive strength (Heveran et al., 2020). The capability for the material to be self-healing is not yet determined and similar to the fungal-based material, the long-term health effects of the material are not known. An additional concern is the foul odor associated with the material (“Building Materials Come Alive with Help from Bacteria” 2020).

2.3.2 Material Properties

2.3.2.1 Structural Strength and Self-healing

The self-healing enzymatic construction material (ECM) described in “*A Self-Healing Enzymatic Construction Material*” is composed of a polymeric network and an enzyme-based healing system. Specifically, the polymeric network is formed by a mixture of polyethylene glycol diacrylate (PEGDA) and a photoinitiator, which is then polymerized using ultraviolet (UV) light. The enzyme-based healing system consists of glucose oxidase (GOx) and catalase (CAT), which are encapsulated in separate liposomes and incorporated into the polymeric network. When the material is damaged, the liposomes containing the GOx and CAT are ruptured and then release enzymes into the damaged area. The GOx then catalyzes the oxidation of glucose, producing hydrogen peroxide. The CAT then catalyzes the decomposition of hydrogen peroxide into water and oxygen (Wang et al., 2022). The oxygen reacts with the photoinitiator in the surrounding polymeric network, triggering a polymerization reaction that binds the broken parts of the material back together. This healing process can be repeated multiple times, allowing the material to repair itself even after repeated damage.

The structural strength of the ECM-n was evaluated in the publication and can be compared to other alternatives including self-healing concrete. The authors of the ECM-n publication: Wang, Scarletta, and Rahbar, were able to demonstrate that the material had a compressive strength of 2.03 MPa, which is comparable to self-healing concrete. This value for the compressive strength, as well as Young’s modulus, is also more than twice that of the minimum acceptable for cement mortar and other alternative building materials. Furthermore, the ECM-n exhibited a significantly higher flexural strength compared to self-healing concrete. The ECM-n is also capable of retaining its mechanical properties even after repeated damage and repair cycles. Alternatively, the self-healing concrete showed a decrease in strength after multiple repair cycles. The ECM publication, “*Curing and Self-Healing of Enzymatic Construction Materials Using Nanoparticles*,” references back to the growth of mineral bridges that hold the sand particles in the ECM together; these bridges that provide the structure of the material have been modeled and studied by other researchers.

With the addition of nanoparticles, the new ECM-n retained all previously explained ECM characteristics. However, the Iron Oxide (III) nanoparticles act as a curing agent by reacting with the polymeric network to increase its strength and stability. The nanoparticles make the ECM receptive to light, adding more applications to the material. It was determined that modified ECM can be cured with a radiative heating method. In previous experiments, the research team used a laser to increase the material's incident surface temperature (Wang et al., 2022). The heat from the surface then dissipates and reinforces the crystal scaffold of the material.

It was determined that the material’s compressive strength fluctuates between 10 and 15 MPa, which is lower than that of traditional self-healing concrete (20 MPa) but still higher than any other carbon-negative structural material that exists today. Overall, these results suggest that

the self-healing enzymatic construction material could offer a promising alternative to traditional construction materials and lead to more sustainable and resilient infrastructure.

2.3.2.2 Photothermal Capabilities

Although the mechanical properties of the material were found and published in the literature, the photothermal properties are unknown. Thermal properties such as thermal conductivity are anticipated to be similar to those of concrete. One of the main differences between the materials is the presence of nanoparticles (Iron Oxide III) in ECM-n that convert any propagated electromagnetic radiation into heat. Iron Oxide (III) is widely used in photothermal therapies to treat tumors. During treatment, cells are illuminated with a laser at near-infrared range (NIR). The addition of nanoparticles to the cells increases energy-to-heat conversion, improving process efficacy (Estelrich, 2018).

To achieve similar results, iron oxide nanoparticles were added to the Enzymatic Construction Material. This modification increased the material's absorptivity and conversion rate for radiative heat. In turn, laser-aided curing was shown to work well with smaller samples. Photon Diode Laser 3W at 810 nm wavelength was used to cure ECM-n samples (Fig. 10). Another experiment was set up to investigate the curing process under tungsten light (Wang et al., 2022) and it took 12 hours for the same sample to fully cure. These results inspired further investigation into the optical properties of ECM-n that have not been studied before.

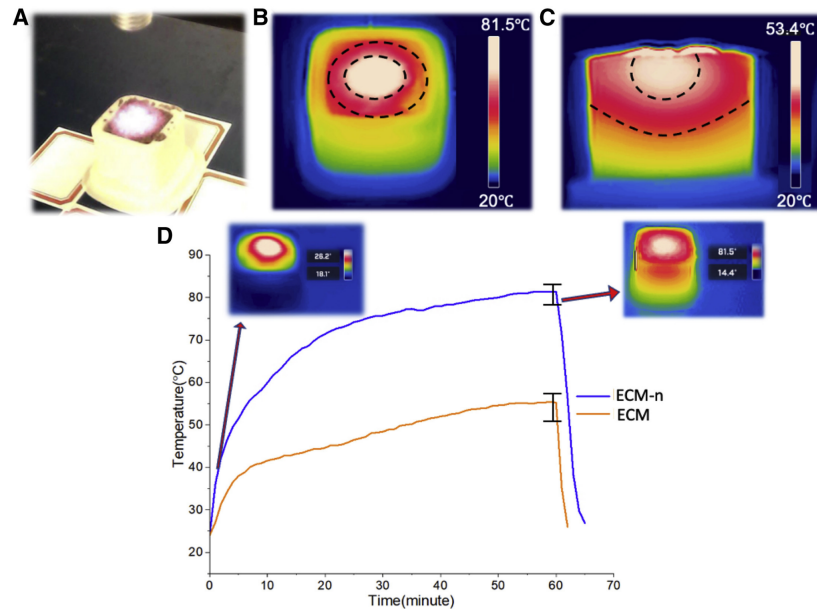


Figure 10. Laser-Induced Curing of ECM-n.
Citation, (Wang et al., 2022).

- (A) The picture of the experimental setup.
- (B) Top view of the temperature variation of ECM-n. The maximum temperature rises to 81.5°C at 60 min ($n = 5$, $med = 81.5$, $SD = 3$).
- (C) The side view of the temperature contours in ECM-n.

(D) The temperature as a function of curing time at the center of a 0.1% nanoparticle-modified ECM-n 12.5 mm cubic sample surface under 3W laser induction compared with ECM without nanoparticles. The data of ECM and ECM-n were taken from a median group of 5 independent samples ($n = 5$).

When considering absorbance and transmittance, optical properties, it is difficult to make an assumption for a similar material. The ECM-n is composed of a variety of components: sand, calcium carbonate, gelatin, and nanoparticles. Fortunately, there is absorbance data available for some of these elements alone. In fact, Iron Oxide (III) nanoparticles display peak absorption in the UV-VIS range at 295-301 nm (Wang et al., 2022). To optimize light-induced heating for the material, the selected light source can only emit wavelengths between 295-301 nm. This can be assumed if nanoparticles are homogeneously distributed throughout the sample.

Yet unknown photothermal properties can be explored to then use the ECM-n as a heating element. After the quantification of these photothermal properties, the design of the heating system can take place to produce the strongest proposed system dependent upon its specification.

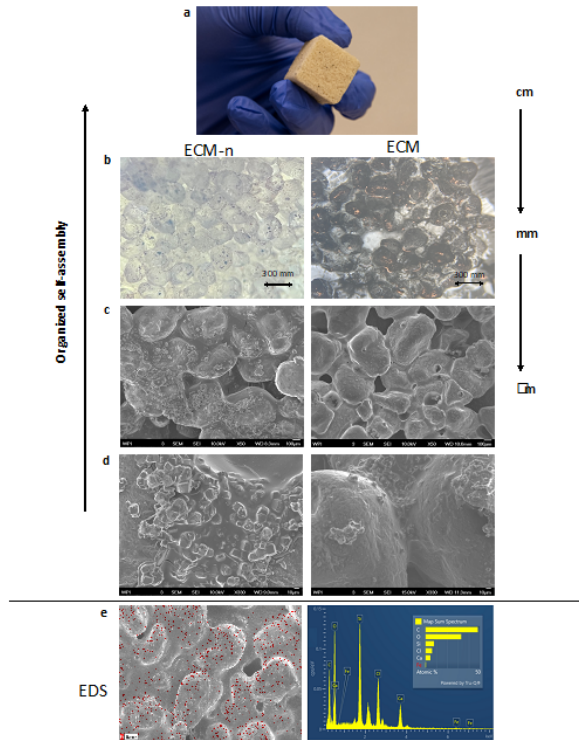


Figure 11. Comparison of Multiscale Microstructure and Mineralization. ECM-n (left) and ECM (right). Citation, (Wang et al., 2022).

2.3.3 ECM-n as a Heating Element

According to the ECM-n's unique properties, the material can be used in buildings for its strong mechanical and photothermal properties. ECM-n's unique set of properties singles it out from other emerging and existing construction materials. Based on the observed success of laser curing (Wang et al., 2022), it is proposed that ECM-n is used as a heating element in building

structures. The ECM-n would have the capacity to function as a large thermal mass similar to the thermal masses used in radiant systems as described in Section 2.1.1.2.

Thermal masses need a heat source before they are able to store and radiate absorbed heat over time. The heat source could come from a laser, as it is known that the laser is capable of curing the ECM-n. Alternatively, electric wires or hydronic piping could be used similarly to the existing radiant systems. A furnace could be used to warm the space and ‘charge’ the ECM-n with heat energy, which could slowly radiate into the space.

As proven in the Background Chapter 2.1, heating systems that promote better heat distribution provide more efficient and homogeneous conditioning of spaces. The technology of heat delivery systems has progressed since the first invention of stove furnaces, introducing new devices that promote air circulation. However, contemporary radiative systems have limitations for greater heat distribution due to the high costs of installation. The hypothesis is that greater distribution of many-point heat sources increases the efficiency of space heating. It also provides a more comfortable environment for occupants. The ECM-n can be used with smaller but many distributed heat sources ‘charging’ the mass with heat energy and radiating it across the heated surface.

2.4 Data Retrieval

2.4.1 Quantification of ECM-n Properties

To design and estimate the effectiveness of any engineering system, quantifications of material properties must be known. Previous research showed structural and self-healing characteristics of the ECM. All of those had been quantified and described in greater detail in earlier papers (Wang et al., 2022). However, the thermal and optical properties of the materials are yet unknown. This section highlights the preliminary information about instruments and machines which have been used throughout this research to identify ECM-n’s properties.

2.4.1.1 Thermal Properties - Instruments & Processes

Thermal Conductivity

The thermal conductivity of a building envelope material is an important property when considering the efficiency and design of a new heating system. Thermal conductivity is a fundamental material property that describes the ability of a material to conduct heat. It is defined as the rate at which heat flows through a material per unit time and per unit area, under a temperature gradient. Materials with high thermal conductivity conduct heat quickly, while those with low thermal conductivity conduct heat slowly.

Thermal conductivity can be quantified using various methods. One of the methods is the steady-state method, which involves measuring the temperature difference across a sample of known thickness and area, and by measuring heat flow through the sample using a heat source and a temperature sensor. After measuring the temperature difference and heat flow, the thermal conductivity can be calculated. Let dQ/dt be the rate of heat flow across the bar at A, the cross-sectional area of a material, as shown below. The temperature gradient is shown by the

blue arrow across the length of the bar. At distance x from the end of the bar, the temperature is T . At distance $x+\delta$, the temperature is $T+\delta T$, which represents the temperature gradient, dT/dx . To find the thermal conductivity, K , Equation 1 can be used (Tatum, 2017).

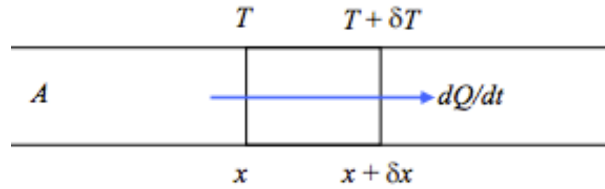


Figure 12. Temperature Gradient.

Heat flows through a material to show a temperature gradient, Citation, (Tatum, 2017).

$$\frac{dQ}{dt} = -KA \frac{dT}{dx} \quad \text{Eq. (2-1)}$$

Another method is the transient method, which involves measuring the time-dependent temperature response of a sample to a heat pulse. By analyzing the time-dependent temperature response, the thermal conductivity of the material can be determined through the transient plane source method, the transient line source method, or the laser flash method (Shah, 2019).

Several scientific instruments can be used to measure the thermal conductivity of a sample of a material. These scientific instruments include the thermal conductivity meter, hot-wire instrument, guarded heat flow meter, and transient plane source technique. A thermal conductivity meter measures the steady-state heat flow through a material. The hot-wire instrument measures the resistance of a heated wire in contact with the material. The guarded heat flow meter measures the heat flow through a sample under controlled environmental conditions. The transient plane source technique measures the time-dependent temperature response of a sample to a heat pulse.

Generally speaking, these instruments all work fairly similarly. By applying a temperature gradient across a sample of the material and measuring the resulting heat flow or temperature response; the produced data can be used to determine the thermal conductivity of the material. These methods and instruments are widely used in various fields, including materials science, engineering, and physics, to study the thermal properties of materials and to develop new materials with improved thermal properties (Coolmag, 2021).

A Guarded Longitudinal Comparative Calorimeter (GLCC) was selected as the instrument to quantify the thermal conductivity of the ECM-n material. This instrument utilizes the steady-state method described above. Further information about the testing can be found in Section 3.2.3.

Heat Capacity

Understanding and quantifying the heat capacity of a material allows you to understand a material's compatibility with other materials in a designed system. Heat capacity is a physical

property that describes the amount of heat required to raise the temperature of a material by a certain amount. It is defined as the amount of heat energy required to increase the temperature of a material by one degree Celsius or one Kelvin. Materials with high heat capacity require more heat energy to raise their temperature compared to materials with low heat capacity (Mettler Toledo, n. d.).

Heat capacity can be determined through various different methods. One common method is the differential scanning calorimetry (DSC) technique. DSC involves measuring the amount of heat absorbed or released by a sample as its temperature changes over time. By analyzing the temperature-dependent heat flow data, the heat capacity of the material can be determined (Mettler Toledo, n. d.). Alternatively, another method for defining a material's heat capacity is the adiabatic calorimetry technique (Fauske, 2018). This technique involves measuring the change in temperature of a sample as it undergoes a chemical or physical change in an insulated environment. By analyzing the temperature change data, the heat capacity of the material can be calculated.

There are several scientific instruments that can be used to carry out the techniques given above. To measure the heat capacity of a material, a DSC, adiabatic calorimeter, or heat flow meter can be used. The DSC measures the heat flow into or out of a sample as it is heated or cooled at a constant rate. The adiabatic calorimeter measures the heat change in a sample as it undergoes a chemical or physical change in an insulated environment. The heat flow meter measures the amount of heat flowing through a sample under controlled temperature conditions (Fauske, 2018).

Through the application of controlled heat to a sample or a material and by measuring the resulting temperature change or heat flow, the data from these processes can be used to calculate heat capacity. These methods and instruments are widely used in various fields, including materials science, engineering, and physics, to study the thermal properties of materials and to develop new materials with improved thermal properties.

A Differential Scanning Calorimeter was selected as the instrument to determine the heat capacity of the ECM-n material. This instrument utilizes the steady-state, differential scanning calorimetry (DSC) technique, described above. Further information about the testing can be found in Section 3.2.2.

2.4.1.2 Optical Absorbance - Instruments & Processes

The attempt of this paper is to show if the proposed mechanical system is capable of heating the space using ECM-n's photothermal features. Even though it is known that Iron Oxide (III) has its peak absorptivity in the region between 295 and 301 nm (Estelrich, 2018), the absorbance and other optical characteristics of the ECM-n material itself are unknown. Light absorptivity of the ECM-n is important, it shows the fraction of the total incident light the energy of which is converted to heat.

The light can simultaneously be absorbed, transmitted, and reflected by the surface of the material the light is projected on. By the equation of conservation of energy in optics, it is known

that the light that is incident to the surface of any material is trisected into reflected, transmitted, and absorbed light. Each material under different conditions makes the light take different fractions of those three types, the sum of which must always equal one.

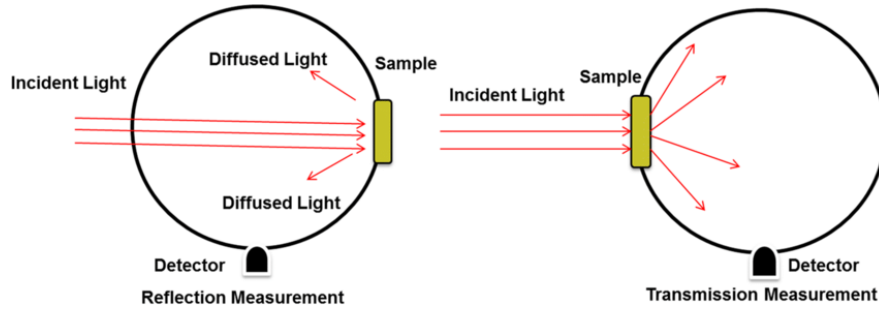


Figure 13. Experimental Setups to Measure Reflected and Transmitted Light. Reflected (left) and transmitted light (right) were measured using the integrating sphere method, Citation, (Hamdy et al., 2021).

One of the methods used to determine the reflectance and transmittance of the material is called the integrating sphere method. Shown above, Figure 13 depicts two ways in which the integrating sphere device can be used in the experiment. The instance on the left shows the method that captures the reflected portion of the light exposed onto the surface of a sample. Usually, if the sample is made of solid material, the device is placed on top of the sample to emit light. In the cavity of the sphere sensors are placed to record the amount of diffused light that was reflected off the sample's surface. Measurement of transmittance takes a similar approach, however, the sphere is now the receptor of the incident light that is transmitted through the sample.

Neither of the methods yields the absorbance data, but it can be computed using transmittance and reflectance. If the transmittance and the reflectance of the material are known, then the energy conservation equation can be used to calculate the absorbance. However, if there is no device available to determine reflectance, transmittance alone can show absorbance.

The value of transmittance is defined by the relation of total incident light intensity (I_0) to transmitted light intensity (I). When both of the values are equivalent to each other, then all light that was propagated to the surface is transmitted. With absorbance, however, the result is inversely proportional to transmittance and is shown:

$$A_\lambda = -\log_{10}(T) \quad \text{Eq. (2-2)}$$

2.4.2 Software

For this section, background information and an explanation for the use of the software will be given.

2.4.2.1 COMSOL

COMSOL is a software platform that is used to solve physics-based problems. It can be used to model the physical behavior of 2D or 3D objects. The objects are either imported from Computer-Aided Design (CAD) programs or built in place in the software itself. COMSOL is widely used as a computational tool by engineers, scientists, and professionals. For this project, COMSOL was used to quantify heat losses through the ECM-n walls of the modeled box-shaped space.

COMSOL provides a flexible workflow as it can couple multiple physics interfaces simultaneously, applying single input throughout interfaces. The aim of the model is to compute and show the amount of heat transferred from colder outside to warmer inside under certain conditions. If the outside temperature is set as fixed, the inside temperature is a result of a conductive heat transfer equation that then can be used as an input for convection and fluid flow physics interfaces. It streamlines the computational process making it more versatile.

All model inputs can be modified and even parameterized if needed. Heat transfer rate depends on the model input, which includes temperature difference, wall thickness, and room dimensions. For instance, with the room, making its dimensions parametric can save a lot of time modeling the same object of different scales.

Working with data in COMSOL is easy and straightforward. The results can be plotted in the software itself once the simulation is completed. There are numerous types of data visualization from dynamic 3D graphics to simple line graphs.

3.0 METHODOLOGY

This chapter presents a sequence of objectives that were identified as necessary to execute the project in full. Each following objective is based upon its predecessor and is stated in such a way as to provide a logical structure of the project timeline and phases.

3.1 Photothermal Heating System Design

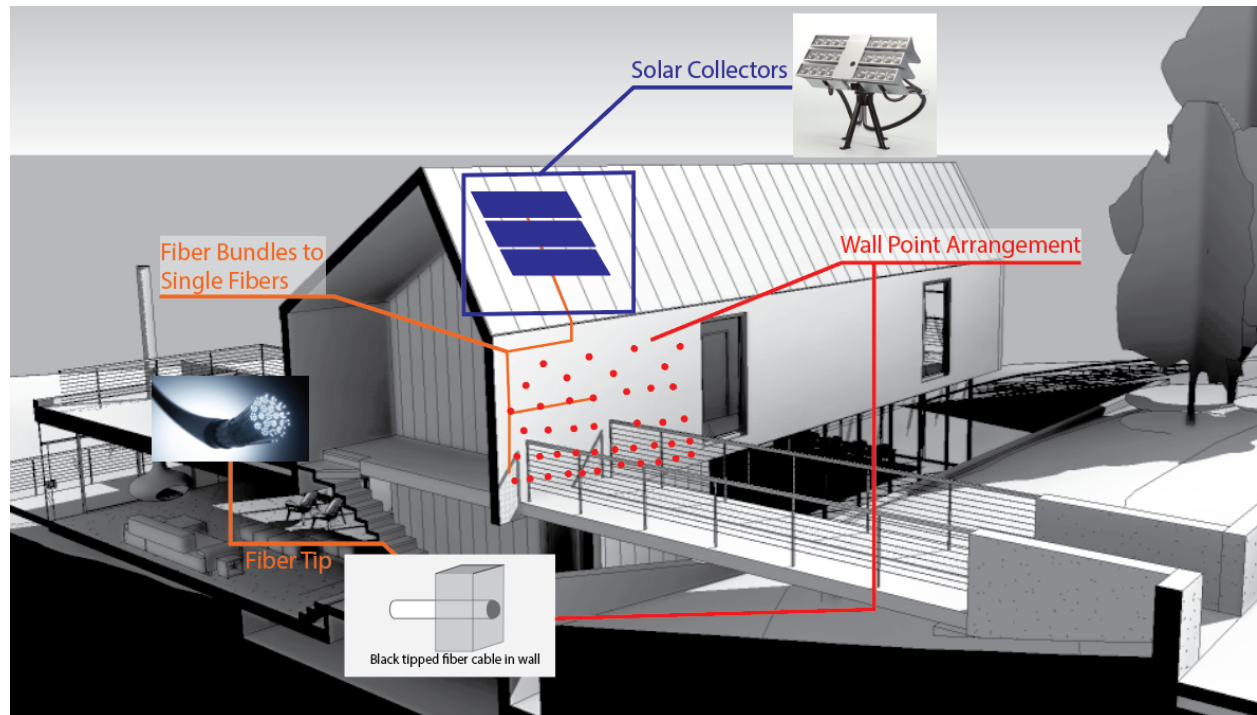


Figure 14. Passive Photothermal Heating System Design.

Citation, (“REVIT 2023” n.d.)

(“PARANS SYSTEM: SP4-12.2 SUNLIGHT COLLECTOR” n.d.)

(“Mechanism of Himawari Solar Lighting System” n.d.)

3.1.1 System Context

The goal of the project addressed the urgent need for zero-carbon emission building operations. As given above in Section 2.2, building heating systems are large contributors to carbon emissions. Although there are several alternative heating systems that rely on passive or clean energies, most of these solutions are not applicable to colder climates. The project’s proposed system aimed to be capable of year-round space heating, even in colder climates. Additionally, to compete with the existing varieties of heating systems on the market, the proposed system needed to be efficient in its conversion of solar power to heat.

Section 2.3.3, describes in detail the concept of heat delivery and how crucial it is for heat efficiency and occupant comfort. This photothermal heating system will use numerous point heat sources densely mapped across the length of the walls to foster an even distribution of heat. Positioning active heat points in the lower half of the wall will develop better air circulation.

3.1.2 System Composition

The proposed system utilized solar collectors, light-pipe fiber cables, ECM-n, and insulation to collect and convert solar energy into heat for a building enclosure. Solar collectors are a large initial investment but ultimately worthwhile as they supply the system with a free energy source. Having heat energy produced on-site makes the system more efficient as the heat loss in energy transfer from generation to consumption was reduced significantly. A network of fiber cables transports the light from the solar collectors to the wall composition. Like the solar collectors, the fiber cables are an expensive initial cost but ultimately worth the added expense. The wall composition includes a solid core of ECM-n with the fiber cables depositing the energy throughout the mass and two layers of Extruded Polystyrene Insulation (XPS) on each side of the ECM-n. A summary of the system components and energy transport through the system can be shown in the flowchart below:

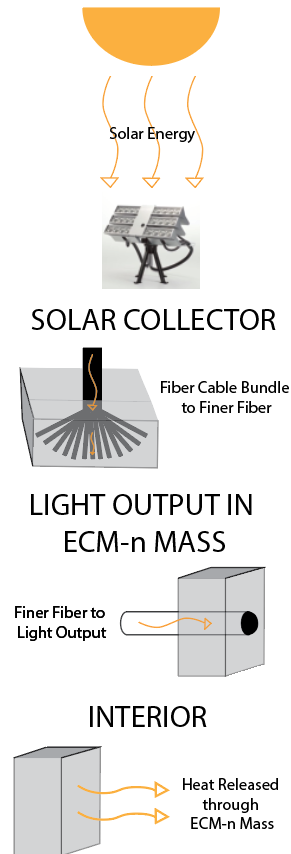


Figure 15. System Energy Flow Chart.

Citation, ("PARANS SYSTEM: SP4-12.2 SUNLIGHT COLLECTOR" n.d.).

3.1.3 System Overview

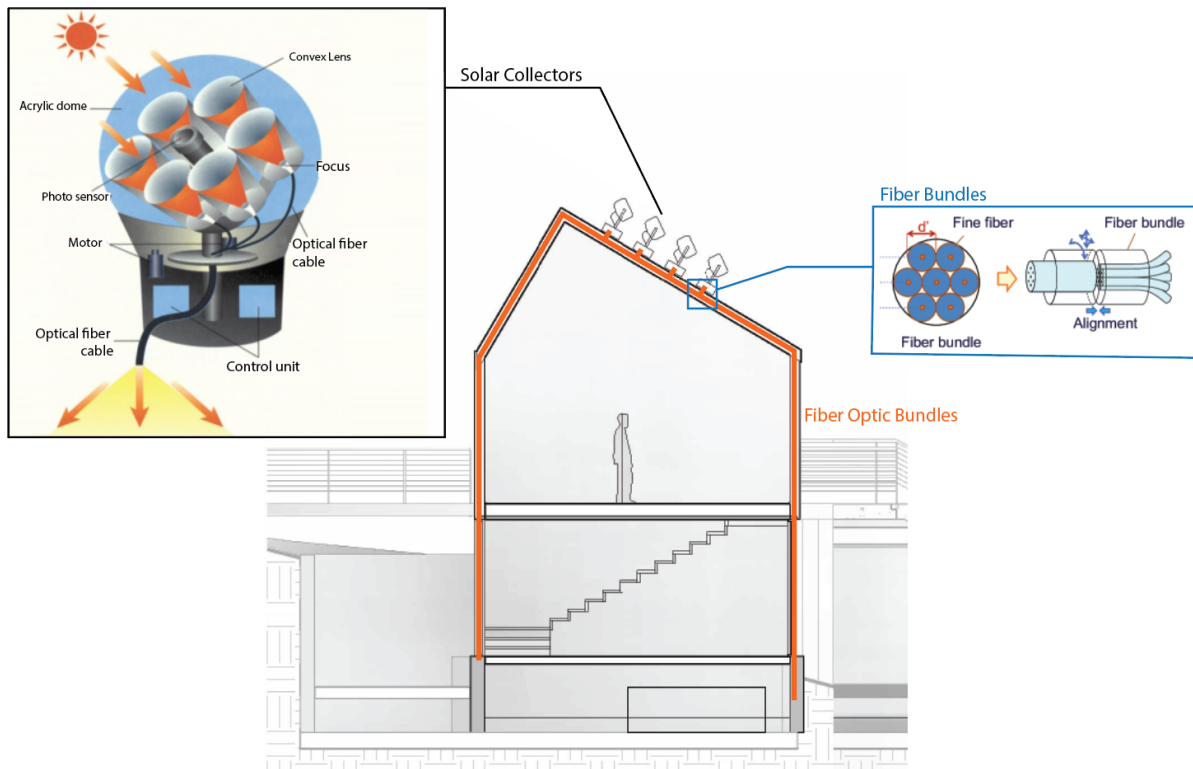


Figure 16. System Section with Solar Collectors.
Citations, (“Mechanism of Himawari Solar Lighting System” n.d.)
 (“Figure 2. Example of Fiber Bundle Type Optical FI/FO Device.” n.d.)
 (“REVIT 2023” n.d.).

A section view of a building given above shows a visual summary of the system with detailed callouts of the various components listed in Section 3.1.2. For the purposes of this preliminary design, the system was specified to meet the codes and be used in Boston, Massachusetts. The choice of a location that is subject to colder climate conditions was intentional so that the system could be optimized and proven to work in cold climates. As the report identifies, it is a currently untapped niche. The proposed functional and efficient system was designed to service cold climates through passive or low energy usages, specifically to meet the goals of the project.

The solar harvesting area required to heat modeled space is calculated in Section 3.5, and most small residential buildings can provide space on their roofs to serve that purpose. The fiber cables are small and the whole network of them can be cast in the ECM-n wall during the manufacturing process. From there, prefabricated panels of ECM-n can be then assembled into a structural frame and form a whole fiber cable network that is woven into the walls. Alike modular construction technology has proven to minimize on-site fabrication. Fiber cables are fragile and should be handled outside of busy construction sites.

Due to novel advancements in the building enclosure design, structural elements are frequently encapsulated in protective products to improve thermal insulation, waterproofing, and air tightness of buildings. A network of fiber cables provides even distribution of sunlight for the hidden ECM-n core of the building. The tips of light cables are arranged in a checkerboard pattern to ensure homogeneous heat distribution.

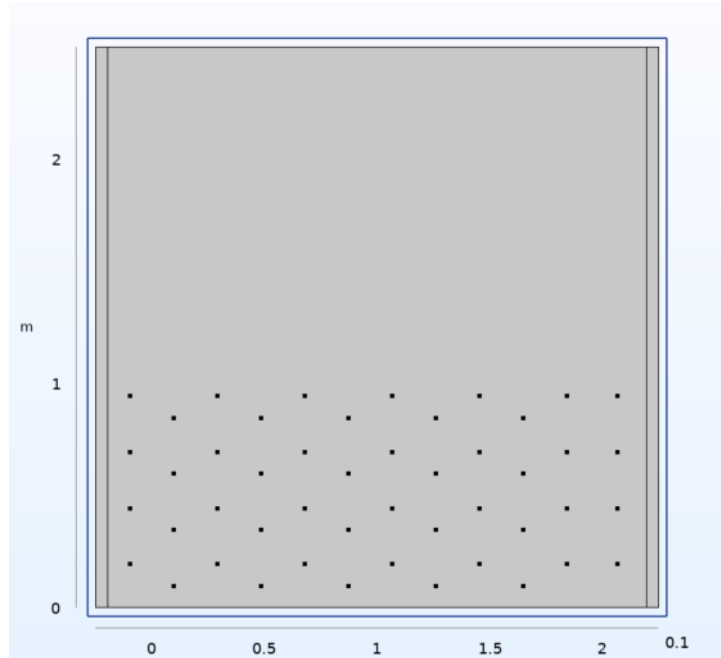


Figure 17. COMSOL Section Cut of ECM-n Wall Depicting Point Heat Source Distribution.

With the connections of the system's components outlined, the next step was to further develop the design to meet the project goal of energy efficiency. To do this, ECM-n's thermal and optical properties needed to be quantified. Energy simulation models allowed the design to be iteratively modified and tested to optimize energy distribution and component thicknesses. Once the system was designed to heat a building environment, an analysis of the energy source was performed to determine the number of solar collectors and specifications needed to support the proposed passive photothermal heating system.

3.2 Creation of ECM-n Sample

ECM-n is an innovative construction material that is composed of sand, calcium carbonate crystals, gelatin, and nanoparticles. In order to make the sample of the ECM-n material, all the components had to be combined following the procedure and then thermally cured to gain strength (Wang et al., 2022). The curing process is usually performed in a custom-designed mold so that the sample is the correct dimensions for the desired testing apparatus. Required dimensions vary between the testing apparatuses used and can be found in

the respective owner's manuals. Further information regarding the sample creation procedure can be found in Appendix B.

3.2.1 Mold Making

The longitudinal guarded calorimetry test using the AHP-1200CPV/ LHP-1200CPV Cold/Warm Plate instrument by ThermoElectric Cooling America Corporation (TECA) can be used with varying sample sizes. In the case of testing the thermal conductivity of materials, the sample's dimensions are dictated by an additional shell structure that is necessary to keep the sample and the meter bars in place (ASTM E1225-20). The lab the team used had one such shell made of rigid insulation which was built by the faculty members for another thermal conductivity experiment. The shell's cavity was designed to be compatible with a 2" x 2" x 2" sample cube.

Before curing the ECM-n sample, sand with nanoparticles had to be mixed with a liquid solution containing calcium carbonate crystals. The resulting "slurry" would then take the shape of the surrounding body it is in. Since the contained gelatin in the ECM-n mix makes it stick to the surfaces, the mold had to deform to release solid samples without breaking the sample's geometry. For such purposes, silicone is a common material to make reusable molds.

To make a silicone rubber mold, the silicone had to be cured in a disposable shell first. CAD software was used to model a plastic mold for the silicone to be poured into and set. A 3D printer produced the plastic shell. Once the shell was complete, the rubber silicone was prepared per the associated instructions. Once a viscous consistency was reached, the rubber silicone could then be poured into the 3D mold shell. Following that, the shell was placed on a vibration plate for 10 to 15 minutes to eliminate air bubbles. Then, the mold was able to be set for the duration listed in the instructions. Once the silicone rubber was fully set to the required duration, the shell was then removed. In some cases, the shell may need to be destroyed to remove the silicone mold intact. The cavity of the cured silicone mold was the intended and required a 2" x 2" x 2" cube desired for the experiential setup. This process was used for any other needed sample sizes.

3.2.2 ECM-n Mixing Procedure

An enzymatic solution was required to be prepared for the first step of the ECM-n sample creation procedure. To do this, 5 mg of enzymes, stored frozen, were combined with 2mL of reagent-grade water. The procedure required 10 microliters of enzymatic solution and the combination was pipetted into canisters each containing 10 microliters.

The following measurements of the procedure are dependent on the size of the sample being created. For a 2"x 2"x 2" sample, either 26g of calcium formate or 58.08g of calcium chloride should be used. The procedure requires the combination of the calcium compound with 410mL of reagent-grade water. Once this has been stirred together, 2.422g of Trizma Base, trace buffer, was added. The solution was then kept stirring for an additional 10 minutes. It is

recommended to use a stir plate and stir bar. The enzymatic solution was then added to the calcium chloride, water, and trace buffer solution.

Once completed, the solution from the above steps was placed under the hood. Under the hood, in that solution, a calibrated pH sensor probe with a tube connected to the carbon dioxide tank was added. From there carbon dioxide was added to the solution until the pH level dropped to 7. The beaker was covered and set in the hood for 6 hours until white calcium carbonate crystals formed. The excess water was drained, leaving the crystals in the bottom of the beaker.

For efficiency in timing purposes of the procedure, the team determined that the sand gelatin mixture should be started closer to the time at which the crystals are formed. The sand gelatin mixture required measuring 180g of sand out and 5.25g of gelatin. The sand and gelatin were then mixed thoroughly for about 5 minutes until there was no accumulation of gelatin particles at the bottom of the mixture. The sand-gelatin mixture was poured into the silicone mold. The nanoparticles were measured to be 0.1% of the sand weight. The crystal solution was combined with the nanoparticles and once combined, poured over the sand-gelatin mixture in the silicone mold without overflowing. It was then placed under a 3W laser to be cured. The ECM-n 2"x 2"x 2" block was cured on the exposed surface for 72 hours. The laser would heat the sample for 12-15 hours at each of the 5 points on the sample's surface. The points were distributed with the same layout as the five dots on a die's face.

3.2.3 Procedure Modifications

3.2.3.1 Alternative to Laser Curing

The laser curing method with a 3W laser had worked for smaller samples in previous research (Wang et al., 2022). An attempt to cure bigger-size samples with the same method did not show similar success. To make laser curing able to cure the sample homogeneously, the process was modified to have 5 points of incidence on the surface instead of just one. Each point was exposed to radiation for 12-15 hours. Although the modifications intended to increase the chances of sample curing, the power of the given 3W laser was not enough to let the heat dissipate effectively through the whole sample. At the end of the total curing time, the sample showed only 1 inch of top cover cured (Figure 18).



Figure 18. Partially Cured 2" Cube ECM-n Sample Flipped Upside Down.

Therefore, a procedure with a 2"x 2"x 2" sample was modified to use an oven instead of lasers to cure the sample, as tested previously with ECM samples (Wang et al., 2022). The oven was set to 90-100°C, and the sample cube was kept in the oven for a minimum of 24 hours.

3.2.3.2 Slurry Modification

Another challenge in the sample creation process was the nonuniform distribution of nanoparticles throughout the sample. To combat this, CaCO₃ crystals, gelatin, and nanoparticles were mixed together before going into the mold to form a slurry. In this modification, the crystalline suspension in water was preheated to 40°C and the corresponding amount of gelatin was added. Once the gelatin melted down under the increased temperature, it would become a viscous liquid. Following that, 0.18g of nanoparticles (0.1% by sand weight) was added. From then on, only glass stirring rods could be used, because metal stir bars would attract nanoparticles. Once well mixed, sand was added to the beaker in small increments and mixed for 5 minutes, while still keeping the beaker's temperature above the melting point of gelatin - around 32 degrees Celsius. Then, the slurry was poured from the beaker into the mold.

3.2.3.3 Slurry with Surfactant Modification

A surfactant in the ECM-n sample creation was used to provide a more homogeneous distribution of nanoparticles within the slurry mixture. To modify the slurry procedure given above, perform the steps same up to the calcium crystals. While the suspended calcium carbonate crystals precipitated in the solution, the surfactant mixture was prepared. To do this, a bigger beaker was picked and 10 ml of reagent-grade water (RGW) was added to it. Then, in the hood, 1.65g of oleic acid and 0.18g of nanoparticles (0.1% by sand weight) were added. Before going to the sonic bath, the beaker had to be sealed at the top. While the surfactant beaker was in the sonic bath, the oven was set to 60°C. Once the 30 minutes in the sonic bath were finished, the beaker was placed in the oven for 24 hours.

After 24 hours of the surfactant and nanoparticles sitting in the oven, an additional 10 ml of acetone was added to let the nanoparticles separate. Then, 10 ml of toluene acid was added to the suspension and placed in a sonic bath for another 30 minutes. For a homogeneous distribution of gelatin in the mix, the crystal suspension was preheated to 40°C and the corresponding amount of gelatin was added. Once the gelatin has melted, the stir bar was removed and the surfactant suspension with nanoparticles was added to the crystalline mixture. From this point on, only glass stirring rods could be used.

Once everything was well mixed, the sand in small increments were added to the beaker and mixed for 5 minutes holding the beaker in the oven at 40 degrees Celsius. The well-mixed slurry was poured out of the beaker into the mold and put in the oven at 100 degrees Celsius. Note that this time a ventilated oven must be used due to the presence of hazardous acids in the mixture. The mold was left undisturbed for a minimum of 30 hours until fully cured.

3.3 ECM-n Properties - Tests and Experiments

The thermal properties of the ECM-n were not quantified which was necessary for the design development of the system. The project aimed to quantify the thermal conductivity, heat capacity, and light absorbance of ECM-n. With data specific to this material, the thermal properties would then be inputted into a software model of the system and used to optimize the system. To quantify the heat capacity, the team used a differential scanning calorimeter. A guarded longitudinal comparative calorimeter, known as a cold plate, was used to determine thermal conductivity. Two different spectrometers, IR range, and UV-VIS range, were used to find the material's absorbance.

3.3.1 Thermogravimetric Analyzer (TGA)

To use the differential scanning calorimeter, the thermal stability of the material had to be deemed safe. The TGA measures a material's stability and fraction of volatile components by monitoring the weight change that occurs as a sample is heated at a constant rate. For the purposes of the planned experimental range for the DSC, the sample was heated from 100°C to 250°C. The DSC will only reach 110°C but to ensure the safety of the equipment the TGA tested an additional 100°C as a precaution.

To conduct this experiment the sample was prepared in a crucible. The crucible could only be handled with tweezers. The crucible was then burned out over a Bunsen burner for a few seconds until it glowed. The crucible then cooled for one minute before its mass was recorded. After the mass was recorded, 10 mg of the sample was added to the crucible. The combined crucible and sample mass was then recorded and the sample mass was deduced.

Once the sample was ready, the NETZSCH-PROTEUS-70 software had to be synched to the TGA instrument. Next, the verification that the chiller was running and displaying a temperature of 30°C or below had to be checked. The settings given in Appendix C were applied for the method settings. For data acquisition, the safety button, on the right side of the instrument, and the open button on the furnace cover had to both be pressed and held until the furnace was fully opened. This could be checked by the light remaining lit rather than blinking. Using tweezers, the crucible, holding the sample, was loaded into the ceramic trident-shaped stand. It is essential that the crucible is precisely centered on the trident. Once loaded, the same buttons had to be pressed and held until the lid was fully closed and the light was on and not blinking.

The data measurement was run by using the data acquisition steps in Appendix C. Once the measurement settings had been entered, in the view signals window, the user had to monitor the TG value until it was stabilized and then selected 'Tare' and then 'Start.' The measurement would then run and the data would become available. To stop collecting data, the 'Stop' button, which is displayed as a red square, could be selected. The data analysis was done using compatible software and the specific settings are given in Appendix C. All data from the NETZSCH-PROTEUS-70 software were saved and exported as a print result, raw data export, or exported as a graphic.

3.3.2 Differential Scanning Calorimeter (DSC)

The differential scanning calorimeter used was a heat flux DSC. A heat flux DSC measures the difference in heat flux, the change in temperature as a function of time, between the sample and a reference. The DSC is primarily used for the quantitative characterization of diverse solids. To run this testing safely, a TGA confirming a material was stable when heated at a steady rate had to be performed before the DSC testing. The specific model used was the Netzsch 214 Polyma DSC (differential scanning calorimeter). This specific model has a range of -40°C to 600°C.

For this experiment, the same sample used in the TGA test was reused immediately following the TGA testing. Given that the sample was already prepared, the next step was to set up the NETZSCH-PROTEUS-70 Software synched to the DSC instrument. The settings given in Appendix D were applied for the method settings.

To collect the data, the outer cell lid had to be removed, in this case, one's fingers could be used. The interior cell lid had to be removed with tweezers. The tweezers were then used to load the reference, left position, and the sample, right position. Each had to be precisely centered on the heat flux sensors. Once completed, both lids were returned to place on the loaded machine. The data measurement was run by using the data acquisition steps in Appendix D. Once the measurement settings were entered, in the view signals window, the tests were initiated by selecting, 'Start.' The measurement ran and the data became available. To end the data collection process, the stop button, displayed as a red square, could have been selected. The data analysis was done using compatible software and the specific settings are given in Appendix D. All data from the NETZSCH-PROTEUS-70 Analysis software was saved and exported as a print result, raw data export, or exported as a graphic.

3.3.3 Guarded Longitudinal Comparative Calorimetry (GLCC)

A Guarded Longitudinal Comparative Calorimeter (GLCC) is used to determine the specimen thermal properties per ASTM standard methods D5470-06 and E1225-09. The GLCC setup consists of a cold plate machine, thermal insulation shell, thermocouples, two standard meter bars (Pyroceram 9606), and a thermal gap filler of known thermal conductivity (Fig. 19). The specifications of the GLCC setup are explained in detail (Y. Farnam et al, 2014).

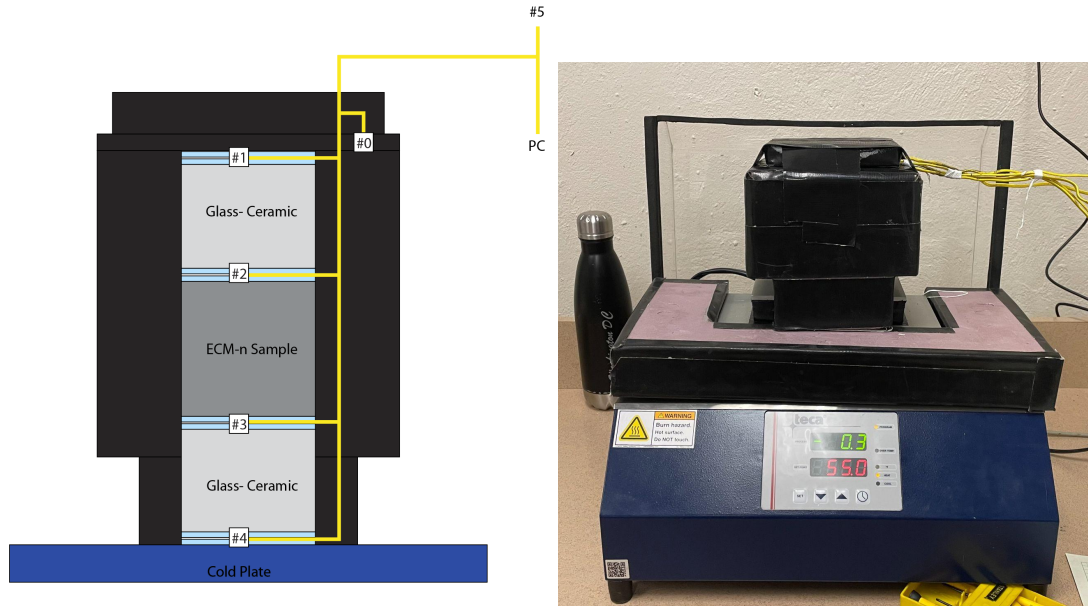


Figure 19. Guarded Longitudinal Comparative Calorimeter Experimental Assembly Section.

Section cut depicting meter bar/sample/meter bar stack, insulation, and thermocouples.

Figure 20. Guarded Longitudinal Comparative Calorimeter Laboratory Setup.

The full assembly of the experimental setup is shown in Figures 19 and 20. The shell is made of XPS insulation and has a rectangular shape (Fig. 19). It is hollow inside to house two meter bars and a sample specimen of length and width no greater than 2 inches. Only one layer of extra XPS is duct taped at the top to reduce heat loss through occurred openings. As it is discussed in Section 3.2.1, the prepared 2 by 2 by 2-inch mold was designed to make an ECM-n specimen to fit into the shell for this experiment. During preparations, the depth of the specimen was decreased with sandpaper from 51mm to 38mm to keep all elements within the shell's walls.

On one of the inner sides of the shell, there is a narrow trench carved out to have extra space for thermocouples. It is not likely for thermocouples to be in direct contact with the sample material or the meter bars (Sharifi et al., 2015). Therefore, to promote a more even distribution of heat at the surface between the sample and the meter bars, a thermal gap filler product from Saint-Gobain (ThermaCool® Silicone Gap Filler, TC3008) is used. Its thermal conductivity is 3.0 W/m-K, and its thickness is 3mm (Saint Gobain, n. d.). Saint-Gobain TC3008 product provides cushion for thermocouples and precision to the temperature measurements. To address that, the tips of thermocouples were sandwiched between two pieces of thermal gap filler (Fig. 19).

To calculate the thermal conductivity of the material, its heat flux at a certain temperature gradient must be known. To provide more accurate thermal conductivity values throughout a temperature range from 55 to -25°C, the GLCC machine was programmed to decrease the temperature of the plate, reaching the bottom threshold, and then increase it to an initial temperature of 55°C. The single experiment took 56 hours to execute. Meanwhile, thermocouples were recording the temperature of the whole system.

Collected temperatures from the experiment were used to compute the thermal conductivity of the ECM-n. Since the specimen has too many unknowns, the first step this method suggests is finding the heat flux of the material with known conductivity. The starting point for calculations is heat flux equations for Pyroceram blocks:

$$q_{standard} = \lambda_{standard} \cdot \frac{T_{top\ of\ standard} - T_{bottom\ of\ standard}}{depth_{standard}} \quad \text{Eq. (3-1)}$$

in which $q_{standard}$ is heat flux (W/m²), λ is the thermal conductivity of Pyroceram 9606 (W/m*K), T is the temperature in degrees Kelvin, and depth is measured in meters. The thermal conductivity of Pyroceram 9606 was calculated using the following equation (Flynn et al., 2021):

$$\lambda_{standard} = -0.0061(T) + 4.2013 \quad \text{Eq. (3-2)}$$

Where $\lambda_{standard}$ is thermal conductivity (W/m K) and T is the temperature (°C) of Pyroceram 9606. Since there are no tools available to measure the overall temperature of meter bars for T value in Eq. 3-2, the median function of two temperature readings on opposite sides of the blocks is taken. The average unit heat flow and total heat flow through the specimen were calculated with:

$$q_{specimen} = \frac{q_{Top\ Standard} + q_{Bottom\ Standard}}{2} \quad \text{Eq. (3-3)}$$

Knowing the depth of the ECM-n specimen and temperature gradient at both of its sides, the thermal conductivity of the material can be therefore calculated:

$$\lambda_{specimen} = q_{specimen} \cdot \frac{depth_{specimen}}{T_{Top\ of\ specimen} - T_{Bottom\ of\ specimen}} \quad \text{Eq. (3-4)}$$

A broader overview of the methods stated above is available in Appendix E. This appendix is intended to serve as a conceptual experiment design basis. There is also material that helped the team initially familiarize themselves with the software interface.

3.3.4 Spectrometry Tests

This section is about the experiments that were set up to measure ECM-n's optical characteristics. The goal is to find all fractions of irradiation (absorptivity, transmissivity, reflectivity) using different methods and devices.

3.3.3.1 UV-VIS Range

UV-VIS is the abbreviation that stands for ultraviolet to visible spectra in optics. The range is defined at wavelengths of 100-400 nm for ultraviolet and 400-800 nm for visible. For ECM-n, the main goal is to identify the absorbance at visible to infrared light range, since the heating of the material is likely to be done using solar power. In order to get the amount of light absorbed from the optical energy conservation equation, it is necessary to find the other two unknowns - reflectance and transmittance.

The experimental setup for reflectance measurement on the UV-VIS range breaks down into four main components. The first component is the Ocean Insight Integrating Sphere 50mm (ISP-50-8-R-GT) (“ISP-50-8-R-GT | Integrating Sphere | Ocean Insight” n.d.). This spectrometer sits on top of the sample and uses an integrating sphere method to capture light reflected off of the exposed surface. More on this method can be found in Section 2.4.1.2. The second component of the system, Ocean Insight DH-2000_BAL external UV-VIS-NIR light source, connects to the integrating sphere with fiber cables to supply the spectrometer with UV-VIS light (“DH-2000-BAL Light Source | Ocean Insight” n.d.). The third device detects all reflected light in the integrating sphere at its output. It is called Ocean Insight OceanHDX miniature spectrometer (“Ocean HDX Spectrometer | High Sensitivity | Ocean Insight” n.d.). It receives the analog signal in the form of light and converts it to digital using a 16-bit encoder. Lastly, OceanHDX sends its digital signal to the computer to record the data.

Before beginning the experiment, the device should be calibrated using reference material provided by the manufacturer. Another recommendation that decreases the amount of unrelated noise suggests identifying the frequency of the interior lightning in the lab where the setup is located. After running the experiment, the wavelength of artificial lighting in the room informs where to pay more attention when analyzing data. Some of the external lighting might get to the internal detector of the device and alter the reflectance data of the investigated material. The best practice, however, is to minimize any lighting that is outside of the experimental setup to exclude any errors.

After the device is calibrated, it is placed onto the surface of the ECM-n sample. The spectrometer is left undisturbed until data collection is finished. Once the device performs all scans, the test is repeated with the remaining surfaces.



*Figure 21. Zoomed Experimental Setup for Measuring Reflectivity of the ECM-n Sample.
Close up of ECM-n sample with UV-VIS Range experimental set up.*

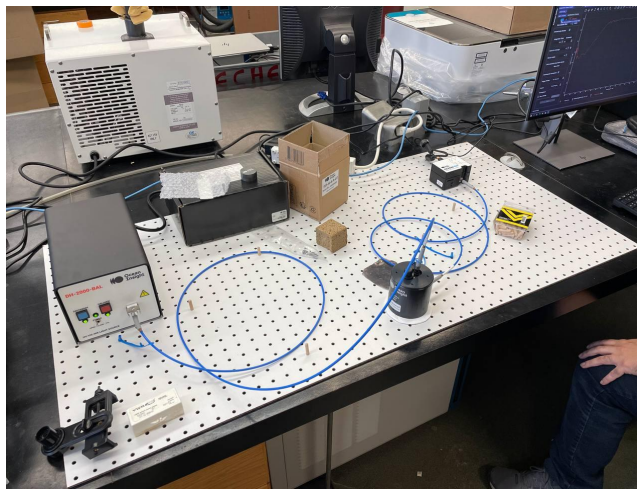


*Figure 22. Full Scope Experimental Setup for Measuring Reflectivity of the ECM-n Sample.
Full depiction of UV-VIS Range experiment components.*

3.3.3.2 IR Range

IR is short for infrared light. Electromagnetic radiation in the range is characterized by longer wavelengths than those of visible light. This means that IR can travel further through denser mediums (“Infrared Waves | Science Mission Directorate” n.d.). Methods for quantifying IR transmittance of some solids, including ECM-n, do not require the dissolution of the material prior to measurements, as opposed to the required procedures for UV-VIS measurements. Infrared light can travel through some thickness of porous solid material to produce results, though with higher material thickness less light will be transmitted. This section contains a description of both the reflectance and transmittance data collection procedures of ECM-n. The reflectance of the ECM-n was tested in the so-called mid-infrared range from 2.5 to 25 micrometers, whereas the absorbance data was collected only within 4 and 10 micrometers. The first conducted experiment was decided based on the availability of the machines on the WPI campus. Perkins&Elmer Spectrum One FT-IR Spectrometer device was provided by the

Department of Chemical Engineering of WPI to measure the transmittance of ECM-n material (“Spectrum™ One FT-IR Spectrometer: Experience the Quality of Spectrum™ One - Best in Class” n.d.).

The methodology of measuring the reflectance at the infrared range does not differentiate from the one described in the preceding section with the UV-VIS experiment, with only one exception. The light source shown in the left part of Figure 22 cannot produce waves with lengths higher than 2,500 nanometers. Herefore, a light source producing wavelength in the mid-infrared range is used to measure IR reflectance, but all other components and procedures are kept the same.

When measuring the reflectance of any material, especially if it produces diffuse reflection due to the higher roughness at the incident surface, the concept of total internal reflection has to be considered. At longer wavelengths, the internally reflected portion of incident light goes deeper into the solid sample, resulting in higher absorbance rates. It creates distortion and adds noise to the collected data (Khoshhesab, 2012).

3.4 Energy Simulation

Energy modeling is an essential tool used to predict the energy performance of a building or system. Both software-based and manual hand calculations were used in the project's analysis of the proposed system. Energy simulation tools allow designers and engineers to understand how energy is used within a building and identify opportunities for energy efficiency improvements and adjustments to ultimately optimize energy usage. By allowing for iterative design options, energy simulation can help to identify the most cost-effective energy efficiency measures and provide critical information for system development. Manual hand calculations are often used in tandem to validate results produced by the energy modeling software, ensuring the accuracy and reliability of the data.

3.4.1 Hand Calculations

Manually conducting hand calculations was essential to validate the data produced by the energy modeling software, COMSOL. Past the scope of the COMSOL modeling, the hand calculations provided an estimate as to how much energy was needed to supply the minimum amount of energy required to sustain a comfortable interior temperature. This was accomplished by considering the total heat loss of the room combined with the heat output of individual point heat sources. These two properties in addition to the COMSOL data were used to confirm the energy required to sustain a comfortable interior temperature.

To confirm the model's results, the team performed independent calculations by hand using the same parameters as COMSOL. To set up these calculations each material in the system and their control surface were accounted for. The properties of the enclosure are given below in a simplified table:

Table 3: Hand Calculation Known Property Summary Table

	Inside Air	Air Film	XPS	ECM-n	XPS	Air Film	Outside Air
Initial Temp (°C)	26°C	-				-	0°C
Thickness (m)	-	0.006	0.091	0.194	0.091	0.006	-
RSI per 25mm (m ² *°C/W) OR Thermal Conductivity (W/(m*K))			1 m ² *°C/W	2.25 W/(m*K)	1 m ² *°C/W		
RSI (m ² *°C/W)		0.00074	3.64000	0.08622	3.64000	0.00021	

The temperatures featured above in Table X, were specified to represent a harsh winter condition, as is common in the Boston, MA climate. The Extruded Polystyrene Insulation (XPS) thermal properties and available thicknesses came from the Dupont Product manufacturer specification sheet, more information about the selected XPS material can be found in Appendix F. The air film RSI Values are from the ASHRAE Standard. The ECM-n thickness was adjusted throughout the design process to get the desired RSI. The ECM-n thermal conductivity value came from the results of Section 4.1.1. The modeled enclosed building environment is designed to a total model exterior surface of 23.880 sq meters. The U-Value equation includes a conversion to SI units with a factor of 5.678 so that the calculated R and U-values could be easily compared to the specified code requirements.

The hand calculations used the following formulas to get the desired properties of the system:

U-Value (SI):

$$U = \frac{1}{RSI_{Total} \times 5.678} = \frac{1}{R} \quad \text{Eq. (3-5)}$$

Heat Flux:

$$q = -k \times \frac{(\Delta T)}{d} = \frac{-(\Delta T)}{RSI} = -\Delta T \times U = (W/m^2) \quad \text{Eq. (3-6)}$$

Heat Loss:

$$Q = q \times A_{surface} = (W) \quad \text{Eq. (3-7)}$$

Minimum Required Power for each Point Heat Source:

$$\frac{Q}{88 \times 2} = (W) \quad \text{Eq. (3-8)}$$

3.4.2 COMSOL

This section covers energy modeling procedures to identify performance of the ECM-n as a heated structural element in the typical building envelope system. Computational Fluid

Dynamics (CFD) modeling was necessary to simulate energy loads and heat flows in the proposed 3-dimensional space. The CFD model was built and analyzed in COMSOL software (“COMSOL Multiphysics® Modeling Software” 2019). These results were translated to maximize the efficiency of the engineered radiative heating system using ECM-n.

3.4.2.1 General

COMSOL is a software platform that is used to solve physics-based problems. It generates 2D or 3D objects which are either imported from Computer-Aided Design (CAD) programs or built in place in the software itself. COMSOL is widely used as a computational tool by engineers, scientists, and professionals. For this project, COMSOL was used to quantify heat losses of the square room with a comfortable temperature inside and the winter-cold temperature outside.

Heat flux, by definition, is the amount of heat flowing in or out of the material per unit area. Heat always travels from hot to cold. In other words, heat travels from the points of high kinetic molecular energy to where that energy is lower. When calculating the rate of heat loss through the wall, the very critical parameter becomes the temperature difference between both sides of this wall. It is directly proportional to the heat flux (Φ_q) in the following equation:

$$\Phi_q = -k \frac{dT(x)}{dx} \quad \text{Eq. (3-9)}$$

The initial values for the outside and inside temperatures in the model are based on the average temperature difference over the cold seasons in the Boston, Massachusetts location. The climate data was sourced from the meteorological database by location. It is usually encapsulated in special file formats, such as EPW (EnergyPlus Weather Data). It was analyzed with Climate Consultant 6.0 for average air temperatures and solar heat gain, which is also used to compare calculations of seasonal solar power intensity over the direct normal and will be discussed later in this paper.

Along with temperature difference, other important variables in the equation are the thickness and thermal conductivity of the media that facilitates conductive heat transfer. In this model, only 3 types of materials were used. The list includes Extruded Polystyrene Insulation (XPS), Air, and ECM-n. Characteristics of the first 2 materials were imported from COMSOL internal library. For the latter, however, the thermal conductivity, heat capacity, and density values were typed in manually because the ECM-n has not been widely researched yet. Results of the experiments conducted with ECM-n showed its thermal conductivity and heat capacity, which are used in this COMSOL model for precise simulation results.

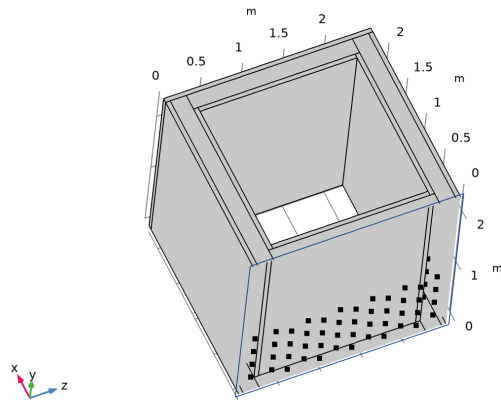
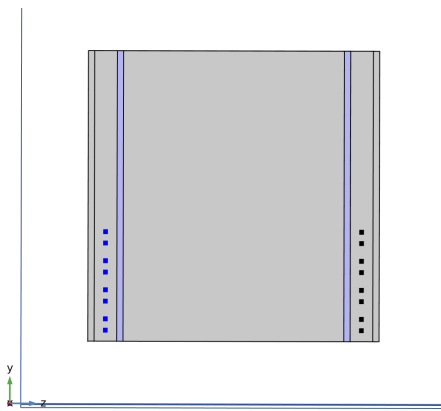


Figure 23. Section Cut View of the COMSOL Model.

Figure 24. Isometric View of the COMSOL Model.

Each view shows the arrangement of point heat sources from different angles.

The geometry of the proposed space is a simple rectangular-shaped box with 4 walls (Figure 24). This shape represents a simplified version of a typical one-story building. Even though the model does not have a roof or a floor, the main purpose of it is to show the efficacy of heat loss compensation. The model runs the simulation only with sidewalls and the interior air. Each wall has an ECM-n structural core that is wrapped in XPS insulation from both sides. The model omits the elements of the building enclosure which do not contribute to the heating of the air inside, so the calculations are performed within the boundary of the walls.

According to the concept of the proposed system, fiber cables pass solar light from the solar collectors to the ECM-n wall. The end tips of fiber cables specify heating points, where the light gets delivered and absorbed by the ECM-n. It is accompanied by the release of heat energy that benefits the heating of the interior space. The current model does not operate a laser heating module. Instead, points of radiance are simplified to point heat sources with fixed spherical diameters. This simplification accounts for less precise but faster execution.

3.4.2.2 Inputs and Outputs

Heating system proposal revolves around maximizing the efficiency of heat delivery and occupational comfort. It is achieved by providing 176-point heat sources which are evenly distributed in the thickness of the ECM-n wall. Points are laid out on a single plane so that each wall has its own distribution plane for these points that is parallel to the surface plane of that wall. To promote the flow of heat towards the inside, the distribution planes are not centered but moved towards the interior by a third of the ECM-n thickness. Each side has 11 columns with 4 points comprising each column. Every following column is also vertically shifted up or down from the preceding one. This geometry feature is added to set point heat sources equally apart from each other. It helps the wall to release heat more homogeneously throughout the surface.

Assuming a steady-state process of compensating for heat loss and sustaining a comfortable temperature inside, the power output for each point heat source must be evaluated prior to the simulation. In order to estimate it, a spreadsheet with R-values (RSI for SI units) and heat flux equations was created. It streamlined the simulation process as well as saved time to learn all parametric advancements of COMSOL software. More details are laid out in the precedent Section 3.4.1.

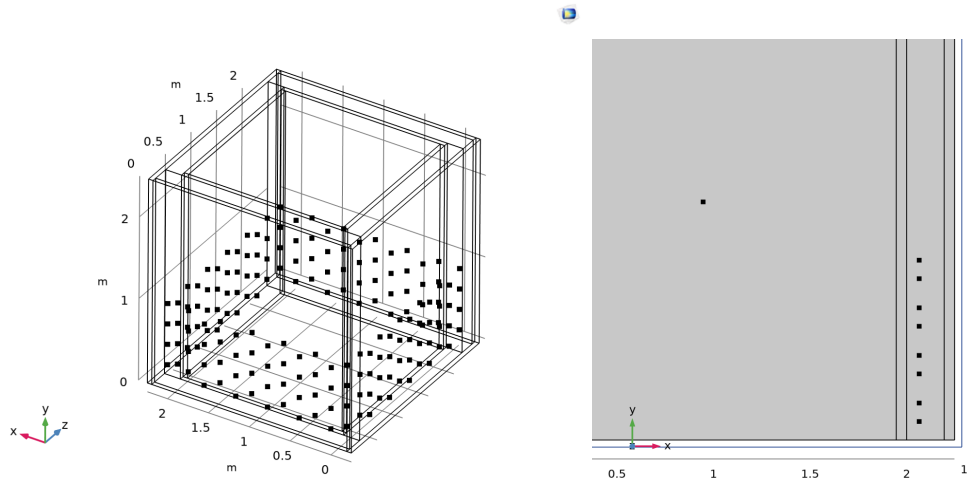


*Figure 25. Isometric Wireframe View.
The layout of 176 point heat sources is shown.*
*Figure 26. Cross Section of Building Envelope Composition.
The thickness of the composition and point heat sources are shown.*

4.0 RESULTS AND ANALYSIS

This chapter of the report will deliver the findings of the research conducted on ECM-n properties – both thermal and optical – as well as provide a detailed analysis of the experimental data, and the results obtained from an energy simulation model. The simulation was run using steady-state conditions, with various parameters and dependencies taken into account. Hand calculations were also carried out to show minimum power input to compensate for heat loss. Furthermore, this chapter delves into the design of a passive photothermal heating system. The proposed design, system overview, system efficiencies, and the building envelope are discussed in detail. Overall, this chapter provides a comprehensive understanding of the research conducted, and its findings that can contribute to the development of innovative passive photothermal heating systems for future buildings.

4.1 ECM-n Properties

The ECM-n properties are essential findings as they provide the information needed to determine the thermal conductivity of ECM-n– which is used to determine the heat loss and efficiency of the system. These thermal properties are relevant parameters for the COMSOL

model. The optical properties of ECM-n define the energy conversion factor and the rate of light dissipation in the material.

4.1.1 Thermal Properties

Thermogravimetric Analysis (TGA) and Differential Scanning Calorimeter (DSC)

The thermogravimetric analysis was conducted to ensure that the use of the ECM-n material in the differential scanning calorimeter was safe. The material was set to heat to 250°C after it stabilized at 100°C. As seen in the results below the material reacted relatively steadily as it heated to the peak of 250°C. From this experiment, it was concluded that it was safe to run the ECM-n in the DSC.

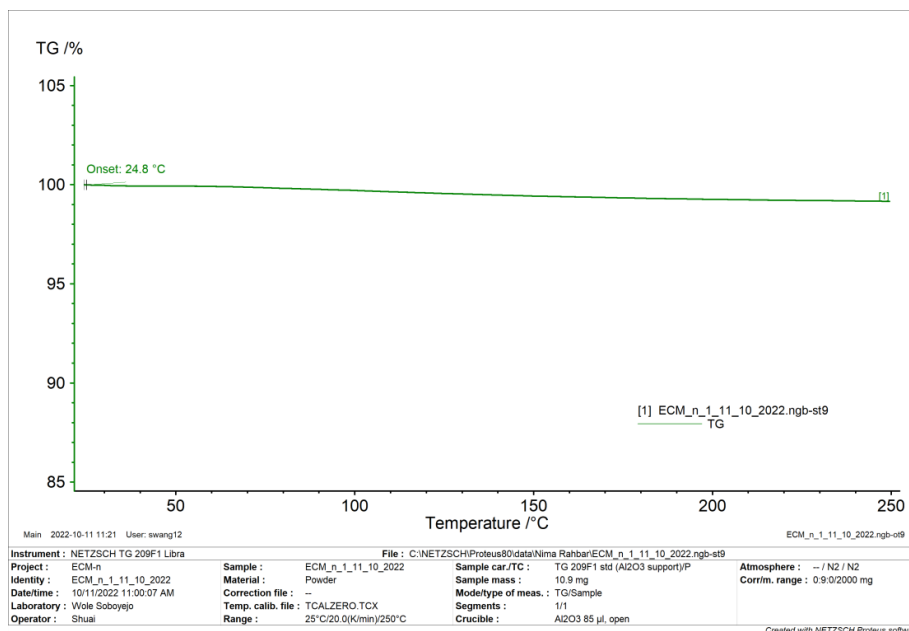


*Figure 27. TGA Data for ECM-n Sample.
The sample was heated to 250°C.*

The differential scanning calorimeter used was a heat-flux DSC which measures the difference in heat flux between the sample and a reference. In this experiment, the sample was heated to 110°C. Since the ECM-n is a mixture of calcium carbonate crystals and gelatin, it can be considered a semi-crystal material. The annotated image below shows where the data gives a peak of crystallization, the unannotated results are available in Appendix G. The curve displayed on the graph shows the glass transition, and cold crystallization processes, as well as how the material temperature stabilizes and stays through the end temperature of 110°C. From the results, it was concluded that the small deviation of heat capacity, 0.037, was negligible. Furthermore, it was concluded that this was likely due to the higher heat capacity of gelatin. Additionally, the slight rise of the line is typical of the phase change behavior of semi-crystals.

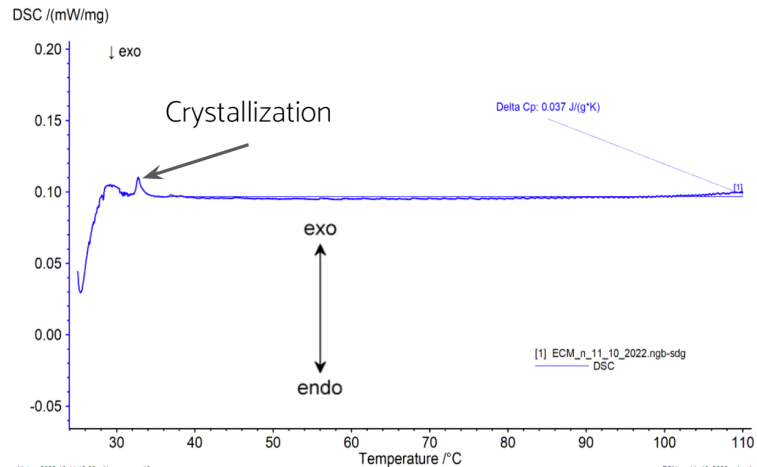


Figure 28. Annotated DSC Data Showing Crystallization.

Guarded Longitudinal Comparison Calorimeter

Data retrieval for this experiment took two steps. The first step was to record temperatures collected with thermocouples. It took 56 hours for GLCC to execute the temperature program in full. The approach was to give 2 hours for the initial temperature of the system to stabilize at 55°C before cooling down for 24 hours. The plate remained at the bottom threshold temperature of -25°C for 4 hours before ramping back up to 55°C (Fig. 29). Throughout the time of 56 hours, thermocouples were reading temperature gradients at different locations of the shell.

Temperature range from -25 to 55 degrees Celsius was selected to 1) represent the operational temperature of the ECM-n as a structural and heating element and 2) minimize the fire hazard of the lab environment. In order to have more accurate values of thermal conductivity, the maximum temperature range was selected. TECA's software EasyLog has a temperature range limitation of 80 degrees Celsius/Kelvin per one running program (Fig. 29).

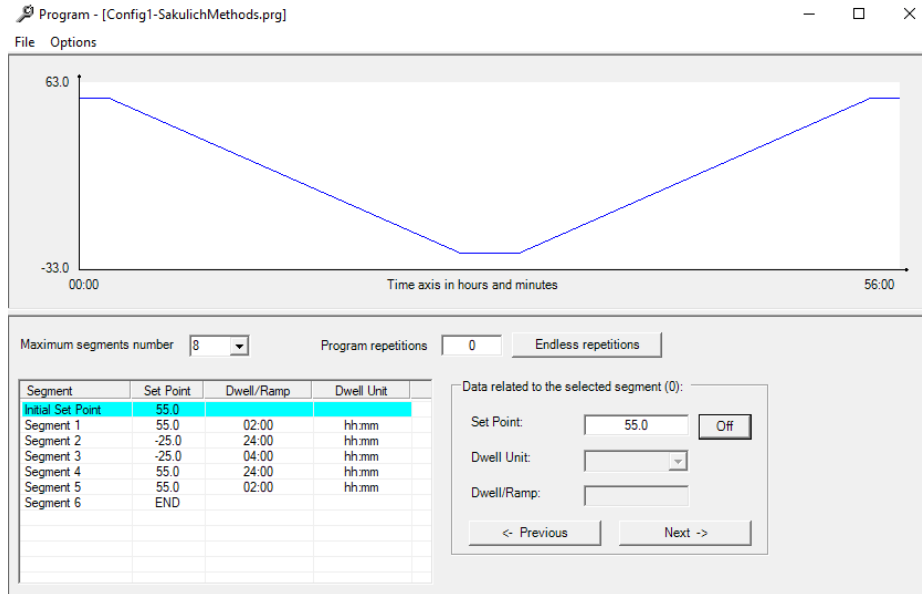


Figure 29. GLCC Temperature Program Graph.
The graph shows the operative setpoint for the experiment.

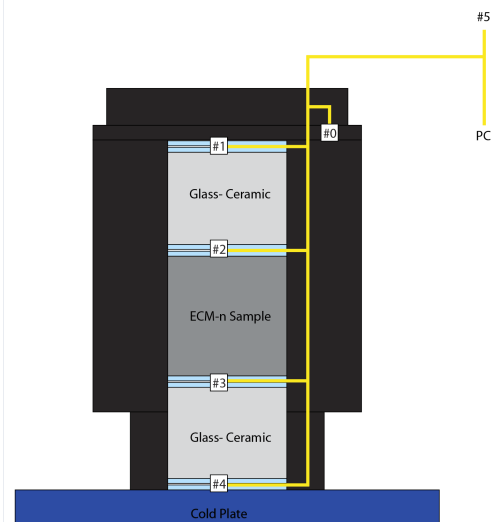
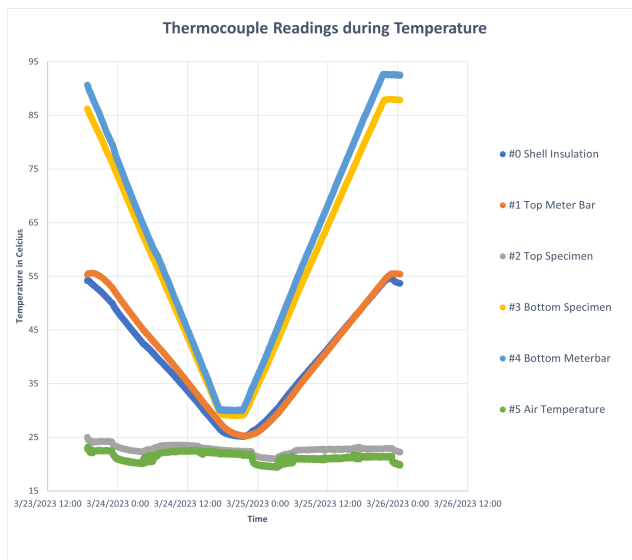


Figure 30. Recorded Temperatures During the Thermal Conductivity Experiment.
Figure 31. Guarded Longitudinal Comparative Calorimeter Laboratory Setup.
The testing apparatus used was the GLCC.

The second step was to calculate the thermal conductivity values of the ECM-n. For this part, an Excel spreadsheet was used to perform iterative calculations with temperatures and compute averages (Fig. 31). Thermal conductivity for each temperature reading was calculated and then a simple arithmetic average of all produced values was taken. The final result of thermal conductivity of the ECM-n material in the temperature range of 55 to -25°C showed $1.5688 \text{ W/m}\cdot\text{K}$.

Device: USB-TEMP							
Serial Number: 210736F							
Channel Count: 6							
Sample Count: 386218							
Start Time: 3/23/2023 6:46:32.0 PM							
Scan Rate: 2							
Sample	Date/Time	AI0 (°C)	AI1 (°C)	AI2 (°C)	AI3 (°C)	AI4 (°C)	AI5 (°C)
0	3/23/2023 18:46	54.15	55.306	25.035	86.222	90.665	22.904
1	3/23/2023 18:46	54.147	55.317	25.041	86.222	90.654	22.904
2	3/23/2023 18:46	54.148	55.309	25.03	86.222	90.662	22.91
3	3/23/2023 18:46	54.148	55.312	25.03	86.215	90.662	22.918

Figure 32. Temperature Measurements at Different Points of the Experimental Setup.

Heat flux (W/m ²) Pyroceram Top Block	Thermal Conductivity (W/m*K) of Pyroceram Top Block	Heat flux (W/m ²) Pyroceram Bottom Block	Thermal Conductivity (W/m*K) of Pyroceram Bottom Block	Heat flux (W/m ²) ECM-n Specimen	Heat flow (W) ECM-n Specimen	Thermal Conductivity of the ECM-n specimen (W/m*K)	Specific Heat of the ECM-n Specimen (J/kg*K)
4277.140891	3.95625995	581.0483439	3.66179465	2429.094617	6.268618734	1.488732053	1.023733929
4277.791301	3.9562081	579.6150922	3.6618282	2428.703197	6.267608618	1.488638137	
4278.277847	3.95626605	580.6574597	3.6618038	2429.467654	6.269581406	1.488839015	
4278.691837	3.9562569	581.5763015	3.66182515	2430.134069	6.271301185	1.489417792	

Figure 33. Calculated Values of Heat Flux and Heat Flow.

Cross section Area (m ²)	0.002581	ECM-n Depth (m)	0.0375	Pyroceram Depth (m)	0.028	ECM-n Sample Mass	0.100075	Pyroceram Mass	0.194495
--------------------------------------	----------	-----------------	--------	---------------------	-------	-------------------	----------	----------------	----------

Figure 34. Geometry Settings and Calculated.

ECM-n Specimen on the temperature range from -25 to 55 degC (W/m*K)	
Simple Arithmetic Average	Average: Pyroceram's thermal conductivity is
1.56883789	1.33462

Figure 35. Results of Thermal Conductivity of ECM-n Based on Excel Calculations.

4.1.2 Optical Properties

Reflectance, UV-VIS Range

This reflectance data was collected when testing the ECM-n sample made using the procedure with surfactant. A faculty member from Clark University, Prof. Granados-Focil provided access to his lab setup for spectrometry measurements. It was used to quantify the percentage of light that was reflected off the sample's surface, as described in Section 2.4.1.2.

Some instruments in the lab setup produced inaccuracies during the experiment which must be addressed. Testings of the material's reflectivity on the UV range (between 200 and 350 nm) produced less accurate results due to integrating the sphere's limitations, as can be seen from the considerable spike on the left side of the graph. In addition to that, there happen to be some parts of data with negative ordinate values between 380 nm and 500 nm which can be disregarded due to roughness of the material.

During the experiment, the total of 4 sides of the cubic sample was tested for a more precise average curve. The trend shows that almost all light that is between 350 nm and 500 nm penetrates the incident surface of the ECM-n. In the NIR range, the reflectance abruptly drops around 3% at 970 nm. The approximate deviation of results is +/- 3%.

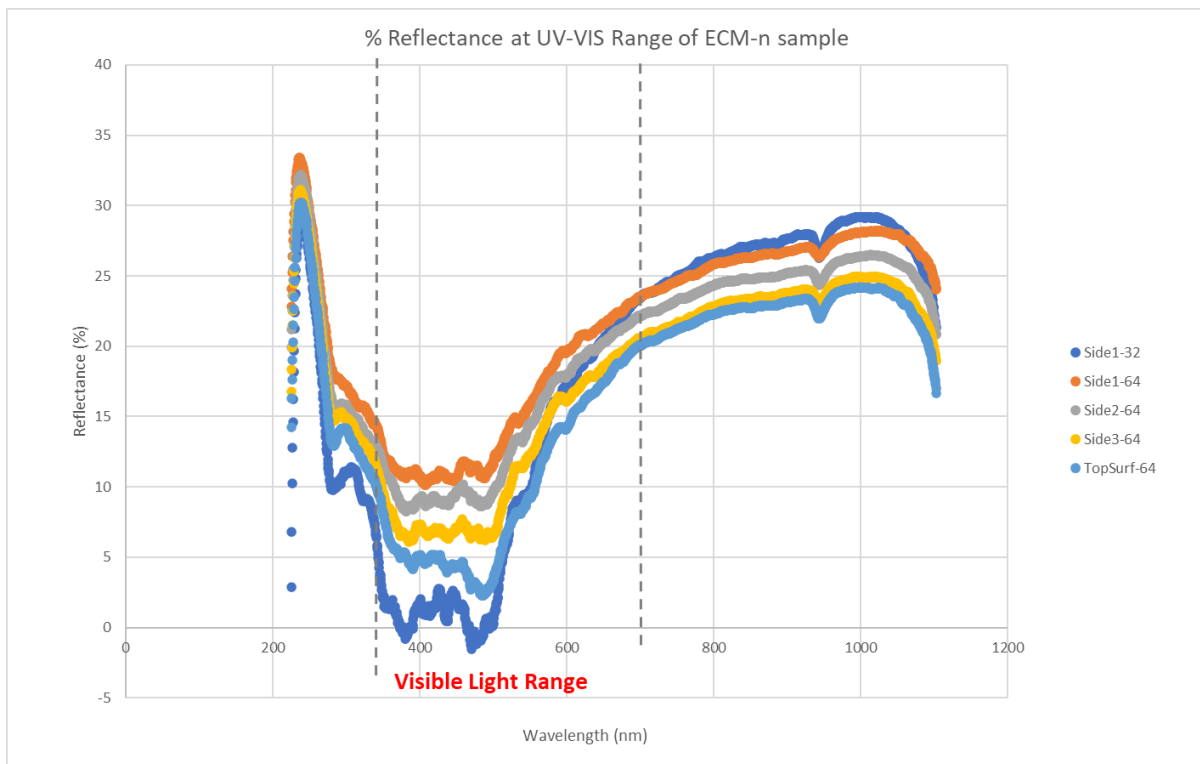


Figure 36. Spectrometry Results Data of ECM-n Specimen. The recorded reflectance was taken at the UV-VIS range.

Spectrometry, IR Range

The following graphs show reflectance and transmittance data of ECM-n collected on the infrared range. Added Iron Oxide III nanoparticles featured new thermal capabilities for ECM,

with which it became possible to heat the material by electromagnetic radiation at different wavelengths. The range of electromagnetic radiation is not limited to visible light range and includes low-frequency microwave radiation, infrared radiation, and high-frequency ultraviolet radiation. The attempt of these measurements was to estimate the amount of IR radiation that is transmitted and reflected from the ECM-n's surface. This data might be used in the future to identify the detailed absorbance of the material, as well as its energy conversion rate.

Figure 37 is representative of IR reflectance for the ECM-n. 3 iterations of the experiment were run to spot the peaks of high reflectance and identify the overall optical performance of the material at the IR range. Even though the values of each test are rather scattered from each other, it was possible to observe the peak reflectance at around 6600 nm and at 9200 nm.

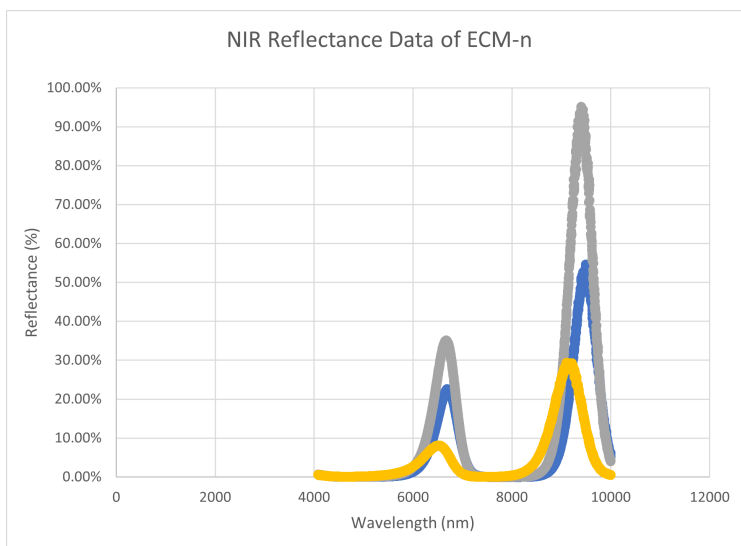


Figure 37. Reflectance Percentage over the IR Range.

To collect absorbance data at various IR wavelengths, 5 iterations of measurements were performed. 2 ECM-n samples with different nanoparticle content (0.1% and 1%) were measured. Figure 38 shows data on the wavelength range 2,500 nanometers (4000 cm^{-1}) and 14,700 nanometers (680 cm^{-1}). Recorded absorbance between 2,500 and 5,700 nanometers ($4000\text{-}1750\text{ cm}^{-1}$) is considered noise due to very dense and scattered values on the graph. The highest peak for both samples is observed at 966 cm^{-1} , which in wavelength is equal to 10,352 nanometers. Green and blue lines on the graph visualize the absorbance of the ECM-n sample with 1% nanoparticle content. Numerical details of other lower peaks can be found in Appendix H.

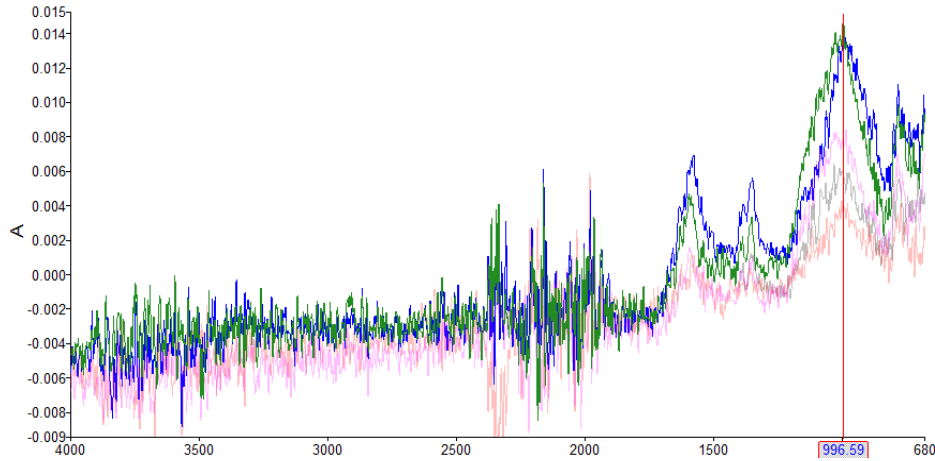


Figure 38. Absorbance of ECM-n Sample at NIR and IR Ranges.
Absorbance Units versus Wavenumber (cm^{-1}).

4.2 Energy Simulation

4.2.1 Hand Calculations

The calculations performed gave heat flux, heat loss, and the U-factors for the designed wall system. With these properties, the minimum amount of energy required to sustain a comfortable interior temperature was also determined. The known inputs and system conditions are listed in Section 3.4.1, in *Table 4*. These are then plugged into the equations given in the methodology to confirm the COMSOL model.

Solving the equations with the values from *Table 4*:

U-Value (SI):

$$U = \frac{1}{RSI_{Total} \times 5.678} = \frac{1}{(0.00074 + 3.64 + 0.08622 + 3.64 + 0.0002) \times 5.678}$$

$$U = \frac{1}{R} = \frac{1}{41.8307} = 0.0239$$

Heat Flux:

$$q = -\Delta T \times U = -26^{\circ}\text{C} \times 0.1357 = 3.5292 \text{ (W/m}^2\text{)}$$

Heat Loss:

$$Q = q \times A_{surface} = 3.5292 \times 23.88 = 84.2766 \text{ (W)}$$

Minimum power required for each Point Heat Source:

$$\frac{Q}{88 \times 2} = \frac{84.2766}{88 \times 2} = 0.2394 \text{ (W)}$$

With these equations, which utilized the properties from the materials or components, and the COMSOL parameters: the hand calculations confirmed the COMSOL energy simulation

results. Additionally, these calculations would provide the energy demand necessary for the sizing of the solar collectors. The results of the hand calculations are summarized in Table 3 below, and further information about these calculations can be found in Appendix I.

Table 4: Hand Calculation Results Summary Table

Results	
U (SI) = 1/R	0.0239
Heat Flux (W/m ²)	3.5292
Model Total Exterior Surface (m ²)	23.8800
Total Heat Loss (W)	84.2766
Power of each Point Heat Source (W)	0.2394

4.2.2 Model Reaches Steady-State Conditions

The following curve generated by the energy simulation software, COMSOL, proves that a steady-state condition can be achieved with our proposed design system. This was achieved when all four walls of the COMSOL model were generating heat at a constant rate in one room.

This data was calculated using only one layer of XPS on the outside of the ECM-n wall to expose the warmer surface of the wall to the inside. The curve shows that in just under 25 days, a constant interior temperature can be maintained in a room. To generate this heat, a total of 176-point heat sources in the room, each at 3W was required. In total, to reach steady-state, 528W needs to be fed to the system continuously. Knowing that the system would need to constantly be running was a major factor in the following design process. This first attempt at energy simulation directly led to the design decision to add lasers that are constantly heating into the system to maintain this steady-state. However, due to technical constraints associated with sharing a single fiber network with two light sources, a laser source is left for future investigators to find the right application in this system.

Steady-State Energy Simulation of Heated ECM-n Room

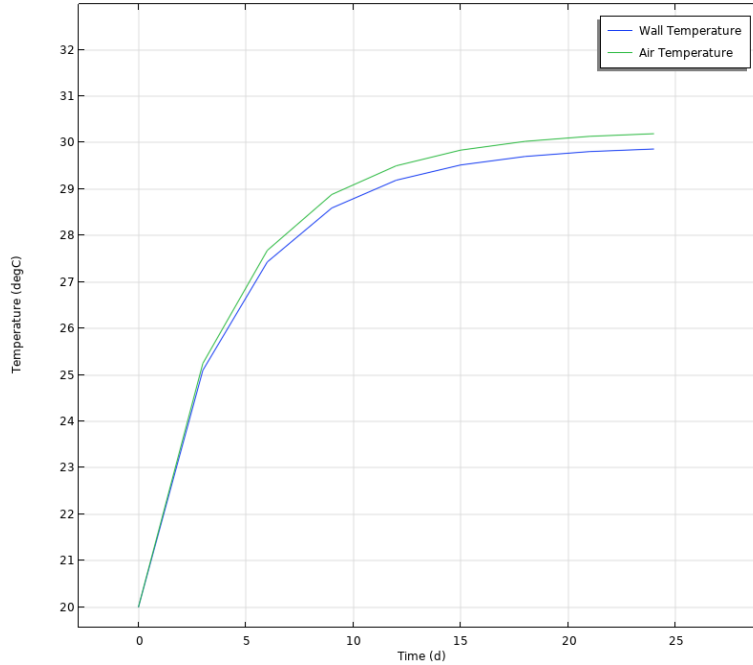


Figure 39. Temperature Integration Results of Interior Walls. Shown per unit time (°C vs. days) of all four surrounding heated walls continuously turned on. The total power required by this system is 528W (3W each, 176-point heat sources).

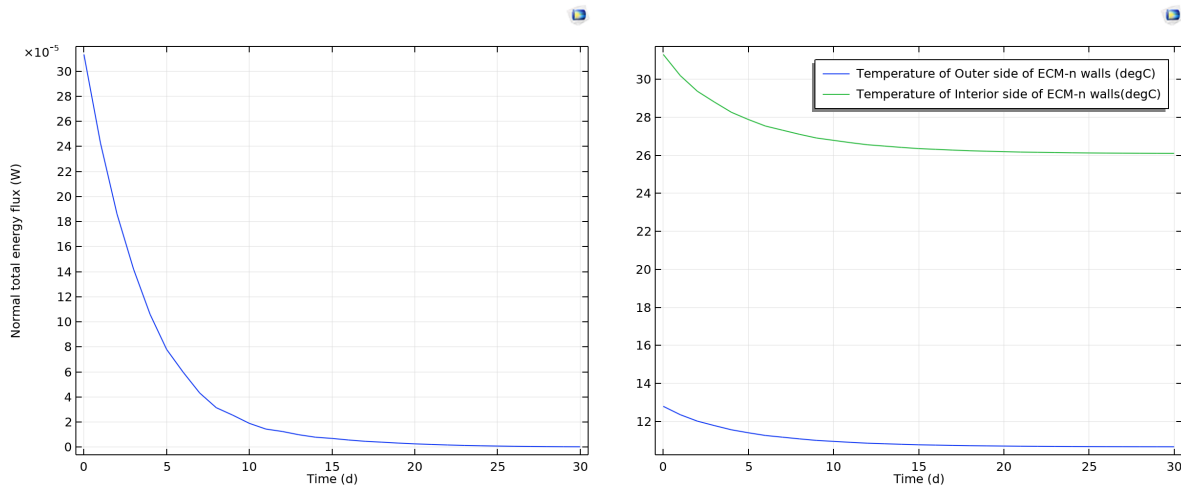


Figure 40. Normal Energy Flux for Interior Surface of Walls. Figure 41. Temperature vs. Time Graph Depicting the Interior and Outer Side of ECM-n Wall.

Figure 39 provides another set of proof that the model reaches steady-state over the course of 30 days at a constant power input of 2.5 watts per point, resulting in 440 watts per total of 176 point heat sources. By attaching another layer of thermal insulation to the interior side of the heated wall, the total power input decreased from 526 watts to 440 watts. Energy flux ramps down as the temperature inside the room stabilizes to a comfortable 26°C.

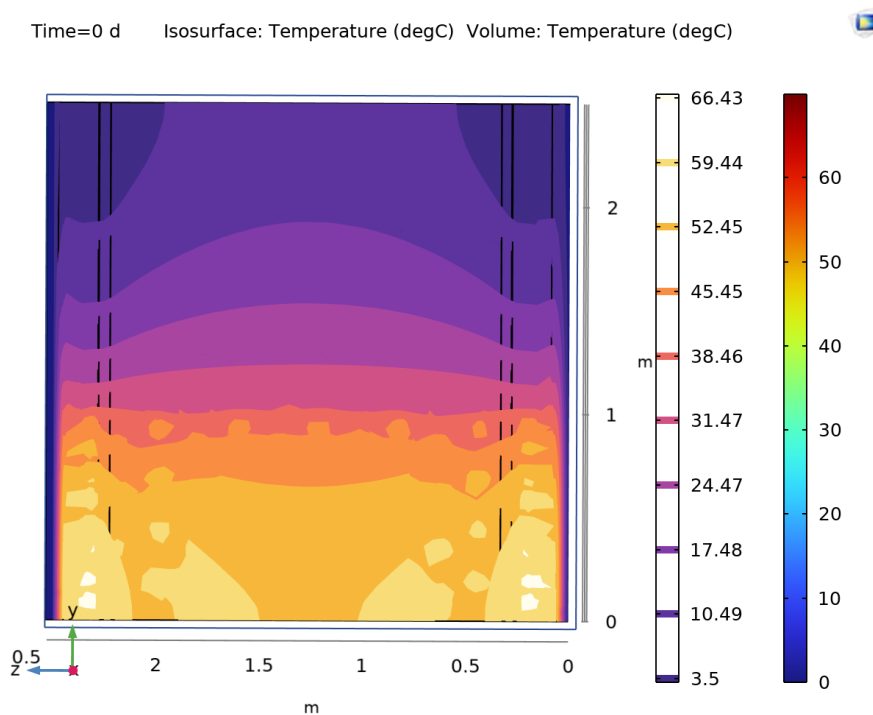


Figure 42. Colored Thermal Gradient for Single Wall.

Similar to the Figure shown above, Appendix J, offers a short rendering from COMSOL giving the dynamic heating of a space.

4.3 Passive Photothermal Heating System Design

4.3.1 Proposed Design

The energy simulation produced many results that provided critical critiques of the system. One such result from the COMSOL simulations was the analysis of the isotherms from the heat point distribution at the lower part of the walls. From the produced data given in Figure 42 above, it was apparent that the current distribution of the heat sources doesn't produce homogeneous heating of the space as anticipated with the design intent. The design intent relied heavily on convective airflow. Although there was some convective airflow as seen in Appendix I, there was not enough to have the entire space remain at a comfortable temperature.

Additionally, the design had been designed with steady-state heating within the ECM-n. After running the simulation and performing calculations, the resulting energy loads were far more substantial than the team anticipated. To run at a steady-state, there was a significant period of time that the model had to run to initially reach the desired steady-state temperature. The energy load to constantly power the model at that steady-state coupled with the initial inconveniences of the model were beneficial critiques of the designed system. To make up for the high energy loads required to power the steady-state system, which resulted in not being very efficient, the team could pivot to utilize a different power source. From the energy simulations, it

was determined that a free energy source such as solar energy would make this system more economical adaptation.

4.3.1.1 Comprehensive Figure of System Overview

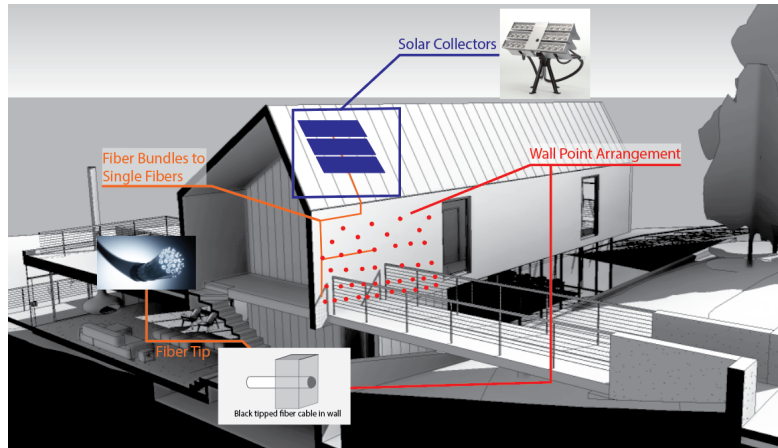


Figure 43. Passive Photothermal Heating System Design.
("REVIT 2023" n.d.)
("PARANS SYSTEM: SP4-12.2 SUNLIGHT COLLECTOR" n.d.)
("Mechanism of Himawari Solar Lighting System" n.d.)

4.3.1.2 Building Envelope

Code Compliance

The preliminary system design is catered to the Boston, Massachusetts location. In the United States, Building Codes are adopted at a state level across the nation. For our purposes, it is essential to note that the Commonwealth of Massachusetts adopts the ninth edition of the 780 Code of Massachusetts Regulations (CMR) at this time. The 780 CMR is based on the 2015 International Code Council (ICC) codes with several amendments. For the code compliance of building envelopes, the International Energy Conservation Code (IECC) can be used. The 2015 IECC, Section R301 has Boston, MA listed as a Climate Zone 5A, cool humid climate. This then dictates that per Table R402.1.2, a Climate Zone 5 building with mass walls must have an R-value of 13 unless more than half the insulation is on the interior of the mass wall, then an R-value of 17 is required. As given above in Section 4.2.3, the design is more than code compliant.

The passive photothermal heating system uses the XPS given in Appendix F. For the purposes of the designed system, an XPS thickness of 91mm with an RSI of 3.52 was used. The Dupont manufacturer produces and distributes this XPS material in sheets that measure 400mm by 2400 mm. This was chosen after testing various other thicknesses in the COMSOL model. The iteration of the design was aimed to increase the efficiency of the system. Similarly, the system efficiencies were increased by manipulating the end of the fiber cable tip to be a matte black within the ECM-n mass. This increases the ECM-n's ability to fully absorb the energy

from the fiber cable. By having high absorbance, the system is able to utilize every watt the solar collectors harvest. A visual of the black tip on the fiber cable is shown in Figure 44.

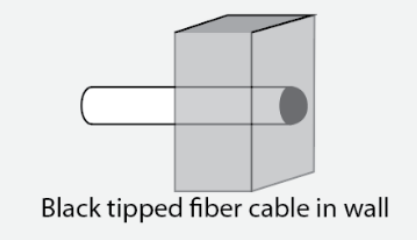


Figure 44. Altered Imbedded Fiber Cable in ECM-n Wall.

4.3.1.3 Efficiencies

To estimate solar radiance that will feed the heating system in Boston, Massachusetts location, Climate Consultant 6.0 tool was used. Figure 45 shows seasonal solar energy data for different solar collector orientations. Direct normal orientation values will be used to estimate the required area for solar harvesting. The annual average radiation per square meter per day for the current location is 300 watt-hours. In other words, at one square meter of collected sunlight, 300 joules of energy are generated every second. According to the simulation data from the COMSOL model, the total required power input is 440 watts per 4 square meters of heating space. To provide a power output of 440 watts, solar collectors need to cover up to 1.5 square meters of space. The efficiency of the system at the current setting can be rewritten as a 7:20 harvested solar-to-heated floor area ratio.

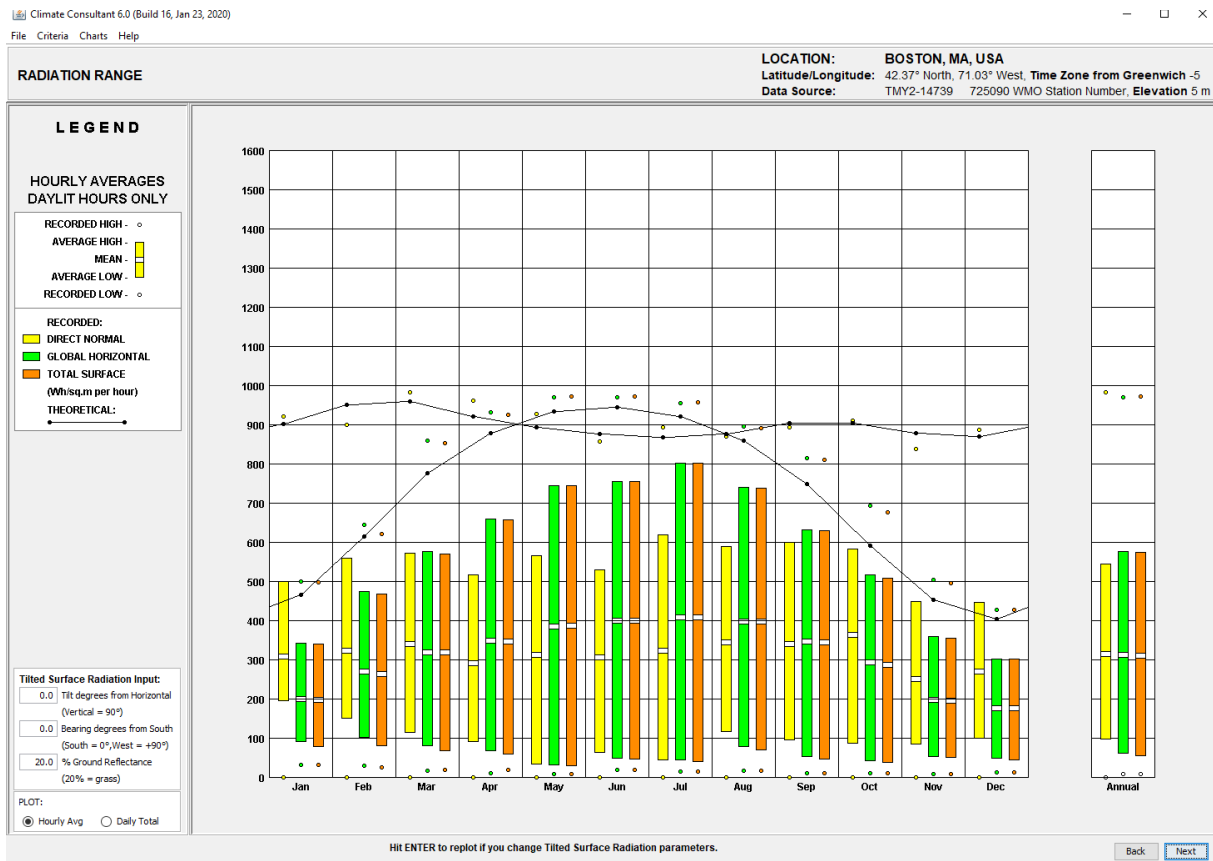


Figure 45. Seasonal Solar Power Intensity in Boston, Massachusetts. Climate Consultant 6.0.

5.0 DISCUSSION & CONCLUSION

5.1 Heating System Considerations

The energy simulation model used a continuous power rate input for point heat sources. This simplification assumes that the Sun non-stop supplies solar collectors with power at a constant rate. In the real world, there are only 6 hours (annual average of sunlight per day for Boston, Massachusetts location) of daylight per day (Climate Consultant 6.0, 2020). Additionally, the power input rate depends on the sky's cloud cover and the time of the day. Solar power peaks at noon on a typical day in July, supplying the system with a lot of energy, whereas a rainy day in October at twilight will deliver almost no energy to the system.

These weather-related variables can be factored into the COMSOL model for more detailed analysis. Heating can switch on/off at programmed times if the time-dependent equation under the heating module follows a personalized time setting. Random power drops can also be added if the power equation's time variable gets nonlinear behavior.

5.1.1 Laser Heating

In this project, lasers are not reviewed as the main energy source for the proposed heating system. Besides the importance of the optical properties of the material, the rate of energy conversion significantly depends on the wavelength of irradiation. The laser heat transfer process can be added to the COMSOL model to account for potential energy losses.

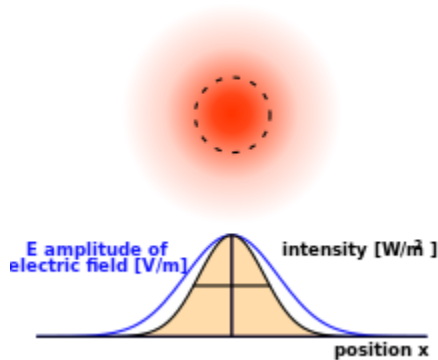


Figure 46. Transverse Intensity Profile of a Gaussian Beam.

In this, the beam is propagating out of the page. Blue curve: electric (or magnetic) field amplitude vs. radial position from the beam axis. The black curve is the corresponding intensity. Citation, ("User: FDominec - Wikimedia Commons" n.d.)

The Gaussian beam concept is usually applied when calculating the radiation heat transfer of monochromatic light (Caiazza et al., 2018). Continuously propagated Gaussian beam has a transverse behavior that defines its intensity profile (Fig. 46). Lasers are monochromatic light sources featuring Gaussian beam physics when propagated onto the surface. This concept

was studied for laser curing of ECM-n for more accurate heat transfer results of defocused laser beams (Wang et al., 2022).

There is potential for a laser source to be used in place of solar collectors when solar output is not powerful enough to supply the building with heat. The light source must be set at a wavelength that is absorbed best by ECM-n, which would be within the visible light range, to maximize energy conversion and minimize further light propagation into the material.

5.1.2 Building envelope

Besides walls, there are more structural elements of the building that can be built using ECM-n. The heating system can extend from walls to, for example, floor slabs and columns. For a more comprehensive understanding of the system's efficiency, it is recommended that more complicated energy simulation models are built and analyzed using the COMSOL template model.

5.2 ECM-n Properties

5.2.1 Thermal Properties

GLCC Procedure - Thermal Conductivity in Temperature Range

Thermal conductivity of the ECM-n in the range of 55°C to -25°C is equal to 1.5688 W/m*K. For comparison, the thermal conductivity of self-consolidating concrete (SCC) at room temperature ranges between 2.8 and 3.5 W/m*K (Asadi et al. 2018). As a heating element, it prompts the ECM-n to conduct heat faster than concrete and warm up the interior spaces more efficiently.

If the thermal conductivity of ECM-n at temperatures beyond the experimental range is needed (-25°C to 55°C), cold plate tests can be rerun at different temperature settings, adding more complex temperature parameters to the temperature program. The accuracy of heat conduction by the specimen can be improved by using more elaborative temperature programs where the rate of temperature change is faster and nonlinear.

Thermal Mass

Specific heat capacity is a significant characteristic that defines the capability of a material to store heat. Another colloquial term for it is thermal mass. Specific heat of the ECM-n can be computed using the same dataset collected for thermal conductivity calculations. Here is the equation for specific heat capacity coefficient:

$$C_p = \frac{Q}{m*\Delta T} \quad \text{Eq. (5-1)}$$

Like the thermal conductivity equation, there are two variables that are already recorded and evaluated in the dataset: temperature gradient ΔT (°C) and heat energy Q (J). The only unknown

in the equation is the mass of the specimen m (kg). The mass of the ECM-n sample used in the experiment is measured with a precise scale readily available in the lab.

5.2.2 VIS Range Spectrophotometer

As can be observed from the spectrophotometry of solar spectra (Fig. 47), 47% of the total solar energy is concentrated in the visible light range (380-780 nm), (Bohm et al. 2023). Assuming that ECM-n absorbs 80% of the incoming solar energy, infrared light will most likely be transmitted. The basis for the assumptions used to produce this conclusion is according to the reflectance data given in Section 4.1.2, and the characteristics of longer wavelengths of light to be more easily transmitted. The latter is implied by IR spectrometry results in Section 4.1.2.

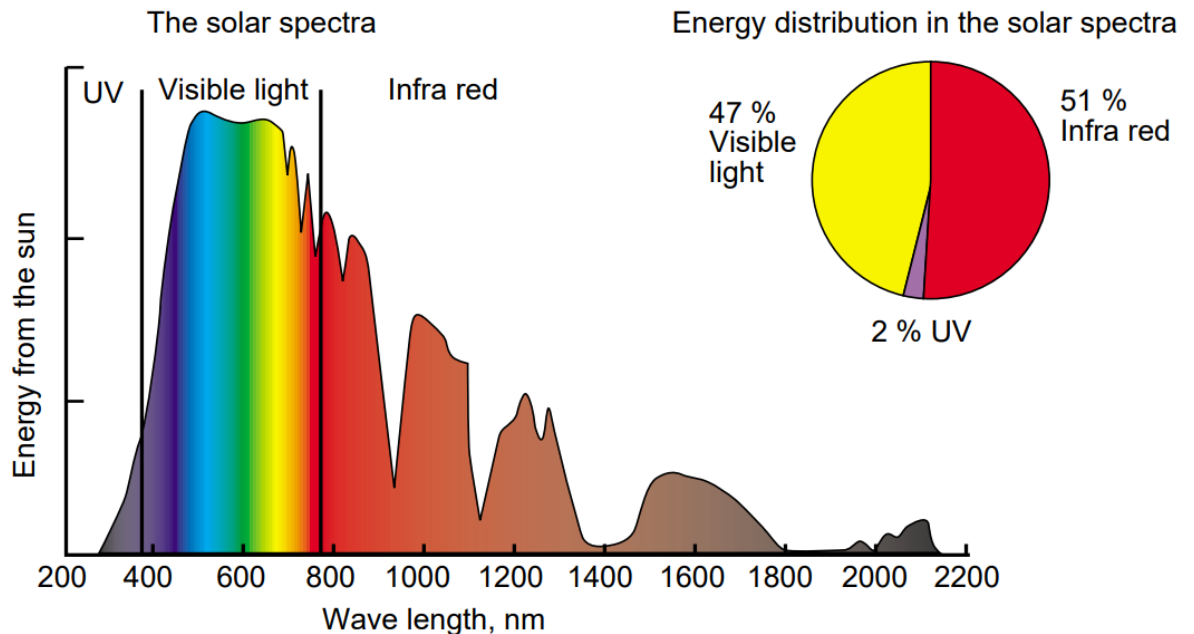


Figure 47. Solar Spectra & Proportional Energy Content of Solar Power. The solar spectra are wavelength (nm) by energy from the sun. (Bohm et al. 2023).

5.2.3 Comprehensive Analysis of Absorbance Data

There are multiple ways the total amount of absorbed light on a specific range of various wavelengths can be computed. For this project, the method of computing the total percentage of light absorbed on the solar spectra includes some integration and the energy equation for a blackbody. Since the absorbance data on the visible light range has not been evaluated, this procedure is recommended for future teams to undertake.

The Planck blackbody equation (5-2) is used to calculate spectral radiance L_{λ} at a specific wavelength λ and temperature T of the source (Ribbing et al., 2013):

$$L_{\lambda}(\lambda, T) = \frac{C_1}{\lambda^4 [\exp(C_2/\lambda T) - 1]} \quad \text{Eq. (5-2)}$$

$$C_1 = 5.99584 \times 1,022 \text{ photons} * \mu\text{m}^5 / \text{s} * \text{cm}^2 * \text{sr}$$

$$C_2 = 14,387.9 \mu\text{m} * K$$

Wavelength and temperature are two variables that control the output value of the equation. This equation also works exclusively with a wavelength parameter. For that, the temperature of the source is made constant.

If equation (5-2) is multiplied by the collected absorbance data of the material, it is converted to the fraction of energy that gets absorbed by the blackbody, which by definition absorbs all light incident to its surface (Ribbing et al., 2013). Hence, this step is done to limit spectral radiance results on the absorbance range of the ECM-n. The units of spectral radiance can be disregarded since it cancels out in the final equation.

Now, it is necessary to map results onto the solar spectra and make sure that spectral radiance units ($ph/s * cm^2 * sr * \mu m$) cancel out to have a unitless output value. First, previously multiplied expressions have to be divided by another (identical to the first) Planck equation. Then, both the denominator and the numerator must be integrated into the solar spectra range (~300nm - 2,000nm). The final equation (5-3), derived by the project team, must take the following form:

$$E_{\lambda} = \frac{\int_{300nm}^{2,000nm} \text{absorbance dataset}(\lambda) * L(\lambda)}{\int_{300nm}^{2,000nm} L(\lambda)} \quad \text{Eq. (5-3)}$$

This method can be used with any material if its optical absorbance is known on the interested wavelength range. The initial scope of this project included experiments to find absorbance at the UV-VIS range, however, the unavailability of required instrumentation made it impossible to perform measurements at the time of the project.

5.3 Takeaways

Based on the energy modeling and experiments conducted, the photothermal radiative heating system utilizing ECM-n did not demonstrate significant efficiency. Despite this, the utilization of solar energy, as a cost-free and renewable source of energy, rendered the system sustainable. Due to the sustainability and productive functionality of the system, it was concluded that the project goal was achieved. Although the system requires only 37.5 square meters of solar collectors to heat 100 square meters of interior space, its versatility can be enhanced by omitting the installation of electrical equipment.

Furthermore, the system is easily and affordably installed with the only required components being, solar collectors, fiber cable bundles, and ECM-n wall masses. As previously discussed, the ECM-n would be manufactured in unitized construction panels with the fiber cables attached. The solar collectors can be readily connected to these ECM-n panels. The system's low maintenance and negligible energy costs for heating contribute to its success.

While more research is required to demonstrate the conceptual design can be implemented, future recommendations to further expand this work include implementing the ECM-n photothermal heating system in floor and column massing. Additionally, other heating alternatives, such as long-term microwaves or electromagnetic fields with lasers, may be explored. In conclusion, further development and exploration of this system could lead to more efficient and sustainable heating solutions for buildings.

6.0 ACKNOWLEDGEMENTS

We would like to extend our thanks first and foremost to our advisors, **Professor Nima Rahbar** and **Professor Steven Van Dessel**. It was with their guidance, expertise, creativity, and support that we were able to complete this work. Furthermore, we would like to thank the WPI professors and Ph.D. students who assisted us in the experiential and design development processes: **Professor Aaron Sakulich**, and Ph.D. Students: **Shuai Wang**, **Zhiying Xiao**, and **Jihan El Ouaragli**. Their generosity in sharing their time, knowledge, and materials was critical to the quantification aspect of our project. In a similar vein, we extend our thanks also to lab manager **Russ Lang** for providing us with the necessary materials, lab space, and general assistance throughout the duration of the project. Another person we'd like to thank is our undergraduate peer who assisted us in the analysis of our data, **Abigail Holmes**, a biomedical engineering student in Professor Rahbar's lab.

Throughout our major qualifying project, we were fortunate to have the support of a handful of mentors outside of the Architectural Engineering realm. They provided guidance as we learned new skills in a subject matter outside of the majority of our undergraduate coursework. From the Chemistry and Biochemistry department, we'd like to thank lab manager **Nick Bold** for his expertise and guidance in spectrometer testing. We'd also like to thank Instrument Core Technician **Daryl Johnson** of the Life Science and Bioengineering Center at WPI for his assistance in the thermal property testing of our project. From the Physics Department, we'd like to thank **Professor Germano Iannacchione** who we consulted with about the feasibility of the system's design. Outside of WPI, we were able to work with **Professor Sergio Granados-Focil** of the Gustaf Carlson School of Chemistry and Biochemistry at Clark University. We extend our thanks to Professor Sergio Granados-Focil for his assistance with spectrometry testing.

BIBLIOGRAPHY

- “Building Integrated Solar Thermal – BIST - Engineering Services Manfred Starlinger.” n.d. Www.ims-Plan.com. ims Ingenieurleistungen Manfred Starlinger. <https://www.ims-plan.com/building-integrated-solar-thermal.html>.
- “COMSOL Multiphysics® Modeling Software.” 2019. Comsol.com. 2019. <https://www.comsol.com/>.
- “DH-2000-BAL Light Source | Ocean Insight.” n.d. Www.oceaninsight.com. Ocean Insight. Accessed April 27, 2023. <https://www.oceaninsight.com/products/light-sources/uv-vis-nir-light-sources/dh-2000-bal/>.
- “Furnaces: How They Work | AHRI.” n.d. Www.ahrinet.org. Accessed April 27, 2023. <https://www.ahrinet.org/scholarships-education/education/homeowners/how-things-work/furnaces-how-they-work>.
- “Galaxy | Lightway Daylight.” 2014. Www.lightwaydaylight.co.uk. Lightway Crystal Sun Tunnels. 2014. <https://www.lightwaydaylight.co.uk/products/galaxy/>.
- “How Central Heating Works | Gas Furnace | Goodman.” n.d. Www.goodmanmfg.com. Accessed April 27, 2023. <https://www.goodmanmfg.com/resources/hvac-learning-center/?param1=hvac-101¶m2=how-a-central-gas-heating-system-works>.
- “How the Thermal Conductivity Is Measured in a Solid?” 2021. Coolmag. June 29, 2021. <https://coolmag.net/how-the-thermal-conductivity-is-measured-in-a-solid/>.
- “ISP-50-8-R-GT | Integrating Sphere | Ocean Insight.” n.d. Www.oceaninsight.com. Accessed April 27, 2023. <https://www.oceaninsight.com/products/sampling-accessories/free-space-optics/integrating-spheres/isp-50-8-r-gt/>.
- “NCEES Professional Licensure.” n.d. NCEES. <https://ncees.org/licensure/>.
- “Ocean HDX Spectrometer | High Sensitivity | Ocean Insight.” n.d. Www.oceaninsight.com. <https://www.oceaninsight.com/products/spectrometers/high-sensitivity/ocean-hdx/>.
- “PARANS SYSTEM: SP4-12.2 SUNLIGHT COLLECTOR.” 2020. Parans.com. June 2020. <https://parans.com/products/parans-system-sp4-12-2-sunlight-collector/>.
- “Portland Cement : A Brief History.” 2014. The Screed Scientist®. June 20, 2014. <https://www.screedscientist.com/portland-cement-a-brief-history/>.
- “REVIT 2023.” n.d. AutoDesk.
- “Romans in Britain - Roman Central Heating.” n.d. Www.romanobritain.org. Accessed 2023. https://www.romanobritain.org/12_innovations/inv_central_heating.php.
- “Spectrum™ One FT-IR Spectrometer: Experience the Quality of Spectrum™ One - Best in Class.” n.d.
- “Styrofoam-Brand-Cavitymate-Ultra-Pis-43-D100051-EnNA.Pdf,” n.d.
- “TC3008 | Tape Solutions.” n.d. Accessed March 29, 2023. <https://www.tapesolutions.saint-gobain.com/na/products/gasketing-foams/silicone/thermally-conductive-silicone/tc3008>.

- “U.S. Energy Information Administration - EIA - Independent Statistics and Analysis.” n.d. Accessed April 2, 2023. <https://www.eia.gov/todayinenergy/prices.php>.
- “United States Natural Gas Industrial Price (Dollars per Thousand Cubic Feet).” n.d. Accessed April 2, 2023. <https://www.eia.gov/dnav/ng/hist/n3035us3m.htm>.
- “User:FDominec - Wikimedia Commons.” n.d. Accessed April 3, 2023. <https://commons.wikimedia.org/wiki/User:FDominec>.
- “What Is HVAC and How Does It Work?” Accessed March 10, 2023. <https://www.usnews.com/360-reviews/services/hvac/what-is-hvac>.
- “What Is SEER, EER, HSPF, AFUE, and COP?” Accessed March 10, 2023. http://www.central-air-conditioner-and-refrigeration.com/SEER_EER_HSPF_AFUE_COP.html.
- “Why The Building Sector? – Architecture 2030.” Accessed November 7, 2022. <https://architecture2030.org/why-the-building-sector/>.
- 2023 Investor Day, 2023. <https://www.youtube.com/watch?v=Hl1zEzVUV7w>.
- Accelerating Building Efficiency. “Accelerating Building Efficiency: Eight Actions for Urban Leaders.” Accessed March 10, 2023. <http://www.wri.org/buildingefficiency/>.
- Amran, Mugahed, Ali M. Onaizi, Roman Fediuk, Nikolai Ivanovich Vatin, Raizal Saifulnaz Muhammad Rashid, Hakim Abdelgader, and Togay Ozbakkaloglu. 2022. “Self-Healing Concrete as a Prospective Construction Material: A Review.” *Materials* 15 (9): 3214. <https://doi.org/10.3390/ma15093214>.
- ASHRAE, ASHRAE Handbook - Systems and Equipment (SI edition), 2020, TH7015 .A74 2020 (SI)
- Basaran, Tahsin. "The Heating System of the Roman Baths." *ASHRAE Transactions* 113, no. 1 (2007).
- Bean, Robert, and Kwang Woo Kim ArchD. "Part 2: History of radiant heating & cooling systems." *Ashrae Journal* 52, no. 2 (2010): 50.
- Bohm, Mats & Holmér, Ingvar & Nilsson, Håkan & Norén, Olle. (2023). Thermal effect of glazing in driver's cabs Evaluation of the impact of different types of glazing on the thermal comfort.
- Bonnefin, Ilvy. n.d. “Emerging Materials: Mycelium Brick.” Accessed March 10, 2023. <https://www.certifiedenergy.com.au/emerging-materials/emerging-materials-mycelium-brick>
- Carl G. Ribbing, Chapter 8 - Controlling thermal radiation from surfaces☆, Editor(s): Angela Piegari, François Flory, In Woodhead Publishing Series in Electronic and Optical Materials, Optical Thin Films and Coatings (Second Edition), Woodhead Publishing, 2013, Pages 357-387, ISBN 9780081020739,
- Chelsea M. Heveran, Sarah L. Williams, Jishen Qiu, Juliana Artier, Mija H. Hubler, Sherri M. Cook, Jeffrey C. Cameron, Wil V. Srubar, Biomineralization and Successive Regeneration

- of Engineered Living Building Materials, *Matter*, Volume 2, Issue 2, 2020, Pages 481-494, ISSN 2590-2385.
- Chen, Yujiao, Zheming Tong, and Ali Malkawi. "Investigating Natural Ventilation Potentials across the Globe: Regional and Climatic Variations." *Building and Environment* 122 (September 2017): 386–96. <https://doi.org/10.1016/j.buildenv.2017.06.026>.
- Crowley, John E. *The invention of comfort: Sensibilities and design in early modern Britain and early America*. JHU Press, 2003.
- Cullingford, Benita. *British Chimney Sweeps: Five Centuries of Chimney Sweeping*. Rowman & Littlefield, 2001.
- DeLaine, Janet. "Recent research on Roman baths." *Journal of Roman Archaeology* 1 (1988): 11-32.
- Egerton, Michael C. "William Strutt and the application of convection to the heating of buildings." *Annals of Science* 24, no. 1 (1968): 73-87.
- Energy.gov. "Active Solar Heating." Accessed November 29, 2022. <https://www.energy.gov/energysaver/active-solar-heating>.
- Energy.gov. "Heat Pump Systems." Accessed March 10, 2023. <https://www.energy.gov/energysaver/heat-pump-systems>.
- Estelrich, Joan, and Maria Antònia Busquets. "Iron Oxide Nanoparticles in Photothermal Therapy." *Molecules (Basel, Switzerland)* 23, no. 7 (June 28, 2018): 1567. <https://doi.org/10.3390/molecules23071567>.
- Fagan, Garrett G. "The genesis of the Roman public bath: recent approaches and future directions." *American Journal of Archaeology* 105, no. 3 (2001): 403-426.
- Fleming, Donald. "Latent heat and the invention of the Watt engine." *Isis* 43, no. 1 (1952): 3-5.
- Flynn, D. , Yen, J. , Filliben, J. , Zarr, R. and Hohlfeld, E. (2021), *Thermal Properties of Pyroceram Code 9606*, International Thermal Conductivity Conference (Accessed March 10, 2023)
- Fong, Jennifer. 2019. "The Benefits of Earning and Maintaining a Professional Engineer License." *IEEE Innovation at Work* (blog). July 11, 2019. <https://innovationatwork.ieee.org/the-benefits-of-earning-and-maintaining-a-professional-engineer-license/>.
- Gagg, Colin R. "Cement and Concrete as an Engineering Material: An Historic Appraisal and Case Study Analysis." *Engineering Failure Analysis* 40 (May 1, 2014): 114–40. <https://doi.org/10.1016/j.engfailanal.2014.02.004>.
- Garrison, Fielding Hudson. "The history of heating, ventilation and lighting." *Bulletin of the New York Academy of Medicine* 3, no. 2 (1927): 56.
- Go Green Solar. 2017. "How Many Solar Panels Do I Need? Easy Solar Calculator." *Gogreensolar.com*. 2017. <https://www.gogreensolar.com/pages/how-many-solar-panels-do-i-need>.
- Goldstone, Jack A. *Why Europe? The rise of the West in world history 1500-1850*. McGraw-Hill Higher Education, 2009.

- Hamdy, Omnia & Mohammed, Haitham. (2021). Investigating the transmission profiles of 808 nm laser through different regions of the rat's head. *Lasers in Medical Science*. 10.1007/s10103-020-03098-9.
- Hammerl, Christa, P. Albin, and A. Moroni. "The earthquake of January 25th, 1348: discussion of sources." *Historical investigation of European earthquakes 2* (1994): 225-240.
- Hansen, Lee R. 2019. "LEED CERTIFICATION INCENTIVES in OTHER STATES." Ct.gov. 2019. <https://www.cga.ct.gov/2015/rpt/2015-R-0061.htm>.
- Hodgkinson, Jeremy. "Pre-Restoration Iron Firebacks." *Journal of Antique Metalware Society* 20 (2012): 2-5.
- HomeAdvisor, and Robert Tschudi. 2021. "Learn about the Cost of Projects in the Heating & Cooling Category." *Www.homeadvisor.com*. 2021. <https://www.homeadvisor.com/cost/heating-and-cooling/>.
- House, The White. "FACT SHEET: President Biden Signs Executive Order Catalyzing America's Clean Energy Economy Through Federal Sustainability." The White House, December 8, 2021. <https://www.whitehouse.gov/briefing-room/statements-releases/2021/12/08/fact-sheet-president-biden-signs-executive-order-catalyzing-americas-clean-energy-economy-through-federal-sustainability/>.
- IEA. "Buildings – Topics." Accessed March 10, 2023. <https://www.iea.org/topics/buildings>.
- Ihm, Pyeongchan, and Moncef Krarti. "Optimal Control Strategies for Heated Radiant Floor Systems." *ASHRAE Transactions* 111, no. 1 (2005).
- Ilchi-Ghazaani, Maryam, and Parviz Parvin. "Heat Generation and Removal in Fiber Lasers," 321–44, 2016. <https://doi.org/10.5772/62102>.
- Iman Asadi, Payam Shafiqh, Zahiruddin Fitri Bin Abu Hassan, Norhayati Binti Mahyuddin, Thermal conductivity of concrete – A review, *Journal of Building Engineering*, Volume 20, 2018, Pages 81-93, ISSN 2352-7102, <https://doi.org/10.1016/j.jobee.2018.07.002>.
- Inc, Warmup. "Radiant Floor Heating Systems Buyers Guide for 2023." Warmup (blog), December 16, 2022. <https://www.warmup.com/blog/radiant-floor-heating>.
- J.W. Linton, Description and Test Results of a High Temperature Heat Pump Test Facility, Editor(s): TAKAMOTO SAITO, Heat Pumps, Pergamon, 1990, Pages 455-465, ISBN 9780080401935.
- Jandot, Olivier. *The Invention of Thermal Comfort in Eighteenth-Century France*. London: Bloomsbury, 2020.
- Karkanis, P., M. Koumouzelis, J.K. Kozlowski, V. Sitlivi, K. Sobczyk, F. Berna, and S. Weiner. "The Earliest Evidence for Clay Hearths: Aurignacian Features in Klisoura Cave 1, Southern Greece." *Antiquity* 78, no. 301 (2004): 513–25. doi:10.1017/S0003598X00113195.
- Khoshhesab, Zahra Monsef. 2012. "Reflectance IR Spectroscopy." In *Infrared Spectroscopy - Materials Science, Engineering and Technology*, edited by Theophile Theophanides. InTech. <https://doi.org/10.5772/37180>.

Kubba, Sam. Chapter Nine - Impact of Energy and Atmosphere, Editor(s): Sam Kubba, Handbook of Green Building Design and Construction (Second Edition), 2017 Butterworth-Heinemann, Pages 443-571, ISBN 9780128104330

LLC, Sun-Aire Comfort Systems. "Heat Pump: What Is It and How Does It Work?" Sun Aire Comfort Systems (blog), January 18, 2017. <https://sun-airehvac.com/heat-pump-work/>.

Massachusetts Department of Energy Resources. n.d. "Massachusetts Energy Rebates & Incentives | Mass.gov." www.mass.gov. <https://www.mass.gov/guides/massachusetts-energy-rebates-incentives>.

Mori Building Group. n.d. "Mechanism of Himawari Solar Lighting System." Laforet Engineering. <https://himawarisolar.com/himawari-solar-natural-lighting-system/mechanism-of-himawari-solar-lighting-system/>.

Nagase, Ryo. 2014. "How to Connect Multicore and Multimode Fibers." Research Gate. 2014. https://www.researchgate.net/figure/Example-of-fiber-bundle-type-optical-FI-FO-device_fig1_263828871.

NASA. 2010. "Infrared Waves | Science Mission Directorate." [Nasa.gov](http://nasa.gov). 2010. https://science.nasa.gov/ems/07_infraredwaves.

Office of Energy Efficiency & Renewable Energy. n.d. "Radiant Heating." [Energy.gov](http://energy.gov). Accessed 2023. <https://www.energy.gov/energysaver/radiant-heating>.

Patil, Pravin Dilip. "Analysis of Heat Transfer Performance of Automotive Radiator Using MgO-Water Nanofluid." (2018).

Purkey, Sarah G., and Gregory C. Johnson. 2013. "Antarctic Bottom Water Warming and Freshening: Contributions to Sea Level Rise, Ocean Freshwater Budgets, and Global Heat Gain*." *Journal of Climate* 26 (16): 6105–22. <https://doi.org/10.1175/JCLI-D-12-00834.1>.

reserved, Mettler-Toledo International Inc all rights. n.d. "Specific Heat Capacity Measurement." www.mt.com. https://www.mt.com/us/en/home/applications/Application_Browse_Laboratory_Analytics/Application_Browse_thermal_analysis/specific-heat-capacity-measurement.html.

Risto Kosonen, Chapter 8 - Chilled Beams and Radiant Ceiling Systems, Editor(s): Roger Legg, Air Conditioning System Design, Butterworth-Heinemann, 2017, Pages 151-166, ISBN 9780081011232,

Ritchie, Hannah, Max Roser, and Pablo Rosado. "CO₂ and Greenhouse Gas Emissions." *Our World in Data*, May 11, 2020. <https://ourworldindata.org/emissions-by-sector>.

Sam Kubba, Chapter 9 - Impact of Energy and Atmosphere, Editor(s): Sam Kubba, Handbook of Green Building Design and Construction, Butterworth-Heinemann, 2012, Pages 385-492, ISBN 9780123851284,

Saxton, Maria. "Mycelium Fungi as a Building Material." *Rise*, February 13, 2020. <https://www.buildwithrise.com/stories/mycelium-fungi-as-a-building-material>.

Shah, Hetal. "Thermal Conductivity - Definition and Detailed Explanation." *BYJUS*, August 1, 2019. <https://byjus.com/chemistry/thermal-conductivity/>.

- Sharifi, Naser P., Gregory E. Freeman, and Aaron R. Sakulich. "Using COMSOL Modeling to Investigate the Efficiency of PCMs at Modifying Temperature Changes in Cementitious Materials – Case Study." *Construction and Building Materials* 101 (December 30, 2015): 965–74. <https://doi.org/10.1016/j.conbuildmat.2015.10.162>.
- Solar Impulse. "Solutions Explorer." Accessed January 29, 2023. https://solarimpulse.com/solutions-explorer?si_SOLUTIONS%5BrefinementList%5D%5Bguide_sectors_en%5D%5B0%5D=Buildings%20%26%20Shelters.
- Solov'ev, Sergej L. *Ancient Berezan: The architecture, history and culture of the first Greek colony in the Northern Black Sea*. Vol. 4. Brill, 1999.
- Srubar Research Group. 2022. "Living Materials Laboratory / Wil v. Srubar III." [Spot.colorado.edu](https://spot.colorado.edu/~wizr7047/). 2022. <https://spot.colorado.edu/~wizr7047/>.
- Strain, Daniel. 2020. "Building Materials Come Alive with Help from Bacteria." *CU Boulder Today*. January 15, 2020. <https://www.colorado.edu/today/2020/01/15/building-materials-come-alive>.
- Stuart, Robert. *On the History and Art of Warming and Ventilating Rooms and Buildings, by Open Fires, Hypocausts, German, Dutch, Russian, and Swedish Stoves, Steam, Hot Water, Heated Air, Heat of Animals, and Other Methods: With Notices of the Progress of Personal and Fireside Comfort, and of the Management of Fuel. Illustrated by Two Hundred and Forty Figures of Apparatus*. Vol. 2. G. Bell, 1845.
- Tatum, Jeremy. 2017. "Book: Heat and Thermodynamics (Tatum)." *Physics LibreTexts*. January 25, 2017. [https://phys.libretexts.org/Bookshelves/Thermodynamics_and_Statistical_Mechanics/Book%3A_Heat_and_Thermodynamics_\(Tatum\)](https://phys.libretexts.org/Bookshelves/Thermodynamics_and_Statistical_Mechanics/Book%3A_Heat_and_Thermodynamics_(Tatum)).
- Team, The Fauske. "Difference Between Reaction & Adiabatic Calorimetry | Fauske." Accessed March 10, 2023. <https://www.fauske.com/blog/reaction-calorimetry-vs.-adiabatic-calorimetry>.
- Thomas, John Meurig. "Sir Benjamin Thompson, Count Rumford and the Royal Institution." *Notes and Records of the Royal Society of London* 53, no. 1 (1999): 11-25.
- U.S. Energy Information Administration. 2016. "Coal Prices and Outlook - U.S. Energy Information Administration (EIA)." [Eia.gov](https://www.eia.gov/energyexplained/coal/prices-and-outlook.php). 2016. <https://www.eia.gov/energyexplained/coal/prices-and-outlook.php>.
- US Environmental Protection Agency. n.d. "Funding Opportunities | Green Building | US EPA." [Archive.epa.gov](https://archive.epa.gov/greenbuilding/web/html/funding.html#guides). Accessed April 27, 2023. <https://archive.epa.gov/greenbuilding/web/html/funding.html#guides>.
- US EPA, OA. "Overview of Greenhouse Gases." *Overviews and Factsheets*. Accessed March 10, 2023. <https://19january2017snapshot.epa.gov/ghgemissions/overview-greenhouse-gases>.
- US EPA, OAR. "Inventory of U.S. Greenhouse Gas Emissions and Sinks." *Reports and Assessments*, February 8, 2017. <https://www.epa.gov/ghgemissions/inventory-us-greenhouse-gas-emissions-and-sinks>.

- Vogele, Nathan. "Brief History of Central Heating Systems." Cates Heating And Cooling, September 25, 2017.
<https://catesheatingandcooling.com/blog/history-central-heating-systems/>.
- Vogele, Nathan. "How Does an Electric Furnace Work?" Cates Heating And Cooling, November 20, 2018. <https://catesheatingandcooling.com/blog/how-electric-furnace-work/>.
- Wang, Shuai, Suzanne F. Scarlata, and Nima Rahbar. "A Self-Healing Enzymatic Construction Material." *Matter* 5, no. 3 (March 2, 2022): 957–74.
<https://doi.org/10.1016/j.matt.2021.12.020>.
- Wang, Shuai, Suzanne Scarlata, and Nima Rahbar. "Curing and Self-Healing of Enzymatic Construction Materials Using Nanoparticles." *Cell Reports Physical Science* 3, no. 9 (September 21, 2022): 101039. <https://doi.org/10.1016/j.xcrp.2022.101039>.
- WarmupUK. 2022. "Radiant Floor Heating Systems Buyers Guide for 2022." Warmup. March 11, 2022. <https://www.warmup.com/blog/radiant-floor-heating>.
- Watts, Jonathan. "Concrete: The Most Destructive Material on Earth." *The Guardian*, February 25, 2019, sec. US news.
<https://www.theguardian.com/cities/2019/feb/25/concrete-the-most-destructive-material-on-earth>.
- Weinberger, Dawn. "What's The Most Efficient Heating System For Your Home?" *Forbes Home*, September 26, 2022.
<https://www.forbes.com/home-improvement/hvac/most-efficient-heating-systems/>.
- Y. Farnam et al., Measuring freeze and thaw damage in mortars containing deicing salt using a low-temperature longitudinal guarded comparative calorimeter and acoustic emission, *Adv. Civ. Eng. Mater.* 3 (1) (2014) 23.

APPENDIX

Appendix A – Visual Summary of Heat Pumps

A visual summary of the components and process of a heat pump is included in the visual summary provided. The example shows an air-source heat pump in heating mode for a split system heat pump. The components as well as some variations are called out and explanations are given.

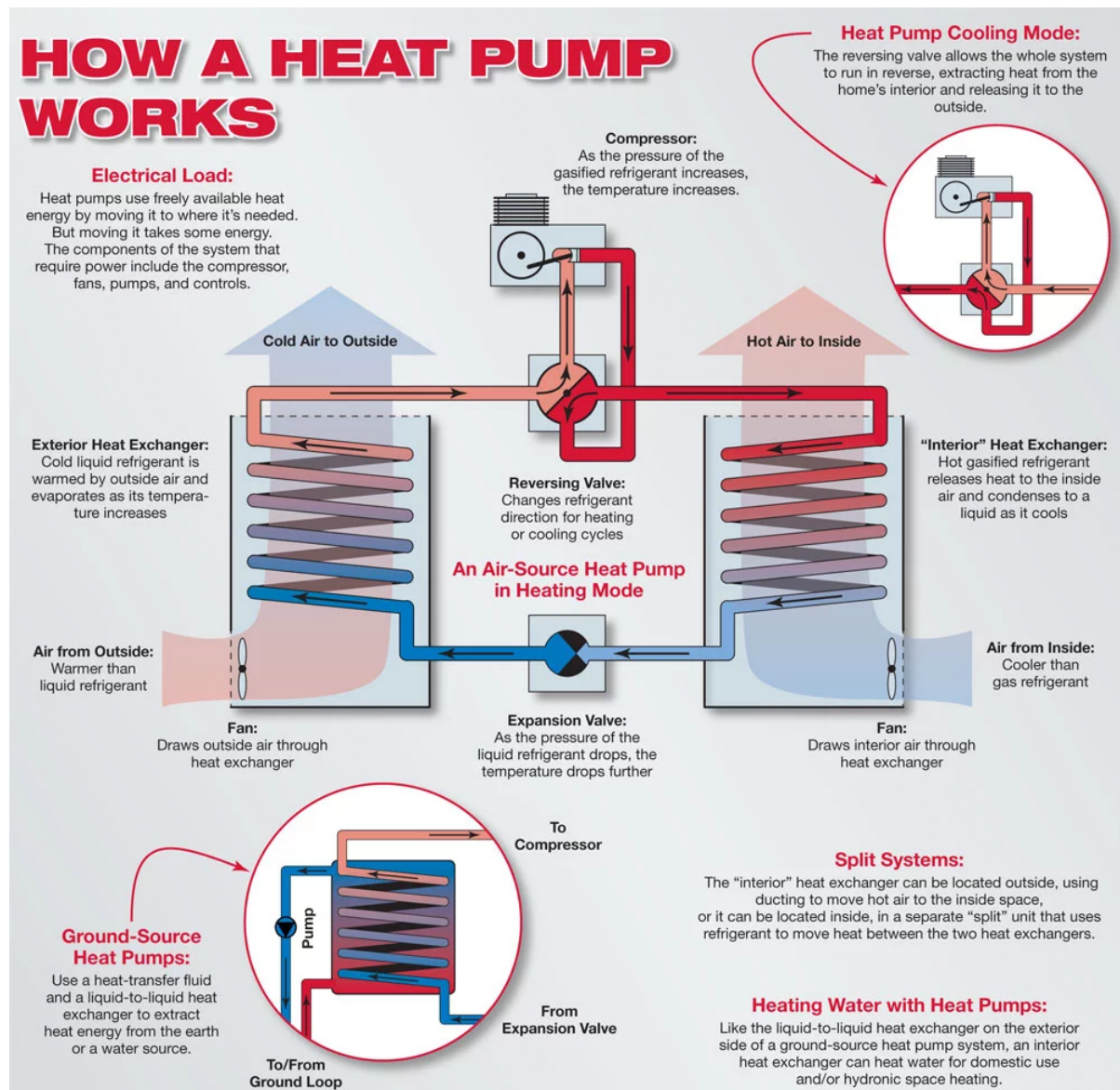


Figure 48. Heat Pump Visual Summary.
Citation, (Sun-Aire, 2017).

Appendix B - ECM-N Sample Creation Procedures

Proposed Procedure:

ECM-n Sample Creation (*for a 2''x 2''x2'' cube with calcium carbonate*)

Slurry sample without surfactant

1. Take the enzymes from the freezer in the far lab
2. Take graduated canisters and place them in the canister holder (10 canisters)
3. Take pipettes and replaceable pipette tips
4. Fill the beaker with reagent-grade water
5. Place 5 mg of enzymes on a scale to measure it. Mix it with 2 ml of RG water.
6. Pour the enzymatic solution into the canister, 10 microliters
**For a 2-inch cube, 180g of sand, 7.5 ml CaC solution (calcium carbonate), 5.25g gelatin*
7. 58.08g Calcium Chloride
 - a. Calcium Carbonate CaCO_3 has a different ratio
8. 400ml +10ml of RG water and mix it with the calcium from step 7. Put it on a stir plate and add a stir bar.
9. 2.422g of the trace buffer (Trizma Base) and add it to the enzymatic solution from step 6. Keep it spinning for 10 mins.
10. Measure 180g of sand in one beaker
11. Measure 5.25g of gelatin (kept by the laser in the kool-aid-esque container) and mix it with the sand from step 10.
12. Mix in the enzymes in the solution from step 9 using the canister with enzymes and pipette with the step 9 solution. Repeat the procedure 2 times.
13. In the hood, calibrate the PH sensor with the three solutions rinsing the sensor in between each.
14. Put the beaker from the stir plate, PH sensor, and carbon dioxide tube into the beaker. Wait until the PH level drops to 7 then stop, put aside for 6 hours, and wait for white crystals to form.
15. For homogeneous distribution of gelatin in the mix, preheat the crystal solution to 40C and put a pre-weighted amount of gelatin in. Ensure that the mixture is well stirred by adding a stir bar. Wait until gelatin fully dissolves in the solution, forming a viscous liquid.
16. Remove the stir bar and add 0.18g of nanoparticles (0.1% by sand weight). From now on, only glass stirring rods can be used.
17. Once everything is well mixed, add sand to the beaker and mix for 5 minutes holding the beaker in the oven. It will keep gelatin in a liquid state.
18. Pour well-mixed slurry out in the mold. Set the temperature in the oven to 90-100C and place the mold with the slurry in. Allow for 30-40 hours of curing.

Proposed Procedure:

ECM-n Sample Creation (for a 2"x 2"x2" cube with calcium carbonate)

Slurry sample with surfactant

19. Take the enzymes from the freezer in far lab freezer
20. Take graduated canisters and place them in the canister holder (10 canisters)
21. Take pipettes and replaceable pipette tips
22. Fill the beaker with reagent-grade water
23. Place 5 mg of enzymes on a scale to measure it. Mix it with 2ml of RG water.
24. Pour the enzymatic solution into the canister, 10 microliters
 - *For a 2-inch cube, 180g of sand, 7.5 ml CaC solution (calcium carbonate), 5.25g gelatin
25. 58.08g Calcium Chloride
 - a. Calcium Carbonate CaCO_3 has a different ratio
26. 400ml +10ml of RG water and mix it with the calcium from step 7. Put it on a stir plate and add a stir bar.
27. 2.422g of the trace buffer (Trizma Base) and add it to the enzymatic solution from step 6. Keep it spinning for 10 mins.
28. Measure 180g of sand in one beaker
29. Measure 5.25g of gelatin (kept by the laser in the kool-aid-esque container) and mix it with the sand from step 10.
30. Mix in the enzymes in the solution from step 9 using the canister with enzymes and pipette with the step 9 solution. Repeat the procedure 2 times.
31. In the hood, calibrate the PH sensor with the three solutions rinsing the sensor in between each.
32. Put the beaker from the stir plate, PH sensor, and carbon dioxide tube into the beaker. Wait until the PH level drops to 7 then stop, put aside for 6 hours, and wait for white crystals to form.
33. In the meantime, start preparing a surfactant mixture to let the nanoparticle distribute more evenly throughout the aggregate in the mixture. Take a beaker and add 10 ml of RG water. Then, in the hood, add 1.65g of oleic acid and 0.18g of nanoparticles (0.1% by sand weight).
34. Seal the beaker and put it in a sonic bath for 30 minutes. Set oven temperature to 60C.
35. After a sonic bath, put a sealed beaker in the oven at 60C and wait for 24 hours.
36. Then, add 10 ml of acetone to let nanoparticles participate. Use a magnet to promote separation. Repeat three times.
37. Add 10 ml of toluene acid to the solution and put it in a sonic bath for another 30 minutes.
38. For homogeneous distribution of gelatin in the mix, preheat the crystal solution to 40C and put a pre-weighted amount of gelatin in. Ensure that the mixture is well stirred by

adding a stir bar. Wait until gelatin fully dissolves in the solution, forming a viscous liquid.

39. Remove the stir bar and add surfactant solution with nanoparticles in. From now on, only glass stirring rods can be used.
40. Once everything is well mixed, add sand to the beaker and mix for 5 minutes holding the beaker in the oven. If the resulting slurry is dry, add more water until it is stirring well.
41. Pour well-mixed slurry out in the mold. Set the temperature in the ventilated oven to 90-100C and place the mold with the slurry in. Allow for 30-40 hours of curing.

Appendix C – NETZSCH-PROTEUS-70 Software Settings for TGA Procedure

Start-Up Setting:

Diagnosis→ Gasses and switches: Ensure the following are checked and OK
Purge 2 MFC: NITROGEN – flow 20mL/min, Protective MFC: NITROGEN– flow 20mL/min, Outlet
Diagnosis→ View Signals: Ensure Temp <100°C

Method Settings:

Creating a New Method

Setup Tab:

Crucible: Al₂O₃ (... 1700°C)
Sample Carrier: TG 209F1 std (Al₂O₃ support) TC: P (-200... 1200°C)
TG BeFlat support: On
Super Res: Off
Weighing Mode: Manual Input
Click Forwards

Header Tab:

Measurement: Sample
Laboratory: *provide lab name* (at WPI, “WPI-Professor (PI)”)
Project: *provide project name*
Operator: *provide operator name* (at WPI, your WPI userID)
Material: *select type of material being analyzed from dropdown menu*
Identity: *provide a unique identifier for each analysis* (at WPI, use format YYYY-MM-DD-WPIuserID-SampleName-01)
Click Forwards

Temperature Program:

Note that the instrument’s temperature limits are 25°C to 1,000°C. Additionally, valid heating rates for dynamic steps are 5K/min, 10K/min, and 20K/min.

Step Category: Initial, Category: Start Temperature: 30°C, Add

Step Category: Dynamic, Category: End Temperature: 600°C, Heating Rate 10K/min, Add

Step Category: Final, Category: Emergency Reset Temp: 625°C, Add
Click Forwards

Calibrations: Select “will not be used”

Last Items:

Select data storage location

Data Acquisition:

Measurement → Start Measurement

(On the TG 209F1 Libra Adjustment Window)

Set Initial Gasses: Check the first 3 to be OK

Purge 2 MFC: NITROGEN – flow 20mL/min, Protective MFC: NITROGEN – flow 20mL/min, Outlet

Data Analysis:

Software → NETZSCH-Proteus-70 Analysis

Open the saved file as a .ngb-st9 extension for raw data

Visibility: expand the dynamic node

Uncheck Temp and Additional to hide the temp and gas flow traces from display

Set Y-Axis Units: Right-click the TGA data curve, TG unit → mg or %

To calculate mass change (units mg or % depending upon prior step):

Right-click on TGA data curve, Evaluate → Mass Change, set cursors as desired, Apply, OK

Identify and label peaks, onset, inflection, end etc.:

Right-click on TGA data curve, Evaluate → set as desired

Appendix D – Software Settings for DSC Procedure

Start-Up Setting:

Setpoint Window: Select OK to start setpoint, *the intracooler should turn on*

Diagnosis→ Gasses and switches: Ensure the following are checked and OK

Purge 2 MFC: NITROGEN – flow 20mL/min, Protective MFC: NITROGEN– flow 20mL/min, Outlet

Diagnosis→ View Signals: Ensure Temp <100°C

Method Settings:

Creating a New Method

Setup Tab:

Crucible: Concavus Pan Al(... 610°C), pierced lid

Automatic Cooling: On

Special Instrument Control: None

STC: On

Click Forwards

Header Tab:

Measurement: Sample

Laboratory: *provide lab name* (at WPI, “WPI-Professor (PI)”)

Project: *provide project name*

Operator: *provide operator name* (at WPI, your WPI userID)

Material: *select type of material being analyzed from dropdown menu*

Identity: *provide a unique identifier for each analysis* (at WPI, use format YYYY-MM-DD-WPIuserID-SampleName-01)

Name: *Sample Name*

Mass: *Sample Mass*

Crucible Mass: *Mass of Sample Pan and Lid*

Reference Name: *Name of Reference*

Mass: *Mass of Reference Sample (usually 0mg)*

Crucible Mass: *Mass of Reference Pan and Lid*

Remark: *enter as desired*

Click Forwards

Temperature Program:

Note that the maximum temperature must be at least 50°C below the sample decomposition onset as found by TGA testing. The instrument’s temperature limits are

-40°C to 600°C. Additionally, valid heating rates for dynamic steps are 5K/min, 10K/min, and 20K/min.

STC → controlled by the setup tab selection (on) and should be checked on for all steps

AC → controlled by the setup tab selection (on)

Gasses → Purge and Protective MFC should be on 20mL/min for all steps

Basic Experiment:

Step Category: Initial, Category: Start Temperature: 25°C, Add

Step Category: Isothermal, Category: Isothermal Time 00:02 (hh:mm), Add

Step Category: Dynamic, Category: End Temperature: 200°C, Heating Rate 10K/min, Add

Step Category: Isothermal, Category: Isothermal Time 00:02 (hh:mm), Add

Step Category: Dynamic, Category: End Temperature: 25°C, Cooling Rate: 10K/min, Add

Step Category: Isothermal, Category: Isothermal Time 00:05 (hh:mm), Add

Step Category: Final, Category: Emergency Reset Temp: 225°C, Add

Click Forwards

Calibrations:

Temperature Calibrations: Select the calibration that corresponds with the heating rate, (ex: 10K/min)

Heat Flow Calibrations: Select the calibration that corresponds with the heating rate, (ex: 10K/min), *NOTE: this permits conversion from MV to MW*

Tau-R Calibration: Select the calibration that corresponds with the heating rate, (ex: 10K/min), *NOTE: this compensates for the thermocouples' time constants*

Last Items:

Select data storage location and save the created method

Data Acquisition:

On the DSC 214 Polyma Adjustment Window

Set Initial Gasses: Check the first 3 to be OK

Cooling: Purge 2 MFC: NITROGEN – flow 20mL/min, Protective MFC: NITROGEN – flow 20mL/min, Outlet

Manual Loading

Diagnosis → View Signals to show relevant parameters

Verify P2(N2) and PG(N2), purge and protective gasses are 20mL/min

Click Start on the DSC 214 Polyma Adjustment 1 Window
Click the Stop button, a red square, to end the data measurement

Data Analysis:

Software→ NETZSCH-Proteus-70 Analysis

Open the saved file as a .ngb-st9 extension for raw data

Visibility: expand the dynamic node

 Uncheck Temp and Additional to hide the temp and gas flow traces from display

Right-click on the DSC data→ Split into segments

 Right-click on segments you'd want to hide, select hide segment

Right-click on exo to set Exo Up/ Exo Down

 Right-click on a peak → Evaluate→ Peak, select limits with cursor, set as desired

Appendix E – Methods Summary for Guarded Longitudinal Comparative Calorimetry

Guarded Longitudinal Comparative Calorimetry (GLCC) with ECM-n

Goal: Determine thermal conductivity of Enzymatic Construction Material with Nanoparticles

Proposed Procedure:

1. Prepare a system that houses the sample, thermocouples and Pyroceram cubes:
 - a. The system's outer shell is made of rigid insulation with certain parts having metal for higher conductivity and stability. The shell has a rectangular extrusion in its center forming a 2"x2"x6" void to fit three 2"x2"x2" cubes. Two of the cubes are pyroceram cubes of known thermal conductivity which surround our sample cube with that of unknown value.
 - b. In order to make heat travel homogeneously through the cavities in between the sample and pyroceram blocks, a highly conductive thermal gap filler will be utilized. The thermal gap filler being used is the ThermalCool TC3008.
 - c. To extract data from the experiment, thermocouples will be used to read the temperature at specified locations. The locations will be the cavities with the thermal gap filler between the neighboring blocks. This way, the temperature difference on the opposite sides of the sample is captured and mapped.

2. Running the experiment:
 - a. The procedure will be run for three iterations. Each run of the experiment will have the hot plate decreasing its temperature at a so-called "pulse" setting. Every 10-degree temperature drop will be followed by a 20-second stationary interval for the temperature to level out. The resulting graph with mapped data will take the same shape as the example below:

tecaLOG Main Window Display

File: Parameter Transfers

Settings: Decimal selection

Help: Minimal

Select a Comm Port: Initiates communication

Enable and Disable: Turns functions on and off

Sensor Temp: Displays sensor measured value

Set: Enter value, press "Set" to send to controller

Ramp/Soak: Create and Run profiles

Data Log: Set up and start data logging function

Autotune: Methods of adjusting and saving PID values

Strip Chart: Displays Set, Sensor and Power on a time scale

Strip Chart Set Up: Adjust Strip Chart axis and display

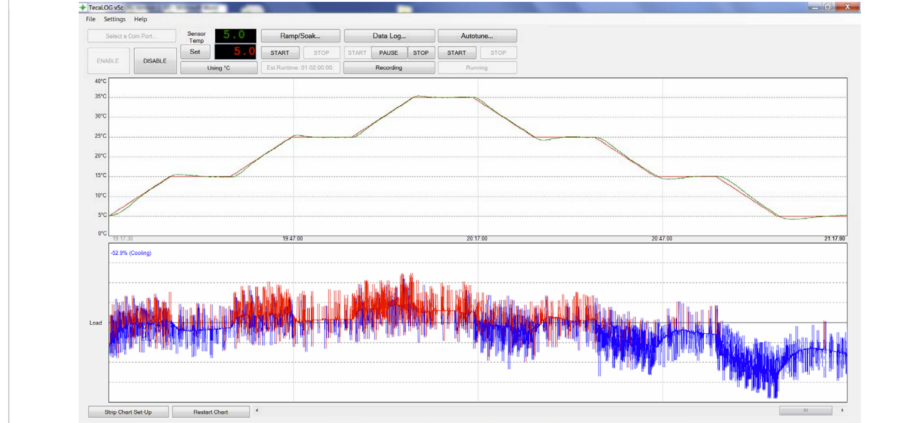


Figure 49. Example Data Given by TecaLog Software Manual.

- b. The specimen sample will begin at 330K and through the duration of the iteration; cool to 130K over approximately 15 minutes.

Appendix F – XPS Insulation Product Specification Sheet

The selected manufacturer model the passive photothermal heating system design uses is Styrofoam™ Brand Cavitymate™ Ultra. The following 2 tables were pulled from the manufacturer’s product specification sheets (“Styrofoam-Brand-Cavitymate-Ultra-Pis-43-D100051-EnNA” n.d.). These sheets provided the relevant material properties needed for the inputs and calculations performed with the model.

TABLE 1: U.S. Sizes, R-values and Edge Treatments for Styrofoam™ Brand Cavitymate™ Ultra XPS Foam Insulation

Nominal Board Thickness ¹⁾ , in.	RSI (R-value) ²⁾	Ultra air barrier wall system Board Size, in.	Board Size, in.	Edge Treatment
2.125	12.0	15 3/4" x 96"	4'x8' with 16" scores longitudinally	Square Edge
2.50	14.0	15 3/4" x 96"	4'x8' with 16" scores longitudinally	Square Edge
3.00	16.8	15 3/4" x 96"	4'x8' with 16" scores longitudinally	Square Edge

¹⁾ Not to be considered sales specifications.

²⁾ R means resistance to heat flow. The higher the R-value, the greater the insulating power. R-values are expressed in ft²·h²·°F/Btu. R-value determined by ASTM C518.

TABLE 2: Canadian Sizes, R-values and Edge Treatments for Styrofoam™ Brand Cavitymate™ Ultra XPS Foam Insulation

Nominal Board Thickness ¹⁾ , mm	RSI (R-value)	Ultra air barrier wall system Board Size, mm	Edge Treatment
75	2.90 (16.5)	400 x 2400	Square Edge
91	3.52 (20)	400 x 2400	Square Edge
75	2.90 (16.5)	600 x 2400	Square Edge

¹⁾ Additional thicknesses available. Contact your DuPont representative for more information. Not all thicknesses available in all regions.

²⁾ RSI or R-value means resistance to heat flow. The higher the RSI or R-value, the greater the insulating power. R-values are expressed in ft²·h²·°F/Btu. RSI values are expressed in m²·C/W. R-value determined by ASTM C518.

Figure 50. XPS R-Values from Dupont.

TABLE 3: U.S. Physical Properties of Styrofoam™ Brand Cavitymate™ Ultra Extruded Polystyrene Foam Insulation

Test Method	Property	Typical Value	Units
ASTM C518	Thermal Resistance ⁽¹⁾ per in.	<u>2.125</u> ² 2.5 ³ 3.0 ⁴ 12.0 14.0 16.8	ft ² x h x °F/Btu, R-value, 1 min. @ 75°F mean temp.
ASTM D1621	Compressive Strength ⁽²⁾	25	psi, min.
ASTM C272	Water Absorption	0.1	% by volume, max.
ASTM E96	Water Vapor Permeance	<u>2.125</u> ² 2.5 ³ 3.0 ⁴ 0.8 0.65 0.50	perm, max.
-	Maximum Use Temperature	165	°F
ASTM D696	Coefficient of Linear Thermal Expansion	3.5 x 10 ⁻⁵	in/in x °F
ASTM C203	Flexural Strength	50	psi, min.
ASTM E84	Flame Spread ⁽³⁾	10	-
ASTM E84	Smoke Developed	155	-
ASTM E84	Surface Burning Characteristics for both foam core and finished product	Class A	
	Flame Spread	<25	
	Smoke Developed	<450	

¹ Values are consistent with the criteria of ASTM C578 and the FTC R-value rule (16 CFR Part 460).

² Vertical compressive strength is measured at 10 percent deformation or yield, whichever occurs first. Since Styrofoam™ Brand Extruded Polystyrene Foam Insulations are visco-elastic materials, adequate design safety factors should be used to prevent long-term creep and fatigue deformation. For static loads, 3:1 is suggested. For dynamic loads, 5:1 is suggested. Contact DuPont for design recommendations.

³ These numerical flame-spread and smoke-developed ratings are not intended to reflect hazards presented by this or any other material under actual fire conditions.

TABLE 4: Canadian Physical Properties of Styrofoam™ Brand Cavitymate™ Ultra Extruded Polystyrene Foam Insulation

Property and Test Method	Value
Thermal Resistance per in. (25 mm), ASTM C518, ft ² ·h·°F/Btu, (m ² · °C/W, R-value (RSI)) ⁽¹⁾ min. @ 75°F mean temp. @ 40°F mean temp. @ 25°F mean temp.	5.6 (0.97) 6.0 (1.04) 6.3 (1.09)
Compressive Strength ⁽²⁾ , ASTM D1621, psi (kPa), min.	25 (170)
Water Absorption, ASTM D2842, % by Volume, max	0.3
Water Vapour Permeance, ASTM E96, perm (ng/Pa·s·m ²), max.	1.5 (90)
Maximum Use Temperature, °F (°C)	165 (73.8)
Coefficient of Linear Thermal Expansion, ASTM D696, in/in·°F (mm/m·°C)	3.5 x 10 ⁻⁵ 6.3 x 10 ⁻²
Flexural Strength, ASTM C203, psi, min.	43.5 (300)
CAN/ULC S1022 Surface Burning Characteristics for both foam core and finished product ⁽³⁾ Flame Spread ⁽⁴⁾ Smoke Developed	<300 <700

¹ Values are consistent with CAN/ULC S7013-17.

² Vertical compressive strength is measured at 10 percent deformation or yield, whichever occurs first. Since Styrofoam™ Brand Extruded Polystyrene Foam Insulations are visco-elastic materials, adequate design safety factors should be used to prevent long-term creep and fatigue deformation. For static loads, 3:1 is suggested. For dynamic loads, 5:1 is suggested. Contact DuPont for design recommendations.

³ Tested per CAN/ULC S1022. Refer to UL and CCMC listings for details on foam thickness and maximum density evaluated.

⁴ These numerical flame-spread and smoke-developed ratings are not intended to reflect hazards presented by this or any other material under actual fire conditions.

Figure 51. Physical Properties of XPS from Dupont.

Appendix G – Supplemental DSC Results

The differential scanning calorimeter used was a heat-flux DSC which measures the difference in heat flux between the sample and a reference. In this experiment, the sample was heated to 110°C. The unannotated data is shown below:

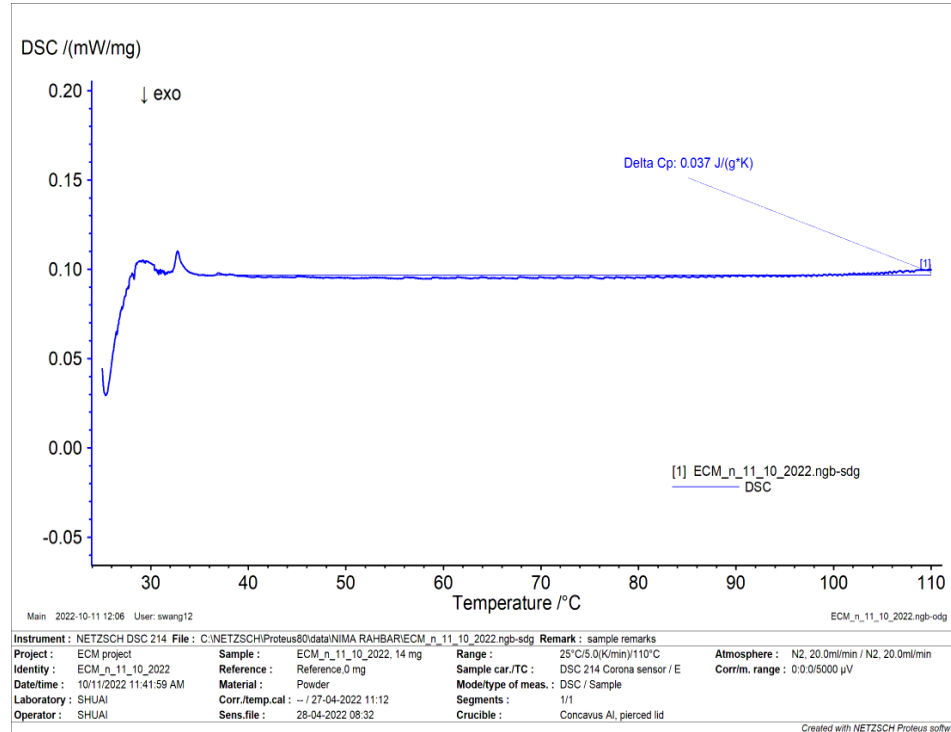


Figure 52. DSC Data for ECM-n Sample.
The sample was heated to 110°C.

Appendix H – Spectrometry Results Data of ECM-n Specimen, Absorbance Peaks

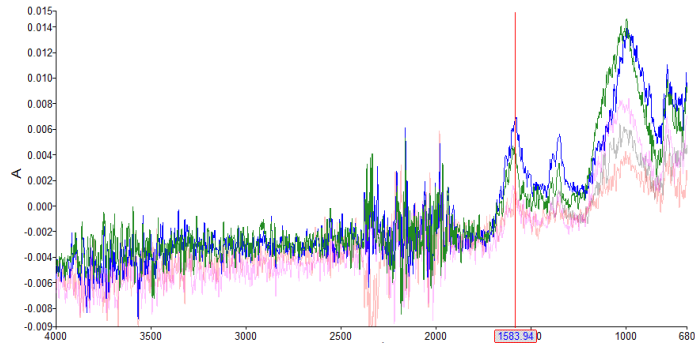


Figure 53. Appendix H, 1 of 4.

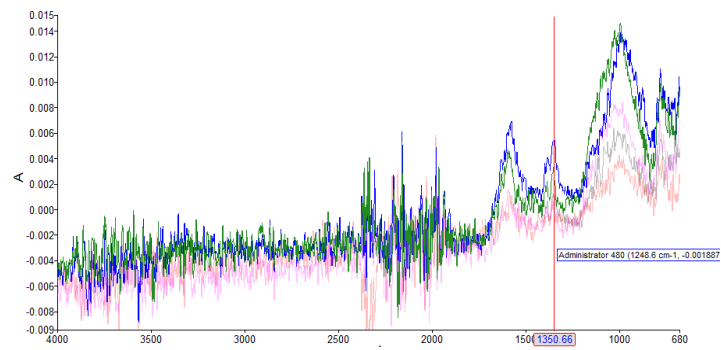


Figure 54. Appendix H, 2 of 4.

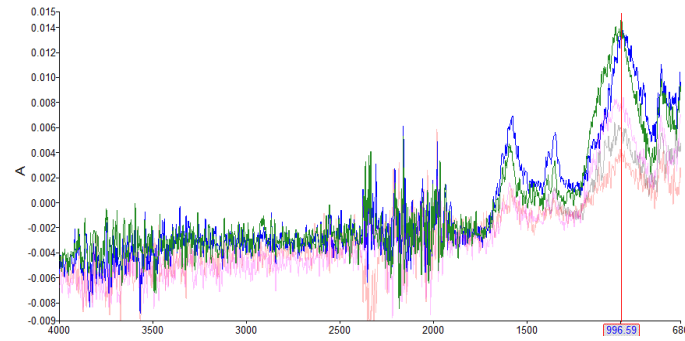


Figure 55. Appendix H, 3 of 4.

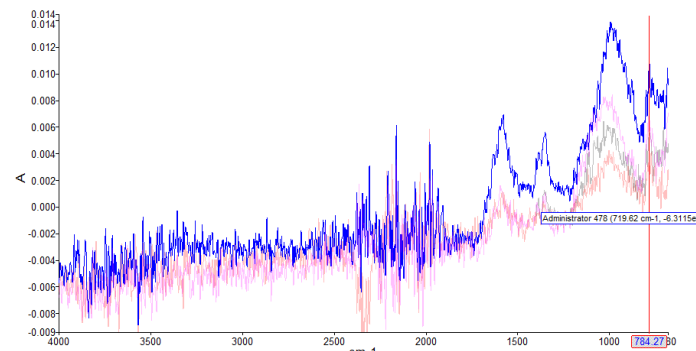


Figure 56. Appendix H, 4 of 4.

Appendix I – Hand Calculations

Using the equations given and combined with the material's properties stated within the report, a Microsoft Excel file was used to perform the hand calculations. All the cells of the file had to be manually formatted together to produce the figures given below.

<p><u>Where:</u> deltaT - temperature gradient Tx - temperature of air outside k - conductivity of material Ty - temperature of air inside d - thickness of the wall q* - heat flux simplified q - vector of local heat flux rho.cp - heat capacity per unit volume alpha - thermal diffusivity [m²/s]</p>	<p><u>Equations:</u> $q^* = -k * (Tx - Ty)/d$ $q = -k * \text{deltaT}$ $q = ((-\text{deltaT})/R)$ $q = (-\text{deltaT}) * U$ $u = 1/R$ $\alpha = k/\text{rho.cp}$</p>
--	---

Figure 57. Variables and Equations Legend.

ECM-n Variations		
#	ECM-n Thickness (m)	Heat Loss (W)
d1	0.194	181.24
d2	0.5	173.03
d3	0.7	168.07

XPS Properties				
Type	Thermal Conductivity	Density	Available Dimensions	Manufacturer
Styrofoam™ Brand Cavitymate™ Ultra	0.025	28	4'x8'	Dupont

Figure 58. Model Component Material Properties.

Type\Layer	Layer 1 (Left)	Control Surface 1	Layer 2	Control Surface 2	Layer 3	Control Surface 3	Layer 4	Control Surface 4	Layer 5 (Right)
Material	Inside Air	Air Film	XPS		ECM-n		XPS	Air Film	Outside Air
Initial Temperature (degrees C)	26								0
Thickness (meters)	-	0.006	0.091	-	0.194	-	0.091	0.006	-
RSI (m ² *°C/W) OR Thermal Conductivity (W/m*K)			1		2.25 [1]		1		
RSI (m ² *°C/W)		0.00074	3.64000		0.08622		3.64000	0.00021	

Figure 59. Wall Model in Excel.

Results	
U= 1/R	0.1357
Heat Flux (W/m ²)	3.5292 [2]
Model Total Exterior Surface (m ²)	23.8800
Total Heat Loss (W)	84.2766
Power of each Point Heat Source (W)	0.2394

Figure 60. Results from Hand Calculations in Excel.

Appendix J – Model Heating Visualization - Isothermal Lines

The figure shows a heat gradient of point heat source distributions. This contributed heavily to the results in Section 4.3.1.

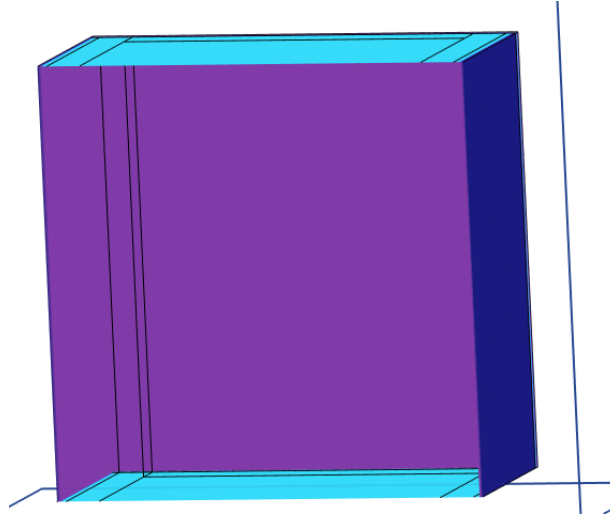


Figure 61. Heat Gradient of Point Heat Source Distributions.